

*Reply to RC1: ' Review of "Influences of hydroxyl radicals (OH) on top-down estimates of the global and regional methane budgets" '*

**Comment:** Zhao et al. assess systematically how uncertainties of OH concentrations affects our inference of the global and regional methane emissions and their decadal changes from the existing surface measurement network. The authors performed a series of inversion experiments using varied OH fields and used the standard deviations of an inversion ensemble to represent the uncertainty due to OH fields. The work is very important, as the uncertainty source of prescribed OH fields have not been quantitatively assessed in previous syntheses (e.g., Saunois et al. 2017, 2019). However, the manuscript can be improved with better presentation and in-depth discussion. I'd recommend the publication of this manuscript if the following issues are addressed.

**Response:** We thank the reviewer for his/her helpful comments. All of them have been addressed in the revised manuscript. Please see out itemized responses below.

**Comments:** 1. The manuscript lacks quantitative comparisons of the results with other uncertainty sources (as assessed in literature) of methane emission estimations. The comparison could provide readers both the context and the insight. For example, I am looking for answers to the following questions:  
1 how large is the uncertainty due to OH compared to other uncertainty sources (e.g., transport)?

**Response:**

**For the uncertainties in global total CH<sub>4</sub> emissions lead by OH, we added the values in section 3.1.1 (L316-326):**

**” The minimum-maximum range of the CH<sub>4</sub> emissions estimated by the 10 OH fields is almost similar to the range estimated by previous bottom-up studies (542-852Tg yr<sup>-1</sup> given by Kirschke et al., 2013 and 583-861Tg yr<sup>-1</sup> given by Saunois et al, 2016) from GCP syntheses and much larger than that reported by an ensemble of top-down studies for 2000-2009 in Kirschke et al. (2013) (526-569Tg yr<sup>-1</sup>), Saunois et al. (2016) (535-566Tg yr<sup>-1</sup>) or the recent Saunois et al. (2019) (522-559 Tg yr<sup>-1</sup>). (Table 2 and Fig. 2). In the three top-down model ensembles, most of the inversion systems use TransCom OH fields, and the reported differences are mainly from different model transport and set-up of the inversion systems (e.g. the observations used in the inversions). Excluding the two**

outliers (MOCAGE and SOCOL-3) in Inv1, we find an uncertainty of about 17% in global methane emissions (518 to 611Tg yr<sup>-1</sup>) due to OH global burden and distributions, while transport model errors lead to only 5% of the uncertainty of the global methane budget (Table 3, Locatelli et al. (2013)). ”

For the regional emissions, we now better compare the uncertainties lead by OH with that lead by model transport errors and set-up of the inversion systems given in Saunois et al. (2016) and of Locatelli et al. (2015). We have inserted a new Table 3 summarizes the results.

**Table 3.** Global, latitudinal, and regional CH<sub>4</sub> emission in Tg yr<sup>-1</sup> (mean ±SD and the [min-max] range of the inversions) calculated by Inv1 and Inv2 during the early 2000s (2000/07/01-2002/06/01) in Tg yr<sup>-1</sup> (excluding MOCAGE and SOCOL-3). The uncertainties (Unc. = (max – min)/multi-inversions mean) lead by using different OH fields are compared with the uncertainties in CH<sub>4</sub> emissions given by Saunois et al. (2016) and Locatelli et al. (2013).

Study	This study (Impact of OH)				Saunois et al. (2016)	Locatelli et al. (2013)
Period	2000/07/01-2002/06/01				2000-2009	2005
Experiment	Inv1 (Original OH)		Inv2 (Scaled OH)		TD ensemble	Transport model errors
Region	Mean ±SD [range <sup>1</sup> ]	Unc.	Mean ±SD [range]	Unc.	Unc.	Unc.
global	567 ± 34 [518-611]	17%	551 ± 2 [548-555]	1%	6%	5%
60 °-90 °N	29 ± 1 [27-30]	12%	29 ± 1 [27-30]	12%	50%	10% (NH)
30 °N-60 °N	174 ± 8 [158-183]	14%	172 ± 6 [159-178]	11%	20%	
0 °-30 °N	199 ± 14 [178-217]	20%	192 ± 1 [191-194]	1%	13% (<30 °N)	
0 °-30 °S	147 ± 14 [121-167]	30%	140 ± 6 [133-153]	14%		
30 °S-90 °S	19 ± 1 [17-20]	18%	18 ± 1 [18-19]	9%	25%	37% (North America)
America	45 ± 2 [42-48]	11%	45 ± 1 [42-46]	8%	70%	23%
Canada	27 ± 1 [24-28]	17%	27 ± 1 [24-28]	13%	31%	
Europe	27 ± 1 [25-28]	12%	27 ± 1 [25-28]	12%	11%	38%
Russia	33 ± 1 [30-35]	13%	33 ± 1 [30-34]	20%	11%	25% (Asia)
China	42 ± 5 [33-50]	39%	40 ± 3 [35-43]	3%	42%	
Southeast Asia	38 ± 3 [34-41]	20%	37 ± 0.3 [36-37]	4%	44%	
South Asia	59 ± 6 [51-66]	24%	57 ± 0.8 [56-58]	17%	44%	48% (South America)
Northern South America	73 ± 9 [58-85]	37%	69 ± 4 [65-77]	20%	94%	
Southern South America	33 ± 4 [27-39]	37%	31 ± 2 [29-36]	6%	42%-45%	30%
Africa	76 ± 4 [68-82]	18%	74 ± 1 [73-77]			

And we added in section 3.2.2 (L387-391 and L400-405):

**“The uncertainties in global OH burden and distributions lead to larger uncertainty (maximum—minimum) in top-down estimated CH<sub>4</sub> emissions over the tropics (>20% of multi-inversion mean) and smaller uncertainty over the northern mid-latitude regions (14%) compare with that lead by transport model errors and different observations given by Saunois et al. (2016) (13% over tropics and 20% over northern mid-latitude regions) (Table 3).”**

**” As shown in Table 3, at regional scales, the uncertainty (maximum—minimum) in top-down estimated CH<sub>4</sub> emissions due to different OH global burden and distributions over Asia and South America (~37% of multi-inversion mean) are of the same order than those lead by transport errors (25% and 48%) or given by Saunois et al. (2016) (~40%). Over other regions, using different OH fields lead to smaller uncertainties (11%-18%) compared to other causes of errors (23%-70%) (Table 3).”**

For emissions changes during the 2000s, we added in section 3.2.2 (L555-566):

**” We now compare the uncertainty of top-down estimated CH<sub>4</sub> emission changes from the early to the late 2000s due to different OH spatial-temporal variations with that ensemble of top-down studies given by Saunois et al. (2017). For the sectoral emissions, the emission changes from agriculture and waste and from wetland show the largest uncertainties (more than 50% of multi-inversions mean, Inv3—Inv2 in Table 6) induced by OH spatial-temporal variations, comparable to that given by Saunois et al. (2017). On the contrary, the uncertainty of fossil fuel emission changes (24% of multi-inversions mean) is much smaller than that given by Saunois et al. (2017). For regional CH<sub>4</sub> emission changes, the uncertainty induced by OH spatial-temporal variations is usually larger than the multi-inversion mean emission changes (except South Asia) and similar to that given by Saunois et al. (2017). The large differences existing in different top-down estimated regional and sectoral emission changes are mainly attributed to model transport errors in Saunois et al. (2017). Here, our results show that uncertainties due to OH spatio-temporal variations can lead to similar biases in top-down estimated CH<sub>4</sub> emission changes.”**

2 Is the uncertainty due to OH the bottleneck for understanding the global and regional methane budget? In which regions, the uncertainty due to OH dominates; and in which regions, they are not that important?

**Response:**

**For the global CH<sub>4</sub> budget, in the conclusions and discussion, we have demonstrated (L640-L645):**  
” **Based on the ensemble of 10 original OH fields ( $[\text{OH}]_{\text{GM-CH}_4}$ :  $10.3\text{-}16.3 \times 10^5 \text{ molec cm}^{-3}$ ), the global total CH<sub>4</sub> emissions inverted by our system vary from 518 to 757 Tg yr<sup>-1</sup> during the early 2000s, similar to the CH<sub>4</sub> emission range estimated by previous bottom-up syntheses and larger than the range reported by the top-down studies (Kirschke et al., 2013; Saunio et al, 2016). The top-down estimated global total CH<sub>4</sub> emission varies linearly with  $[\text{OH}]_{\text{GM-CH}_4}$ , which indicates that at the global scale, a small uncertainty of  $1 \times 10^5 \text{ molec cm}^{-3}$  (10%)  $[\text{OH}]_{\text{GM-CH}_4}$  can result in 40.4 Tg yr<sup>-1</sup> uncertainties in optimized CH<sub>4</sub> emissions.”**

**For the regional CH<sub>4</sub> budget, we added in “Conclusions and discussion” (L647-L654) :**

**“At regional scale (excluding the two highest OH fields), CH<sub>4</sub> emission uncertainties due to different OH global burdens and distributions are largest over South America (37% of multi-inversion mean), South Asia (24%), and China (39%), resulting in significant uncertainties in optimized emissions from the wetland and agriculture and waste sectors. These uncertainties are comparable in these regions with those due to model transport errors and inversion system set-up (Locatelli et al., 2013; Saunio et al., 2016). For these regions, the uncertainty due to OH is critical for understanding their methane budget. In other regions, OH leads to smaller uncertainties compared to that given by Locatelli et al. (2013) and Saunio et al. (2016).”**

Is it adequate to reduce the uncertainty of global mean OH for the purpose of improving estimates for global and regional methane emissions? Or reducing uncertainty in OH spatial distribution is equally important?

**Response: We added in Section 4 “Conclusions and discussion” (L705-L713):**

**” Our results indicate that OH spatial distributions, which are difficult to obtain from proxy observations (e.g. MCF), are equally important as the global OH burden for constraining CH<sub>4</sub> emissions over mid- and high-latitude regions. Constraining global annual mean OH based on proxy observations (e.g. Zhang et al., 2018; Maasakkers et al., 2019) provides a constraint on global total methane emissions, through the necessity of balancing the global budget (sum of source – sum of sinks = atmospheric growth rate). It also largely reduces uncertainties in optimized CH<sub>4</sub> emissions due to OH over most of the tropical regions but not over South America and overall mid-**

**high latitude regions. Also, the spatial and seasonal distributions of OH is found critical to properly infer temporal changes of regional and sectoral CH<sub>4</sub> emissions.”**

These questions are interesting to readers and can be addressed by putting the results of this paper in the context of literature (such as Saunio et al. 2017 from the authors' group).

**Comments:** 2. The regional results are specific to the observing system (i.e., NOAA surface network). Surface observations are relatively dense in North America and West Europe, but very sparse near South America, Tropical Africa, and Tropical Asia. Therefore, the inversion tends to adjust emissions from regions less constrained by observations, if any global mismatch exists, leading to large spread of estimates in these regions. Inclusion of more observations may lead to different spatial patterns in Fig. 3. It is important to acknowledge that the conclusion about regional emissions applies to only this specific observing system. The authors mentioned site locations when explaining the difference between Inv1 and Inv2; however results from other experiments may also be explained by this factor, at least partly. In addition, OH concentrations are highest over tropics, therefore, it is expected that the difference in OH from varied fields is largest over tropics. This could explain the larger posterior flux range in tropics for Inv1.

**Response:** We added in the 3.1.2 (L407-415):

**” The uncertainties in the top-down estimated regional emissions are not only due to inter-model differences of the regional OH fields but also rely on the distribution of the surface observations used in the inversions. Over the regions with large prior emissions but less constrained by observations (e.g. South America, South Asia, and China), our OH analysis leads to larger uncertainties than regions that are well constrained by observations (e.g. the North America and Canada) (Fig. S3). The results may indicate that on the regional scale, the top-down estimated CH<sub>4</sub> emissions and the uncertainties lead by OH are specific to the observation system retained. If more surface observations (e.g. in the southern hemisphere) or satellite columns with a more even global coverage were included in our inversions, spatial patterns of the top-down estimated CH<sub>4</sub> emissions and their uncertainties (as shown by Fig.3) could be different.”**

**Comments:** 38-40: The sentence reads awkward. Physically, increases in OH burden cannot contribute to increases in emissions. Clarify or rephrase to avoid any confusion.

**Response:** We changed the sentence to (L37-L38):

**“From the early to the late 2000s, the optimized CH<sub>4</sub> emissions increased by 21.9±5.7Tg yr<sup>-1</sup> (16.6-30.0Tg yr<sup>-1</sup>), of which ~25% (on average) offsets the 0.7% (on average) increase in OH burden ”**

**Comments:** 53-54: The word “additional” is confusing here.

**Response:** We removed “additional”

**Comments:** 71-72: Unclear what “catalytic chemistry” in this sentence is referred to. Also, the statement “a small perturbation of OH can result in significant change in atmospheric CH<sub>4</sub>” is inaccurate or ambiguous. The author may want to say “. . . significant change in the budget (or budget imbalance) of atmospheric CH<sub>4</sub>”.

**Response:** We rephrased the sentence as suggested:” A small perturbation of OH can result in significant changes in the budget of atmospheric CH<sub>4</sub> (Turner et al., 2019).”

**Comments:** 72-75: There are other OH sources such as O<sub>3</sub>+HO<sub>2</sub>, H<sub>2</sub>O<sub>2</sub> photolysis, and OVOCs photolysis that become important depending on the chemical environment, for example, see Lelieveld et al. (2016).

**Response:** We changed in the text (L70-L75):

**” At the global scale, tropospheric OH is mainly produced by the reaction of excited oxygen atoms (O(<sup>1</sup>D)) with water vapor (primary production) but also by the reaction of nitrogen oxide (NO) and ozone (O<sub>3</sub>) with hydroperoxyl radicals (HO<sub>2</sub>) and organic peroxy radicals (RO<sub>2</sub>) (secondary production). At regional scales, photolysis of hydrogen peroxide and oxidized VOC photolysis can be important depending on the chemical environment (Lelieveld et al. 2016).”**

**And we added in the reference list:**

**Lelieveld, J., Gromov, S., Pozzer, A., and Taraborrelli, D.: Global tropospheric hydroxyl distribution, budget and reactivity, Atmospheric Chemistry and Physics, 16, 12477-12493, 10.5194/acp-16-12477-2016, 2016.**

**Comments:** 78: A direct measurement of OH is challenging but possible. But estimates of global  $\bar{\tau}$  mean from sparse direct measurements is nearly impossible because the large variation of OH as a result of its short lifetime.

**Response:** We rephrased the sentence to (L77-L89) “Tropospheric OH has a very short lifetime of a few seconds (Logan et al., 1981; Lelieveld et al., 2004), hindering estimates of global OH concentrations ([OH]) through direct measurements and limiting our ability to estimate the global CH<sub>4</sub> sink.”

**Comments:**101-103:Optimizations of CH<sub>4</sub> emissions together with OH concentrations have been done using 3-D model inversions (e.g., Cressot et al., 2014, Zhang et al., 2018 and Maasakkers et al., 2019), in addition to two-box model analysis. These studies all used satellite data though.

**Response:** We added in the text (L105-L111):

“The role of OH variations on the top-down estimates of CH<sub>4</sub> emissions has been evaluated using two box-model inversions with surface observations (e.g. Rigby et al., 2017; Turner et al., 2017, Naus et al., 2019) and 3D models that optimize CH<sub>4</sub> emissions together with [OH] by assimilating surface observations (Bousquet et al., 2006) or satellite data (Cressot et al., 2014, McNorton et al., 2018; Zhang et al., 2018; Maasakkers et al., 2019). The proxy-based constraints usually optimize [OH] on a global or latitudinal scale, the impact of OH vertical and horizontal distributions being less quantified to date. Also, proxy methods do not allow to access underlying processes as direct chemistry modeling (Zhao et al., 2019). ”

**Comments:** Line 155: What temperature field do you use to compute [OH]<sub>GM-CH<sub>4</sub></sub> for different models? And how “troposphere” is defined in this calculation? Line 158: Is latitudinal distribution of OH also a factor (and maybe even more important factor) that results in [OH]<sub>GM-CH<sub>4</sub></sub> > [OH]<sub>GM-M</sub> ?

**Response:** We clarified in the text (L167-L169):

“The tropopause height is assumed at 200hPa following Naik et al. (2013) and the 3D temperature field used to compute [OH]<sub>GM-CH<sub>4</sub></sub> is from ERA Interim re-analysis meteorology data (Dee et al, 2011). ”

As we can see in Table 1, if MOCAGE and SOCOL3 OH fields are excluded, differences between [OH]<sub>GM-M</sub> and [OH]<sub>GM-CH<sub>4</sub></sub> are largely reduced. We clarified in the text (L175-L177):

” This is mainly because MOCAGE and SOCOL3 OH fields show much higher [OH] near the surface than in the upper troposphere (Zhao et al., 2019).”, and we removed: ” as some of the OH fields show distinct vertical distributions”.

**Comments:** Eq. 1. The (x-xb) term is repeated twice.

**Response:** Thank you very much for pointing out this, we removed the (x-xb).

**Comments:** Line 172: Since only emissions are optimized in the inversion, it's a bit misleading to say H(x) represents sensitivity to sinks.

**Response:** We removed the "sinks" as suggested.

**Comments:** Line 205: What about Cl?

**Response:** We added in the text (L225-226) "The CH<sub>4</sub> sink by reaction with chlorine is not considered in our LMDz model simulations."

**Comments:** Line 231-232: "To separate the influence of OH spatial distributions from that of global mean [OH]: :". As commented above, it is unclear whether the OH fields vary monthly or annual mean. If the former, then in addition to influence of spatial distribution, the influence of seasonal variation is also embedded. If the latter, then the study design has a major flaw because the latitudinal distribution of OH has a pronounced seasonal cycle.

**Response:** OH fields vary monthly in our inversions, the seasonal variations of OH fields can impact inversion results. Thank you for mentioning the role of the OH seasonal cycle, which is not detailed in our analysis. We clarified in the text (in section 2.2 - L186):

" We conduct an ensemble of variational inversions ... but different prescribed monthly mean OH fields as described in Sect. 2.1."

In section 2.3, to emphasize the impact of OH seasonal variation, although not analyzed separately in this work. we added:

L254-255: "To separate the influence of OH spatial distributions (including their seasonal variations) from that of the global annual mean [OH]."

L257-258: "As such, Inv2 provides the uncertainty range of CH<sub>4</sub> emissions induced by OH spatial distribution in both horizontal and vertical directions as well as seasonal variations..."

**Comments:** Line 239-240: Please denote inv3 and inv4 explicitly after 2007-2009 and 2000-2002 to

make it easier to follow.

**Response: This has been changed as suggested.**

**Comments:** Line 241-243: I don't think Inv4-Inv2 represents the impact of OH spatial distribution.

**Response:** Here we mean the difference in Inv4—Inv2 estimated by different OH fields represents the uncertainties lead by the different OH spatial and seasonal distributions since they are all using OH fields scaled to the same value globally for 2000-2002.

**We clarified in the text (L268-272):**

” Therefore, the difference Inv3—Inv2 reveal the impact of OH on CH<sub>4</sub> emission changes between the early and late 2000s (the yellow box with solid lines of Fig. 1), Inv3—Inv4 separates the impact of OH interannual variations, and the difference Inv4—Inv2 allows assessing the uncertainties of optimized CH<sub>4</sub> emission changes due to different OH spatial and seasonal distributions (the yellow boxes with dashed lines in Fig. 1). ”

**Comments:** Line 250: Which one has the largest trend, which may be more relevant in this setting?

**We added in the text (L279):**

“...shows the largest year-to-year OH variations and a positive trend of 0.35% yr<sup>-1</sup> ...”

**Comments:** Line 269-273: This sentence does not flow smoothly within the context (results from Inv1). Remove it or move it somewhere else.

**Response: We removed this sentence as suggested**

**Comments:** Line 278: Not clear to me how this helps decreasing discrepancies with bottom-up estimates? Fig. 2 does not show the discrepancies are reduced to me. Please clarify. Also please provide the values (and ranges) of bottom-up estimates in the text for a clear comparison.

**Response: We removed “help decreasing discrepancies with bottom-up estimations”, and we added the number in the text (L316-L320):**

”The minimum-maximum range of the CH<sub>4</sub> emissions estimated by the 10 OH fields is almost similar to the range estimated by previous bottom-up studies (542-852Tg yr<sup>-1</sup> given by Kirschke et al., 2013 and 583-861Tg yr<sup>-1</sup> given by Saunio et al, 2016) from GCP syntheses and much larger than that reported by an ensemble of top-down studies for 2000-2009 in Kirschke et al. (2013) (526-

569Tg yr<sup>-1</sup>), Saunois et al. (2016) (535-566Tg yr<sup>-1</sup>) or the recent Saunois et al. (2019) (522-559 Tg yr<sup>-1</sup>). (Table 2 and Fig. 2). ”

**Comments:** Line 284-290: Is it possible that the difference is due to the fact that [OH]<sub>GM-CH4</sub> is used here instead of [OH]<sub>GM-M</sub> (which I assume was used in these studies)? It does not convince me that the difference is due to the inter-hemispheric transport and stratospheric loss in 3-D model vs. 2-box model. Choices of hemispheric mean reaction rate of OH+CH<sub>4</sub> can also introduce biases in 2-box model.

**Response:** For the two-box model inversion, the [OH]<sub>GM-CH4</sub> is the same as [OH]<sub>GM-M</sub> since the air mass and temperature are homogeneously distributed over space. For 3D model inversion, the optimized CH<sub>4</sub> emissions do not show a linear relationship with [OH]<sub>GM-M</sub>. One can see that the [OH]<sub>GM-M</sub> of CMAM OH field ( $11.3 \times 10^5$  molec cm<sup>-3</sup>) is a bit lower than that EMAC-L90MA ( $11.5 \times 10^5$  molec cm<sup>-3</sup>) and CESM1-WACCM ( $11.4 \times 10^5$  molec cm<sup>-3</sup>), but the top-down estimated CH<sub>4</sub> emissions using CMAM OH field (599Tg yr<sup>-1</sup>) is higher than that estimated using CESM1-WACCM (578Tg yr<sup>-1</sup>) and EMAC-L90MA (589Tg yr<sup>-1</sup>).

For the explanation of the difference between two-box model and 3-D model inversions, we agree that the choice of hemispheric mean rate is a more important factor. We added in the text (L342-L345):

“This difference probably results from the different hemispheric mean reaction rates of OH+CH<sub>4</sub> applied in box models, but could also be due to different treatments of inter-hemispheric transport and stratospheric CH<sub>4</sub> loss in global 3D transport models compared to simplified box-models (Naus et al., 2019).”

**Comments:** Line 316: Does the seasonality of OH fields also play a role here?

**Response:** Yes, the seasonality can also contribute to the differences in Inv2. As we cannot separate the contribution from seasonal variations and spatial distribution, we emphasized this in Section 2.3 (L245-L255):

“To separate the influence of OH spatial and seasonal distributions from that of the global mean [OH].”

**Comments:** Line 338: Please explicitly state which uncertainty sources Saunois et al. (2016) considered. The comparison may be misleading otherwise.

**Response:** We clarify in the text (L387-L391):

**“The uncertainties in global OH burden and distributions lead to larger uncertainty (maximum—minimum) in top-down estimated CH<sub>4</sub> emissions over the tropics (>20% of multi-inversion mean) and smaller uncertainty over the northern mid-latitude regions (14%) compare with that lead by transport model errors and different observations given by Saunois et al. (2016) (13% over tropics and 20% over northern mid-latitude regions) (Table 3).”**

**Comments:** Line 343-345: Likely because these regions have high prior emissions, but are not well constrained by surface measurements. So, it should be stated that these regional features are not intrinsic of the atmosphere, but specific to the observing system of interest.

**Response:** As already mentioned in the first comments, we added in the text (L407-415):

**“The uncertainties in the top-down estimated regional emissions are not only due to inter-model differences of the regional OH fields but also rely on the distribution of the surface observations used in the inversions. Over the regions with large prior emissions but less constrained by observations (e.g. South America, South Asia, and China), our OH analysis leads to larger uncertainties than regions that are well constrained by observations (e.g. the North America and Canada) (Fig. S3). The results may indicate that on the regional scale, the top-down estimated CH<sub>4</sub> emissions and the uncertainties lead by OH are specific to the observation system retained. If more surface observations (e.g. in the southern hemisphere) or satellite columns with a more even global coverage were included in our inversions, spatial patterns of the top-down estimated CH<sub>4</sub> emissions and their uncertainties (as shown by Fig.3) could be different.”**

**Comments:** Line 355: what is the “total differences”? How large are they?

**Response:** We clarified in the text (L427-L429):

**”... account for 50% of the differences due to both OH burden and spatial distributions...”**

**Comments:** Line 364-367: I don't understand the logic here. I think it is probably related to OH concentration being much higher in tropics than extra-tropics.

**Response:** When scaling all OH fields to the same total global loss, the inter-model difference of OH is reduced by 33% over northern mid and high latitudes and uncertainties in top-down estimated CH<sub>4</sub> emissions are reduced by only 22%. Over northern tropical regions, the inter-model difference in OH is reduced by 67% but the uncertainties in CH<sub>4</sub> emissions are reduced by 93%, as we show in the text. The explanations here, we think, are similar to the comments for Line 343-345, which related that OH over tropical regions is more sensitive to global OH burdens as less constrained by local/direct observations. We clarified this point in the text (L434-L440):

”Over tropical regions, CH<sub>4</sub> emissions are less constrained (with few to none observation sites near source regions) than in the northern extra-tropics, where several monitoring sites located at or near the regions with high CH<sub>4</sub> emission rates and high OH uncertainties (e.g. North America, Europe, and downwind of East Asia). Thus, CH<sub>4</sub> emissions over the tropical regions mainly contribute to match the global total CH<sub>4</sub> sinks (instead of the sinks over the tropical regions only) estimated by inversion systems. When all OH fields are scaled to the same CH<sub>4</sub> losses (Inv2), differences of emissions over the tropical regions are therefore largely reduced. ”

**Comments:** Line 379: The range of global total CH<sub>4</sub> emissions by Inv2 (551±2Tg a<sup>-1</sup>) should be reported and discussed in 3.3.1, in comparison with Inv1.

**Response:** We added in section 3.1.1 (L347-L350):

” With the OH fields scaled to the same  $[\text{OH}]_{\text{GM-CH}_4}$  ( $11.1 \times 10^5 \text{ molec cm}^{-3}$ ), the Inv2 simulations (assuming a global total OH burden well constrained) estimated global CH<sub>4</sub> emissions of 551±2Tg yr<sup>-1</sup> (Table 3), as expected by the scaling. Differences in OH spatial distributions only lead to negligible uncertainty in global total CH<sub>4</sub> emissions estimated by top-down inversions.”

**Comments:** Line 418: Be clearer what “global scale increase” in this sentence is referred to. It is ambiguous in the current form.

**Response:** We add in the text (L491):” the increase in global mean [OH]”

**Comments:** Line 485-489: The assessment of the uncertainty due to OH fields relative to other uncertainty sources are too qualitative throughout the manuscript. More insight can be gained by quantitatively comparing to uncertainty estimates in literature such as Saunois et al.

**Response:** We added in section 3.2.2(L555-L566):

” We now compare the uncertainty of top-down estimated CH<sub>4</sub> emission changes from the early to the late 2000s due to different OH spatial-temporal variations with that ensemble of top-down studies given by Saunois et al. (2017). For the sectoral emissions, the emission changes from agriculture and waste and from wetland show the largest uncertainties (more than 50% of multi-inversions mean, Inv3—Inv2 in Table 6) induced by OH spatial-temporal variations, comparable to that given by Saunois et al. (2017). On the contrary, the uncertainty of fossil fuel emission changes (24% of multi-inversions mean) is much smaller than that given by Saunois et al. (2017). For regional CH<sub>4</sub> emission changes, the uncertainty induced by OH spatial-temporal variations is usually larger than the multi-inversion mean emission changes (except South Asia) and similar to that given by Saunois et al. (2017). The large differences existing in different top-down estimated regional and sectoral emission changes are mainly attributed to model transport errors in Saunois et al. (2017). Here, our results show that uncertainties due to OH spatio-temporal variations can lead to similar biases in top-down estimated CH<sub>4</sub> emission changes.”

**Comments:** Table 2 Quite confusing. Why global and hemispheric emissions are only shown for Inv1, but the inter-hemispheric differences are shown for both Inv1 and Inv2? Also, unit should be denoted in the caption.

**Response:** We added the global and hemispheric CH<sub>4</sub> emissions estimated by Inv2 to Table2 as suggested. And we included the unit.

**Table 2.** The global total, hemispheric CH<sub>4</sub> emissions, and inter-hemispheric difference of CH<sub>4</sub> emissions calculated by Inv1 and Inv2 during the early 2000s (2000/07/01-2002/06/01) in Tg yr<sup>-1</sup>.

Unit: Tg yr <sup>-1</sup>	Inv1 original OH				Inv2 scaled OH			
	Global	0-90 °N	90 °S-0	N-S <sub>Inv1</sub>	Global	0-90 °N	90 °S-0	N-S <sub>Inv2</sub>
<b>Prior</b>	522	384	138	246	522	384	138	246
<b>TransCom</b>	530	368	162	206	549	377	172	205
<b>INCA NMHC-AER-S</b>	518	380	138	242	553	399	154	245
<b>INCA NMHC</b>	552	392	160	232	552	392	160	232
<b>CESM1-WACCM</b>	587	420	166	254	551	400	151	249
<b>CMAM</b>	599	419	180	239	553	399	154	245
<b>EMAC-L90MA</b>	589	414	175	239	555	396	159	237
<b>GEOSCCM</b>	611	424	187	237	550	392	159	233
<b>MOCAGE</b>	716	/ <sup>a</sup>	/	/	/	/	/	/
<b>MRI-ESM1r1</b>	553	396	156	240	548	396	152	244
<b>SOCOL3</b>	757	/	/	/	/	/	/	/

Mean±SD	601±78	401±21	166±15	236±14	551±2	393±7	158±7	236±14
---------	--------	--------	--------	--------	-------	-------	-------	--------

<sup>a</sup> We do not analyze the hemispheric CH<sub>4</sub> emission estimated with MOCAGE and SOCOL3 OH field since inversions using the two OH fields calculate much higher CH<sub>4</sub> emissions than using other OH fields.

**Comments:** Table 5 With fixed OH field, you still expect an increasing OH sink (and therefore increasing emissions) because of increasing CH<sub>4</sub> concentration and temperature. This should be clarified somewhere in the text.

**Response:** We clarified in the 3.2.1 (L522-L525):

”Keeping OH fields from 2000-2002, top-down estimated CH<sub>4</sub> emissions increase by 16.9±1.9Tg yr<sup>-1</sup> (14.3-19.3Tg yr<sup>-1</sup>, Table 5) between the early 2000s (Inv2) to the late 2000s (Inv4) in response to increasing atmospheric CH<sub>4</sub> mixing ratios and temperature. This represents 75% of total optimized emission changes (Inv3—inv2) between the early and late 2000s (21.9±5.7Tg yr<sup>-1</sup>, Table 5).”

**Comments:** Fig. 2 The R<sup>2</sup>=0.99 line in the right panel: it should be acknowledged that other sinks of methane (such as soil absorption, Cl, and stratospheric loss) are not optimized and are specified with the same field in these inversions. Uncertainty in these sinks, if considered, will certainly create some spread in the data.

**Response:** We added in the Section 3.1.1 (L334-338): ” Where a 1×10<sup>5</sup> molec cm<sup>-3</sup> (1%) increase in [OH]<sub>GM-CH<sub>4</sub></sub> will increase the top-down estimated CH<sub>4</sub> emissions (EMIS<sub>CH<sub>4</sub></sub>) by 40.4 Tg yr<sup>-1</sup>, consistent with that given by He et al. (2020) using full-chemistry modeling and a mass balance approach. Other CH<sub>4</sub> sinks including soil uptake and oxidation by O<sup>1</sup>(D), which are prescribed in this study, remove 66.7Tg yr<sup>-1</sup> CH<sub>4</sub>. If uncertainties in all the CH<sub>4</sub> sinks were also considered, the correlation between optimized CH<sub>4</sub> emissions and the [OH]<sub>GM-CH<sub>4</sub></sub> would be reduced. ”

**Comments:** Fig. 3 To interpret this figure, the author should consider the uneven sampling of the surface network. The ranges of inferred regional emissions are large where observations are sparse, because it “costs” the least for the inversion to adjust in these regions. The inference for regional emissions is specific to the particular observing system. Having more surface stations in the southern hemisphere, or including satellite observations, would change the spatial pattern shown in this figure.

**Response:** As stated in previous comments, we added in section 3.1.2 (L407-L415):

”The uncertainties in the top-down estimated regional emissions are not only due to inter-model differences of the regional OH fields but also rely on the distribution of the surface observations

used in the inversions. Over the regions with large prior emissions but less constrained by observations (e.g. South America, South Asia, and China), our OH analysis leads to larger uncertainties than regions that are well constrained by observations (e.g. the North America and Canada) (Fig. S3). The results may indicate that on the regional scale, the top-down estimated CH<sub>4</sub> emissions and the uncertainties lead by OH are specific to the observation system retained. If more surface observations (e.g. in the southern hemisphere) or satellite columns with a more even global coverage were included in our inversions, spatial patterns of the top-down estimated CH<sub>4</sub> emissions and their uncertainties (as shown by Fig.3) could be different. ”

## ***Reply to RC2: ' Review'***

### 1 Overview:

Review of “Influences of hydroxyl radicals (OH) on top-down estimates of the global and regional methane budgets” by Zhao et al. This review slipped through the cracks as the COVID-19 situation evolved here. My sincere apologies for any hold ups. Zhao et al. present an analysis of a set of methane inversions using a set of 10 different OH fields from the CCMI experiment. They find the magnitude of methane emissions differs by roughly 30% (518-757 Tg/yr) depending on what OH fields they use. Overall, the study is useful in quantifying some of the uncertainties in methane emission estimates due to uncertain OH concentrations. The main shortcoming is the lack of discussion of what actually causes some of the differences (or really any discussion of OH). The figures are high quality but the text is very hard to follow because it's filled with many acronyms and parenthetical expressions. I would recommend major revisions.

**Response: We thank the reviewer for his/her helpful comments. This manuscript is the second step of our previous study, in which we have made a detailed description of the CCMI, INCA and TransCom OH fields and where we analyzed the factors controlling the inter-model differences in OH burden and spatial distribution and the increasing trend of OH simulated by CCMI models (Zhao et al., 2019). This manuscript mainly focuses on the impact of the inter-model differences of different OH fields on the top-down estimates of CH<sub>4</sub> emissions. Thus, regarding discussions on OH, we directly refer to the conclusion from Zhao et al. (2019) (see the response for the comments 2.1) without re-detailing all results. However, we now better explain the link with our first paper in the revised version and include summaries of results from Zhao et al. (2019) in this second paper.**

**Also, we have rephrased large parts of the original manuscript in this revised version, and especially**

**Section 3.2, which includes most of the acronyms and parenthetical expressions. All of the other comments have been addressed in the revised manuscript. Please see out itemized responses below.**

2 Comments:

2.1 What processes actually drive these differences?

The main issue I feel is totally missing from the manuscript is any discussion of what processes are actually driving some of these differences. I believe there was only a single paragraph (Lines 70-79) even mentioning anything about what might affect OH. For example, do some of the CCMI models or inversions show consistent patterns with known climate oscillations? This was surprising given that this is a paper focused on how OH impacts methane. The obvious question is what leads to these differences/similarities in OH. The authors seem to treat the CCMI models as a black box which makes it hard to gain any understanding of what's happening.

**Response:**

**As mentioned in the overview, this paper follows Zhao et al. (2019) where we analyzed in detail OH fields from CCMI models. Including the main conclusions of this first paper in the updated section 2.1 of this paper provides the required elements on what causes OH differences in CCMI models.**

**In the introduction, to clarify the link with our previous paper, we added (L112-121):**

**“This paper follows the work of Zhao et al. (2019), where we analyzed in details 10 OH fields derived from atmospheric chemistry models considering different chemistry, emissions, and dynamics (Patra et al., 2011; Szopa et al., 2013; Hegglin and Lamarque, 2015; Morgenstern et al., 2017; Zhao et al., 2019; Terrenoire et al., 2019). We now aim to build on this previous paper to estimate the impact of these OH fields on methane emissions as inferred by an atmospheric 4D variational inversion system. To do so, we use each of the OH fields in the 4D variational inversion**

system PYVAR-LMDz based on LMDZ-SACS (Laboratoire de Météorologie Dynamique model with Zooming capability-Simplified Atmospheric Chemistry System) 3D chemical transport model to evaluate the influence of OH distributions and variations on the top-down estimated global and regional CH<sub>4</sub> budget. Section 2 briefly describes the OH fields and their characteristics and underlying processes (see also Zhao et al., 2019 for more details)”

In section 2.1, we added (L146-L154):

“The inter-model differences of OH burden and vertical distributions are mainly attributed to differences in chemical mechanisms related to NO production and loss. The differences in [OH] spatial distributions are due to applying different natural emissions: for example, primary biogenic VOC emissions and NO emissions from soil and lightning (Zhao et al., 2019). As a result, the regions dominated by natural emissions (e.g. South America, central Africa) show the largest inter-model differences in [OH] (Fig.S1). The CCMI models consistently simulated positive OH trend during 2000-2010, mainly due to more OH production by NO than loss by CO over the East and Southeast Asia and positive trend of water vapor over the tropical regions (Zhao et al., 2019; Nicely et al., 2020). More details can be found in Zhao et al. (2019) and the herein cited literature.”

In section 3.1.1 (L310-L314), we added:

“The high [OH]<sub>GM-CH<sub>4</sub></sub> simulated by SOCOL3 and MOCAGE are mainly due to high surface and mid-tropospheric NO mixing ratio simulated by these two models (Zhao et al., 2019). As analyzed in Zhao et al. (2019), the lack of N<sub>2</sub>O<sub>5</sub> heterogeneous hydrolysis (by both SOCOL3 and MOCAGE) and the overestimation of tropospheric NO production by NO<sub>2</sub> photolysis (by SOCOL3) are the major factors behind the overestimation of NO and OH.”

Given this, the only major take-away I had from the paper is that “OH can lead to big differences in

methane estimates”, but this was already demonstrated by the box modeling papers (and others) that Zhao et al. are highly critical of. For example, the Rigby paper had error bars on their OH fields that bounded zero and the Turner paper had a case where OH didn’t change. Both of these led to radically different methane emissions.

**Response: Two-box models are an effective tool to assess changes in global CH<sub>4</sub> budget (Rigby et al., 2017, Turner et al., 2017), but we think that 3D analysis is still needed : (i) to check if box-model results are not biased by the oversimplification of atmospheric transport, (ii) to infer the regional CH<sub>4</sub> budgets, and (iii) to estimate methane decadal budgets as box-models are less relevant for estimating budgets than budget changes (Saunois et al., 2019). The study aims to quantify the uncertainties lead by using the prescribed OH fields in 3D model inversions.**

**Also, we have been more precise in the abstract and conclusions for the reader to get a more complete take away of our work (regions that are sensitive/important, quantitative estimates, comparison with other causes of uncertainties).**

**We added in the abstract (L25-L27):**

**“Current top-down estimates of the global and regional CH<sub>4</sub> budget using 3D models usually apply prescribed OH fields and attribute model-observation mismatches almost exclusively to CH<sub>4</sub> emissions, leaving the uncertainties due to prescribed OH field less quantified. ”**

**And we clarified in the text that we conducted inversions using an ensemble of OH fields not only to show that OH can lead to differences in CH<sub>4</sub> emissions but also to quantify the influences at global and regional scales.**

**In “conclusions and discussion”, we compared the uncertainties lead by OH with other causes of uncertainty.**

**For global total CH<sub>4</sub> emissions (L640-L644):**

**” Based on the ensemble of 10 original OH fields ( $[\text{OH}]_{\text{GM-CH}_4}$ : $10.3\text{-}16.3 \times 10^5$  molec cm<sup>-3</sup>), the global total CH<sub>4</sub> emissions inverted by our system vary from 518 to 757Tg yr<sup>-1</sup> during the early 2000s, similar to the CH<sub>4</sub> emission range estimated by previous bottom-up syntheses and larger than the range reported by the top-down studies (Kirschke et al., 2013; Saunio et al, 2016). ”**

**For the regional emissions (L647-L654):**

**” At regional scale (excluding the two highest OH fields), CH<sub>4</sub> emission uncertainties due to different OH global burdens and distributions are largest over South America (37% of multi-inversion mean), South Asia (24%), and China (39%), resulting in significant uncertainties in optimized emissions from the wetland and agriculture and waste sectors. These uncertainties are comparable in these regions with those due to model transport errors and inversion system set-up (Locatelli et al., 2013; Saunio et al., 2016). For these regions, the uncertainty due to OH is critical for understanding their methane budget. In other regions, OH leads to smaller uncertainties compared to that given by Locatelli et al. (2013) and Saunio et al. (2016).”**

**And we emphasized the importance of the OH spatial distributions on the top-down estimation of regional CH<sub>4</sub> budget (L705-713):**

**” Our results indicate that OH spatial distributions, which are difficult to obtain from proxy observations (e.g. MCF), are equally important as the global OH burden for constraining CH<sub>4</sub> emissions over mid- and high-latitude regions. Constraining global annual mean OH based on proxy observations (e.g. Zhang et al., 2018; Maasakkers et al., 2019) provides a constraint on global total methane emissions, through the necessity of balancing the global budget (sum of source – sum of sinks = atmospheric growth rate). It also largely reduces uncertainties in optimized CH<sub>4</sub> emissions due to OH over most of the tropical regions but not over South America and overall mid-**

**high latitude regions. Also, the spatial and seasonal distributions of OH is found critical to properly infer temporal changes of regional and sectoral CH<sub>4</sub> emissions.”**

Back to my point, I would find this manuscript much more useful and compelling if the authors actually highlighted processes and phenomena that lead to similar methane inversion responses. From Holmes et al., ACP (2013; <https://doi.org/10.5194/acp-13-285-2013>) we know some of the major processes that influence OH and Turner et al., PNAS (2018; <https://doi.org/10.1073/pnas.1807532115>) showed how this can with things like ENSO, do the authors see ENSO signals in the methane inversions? A recent paper from Nguyen et al., GRL (2020) tried to look at these feedbacks in a simple model. The authors should at least touch on the processes that influence OH, particularly those that could also influence methane.

**Response: We acknowledge that it is important to analyze processes and phenomena that lead to similar methane inversion responses. During the time period of this manuscript (the 2000s), the CCMI model simulated OH show a consistent positive trend (Zhao et al., 2019; Nicely 2020). As stated in our response to comments 2.1, the positive OH trend is mainly due to more OH production by NO than loss by CO over the East and Southeast Asia and positive trend of water vapor over the tropical regions (Zhao et al., 2019; Nicely et al., 2020). We have analyzed the impact of positive [OH] trend during the 2000s on top-down estimates of CH<sub>4</sub> emissions in section 3.2 and section 3.3. The ENSO signal during the early 2000s is very weak (with small year-to-year variations of [OH]) and the time period of this paper very short. Therefore, analyzing the impact of ENSO seems beyond the scope of this paper. However, please note that we have another manuscript submitted to ACP using CCMI models that analyzes the impact of trend and interannual variability of OH on the CH<sub>4</sub> budget on the decadal time scale (1980-2010) with a focus on the ENSO (<https://doi.org/10.5194/acp-2020-308>).**

**Yet, we discussed shortly the impact of ENSO in Section 4 (L692-L701):**

**“The trend and interannual variations of tropospheric OH burden are determined by both precursor emissions from anthropogenic and natural sources and climate change (Holmes et al., 2013; Murray et al., 2014). Based on satellite observations, Gauber et al. (2017) estimated that ~20% decrease in atmospheric CO concentrations during 2002-2013 led to an ~8% increase in atmospheric [OH]. The El Niño-Southern Oscillation (ENSO) has been proven to impact the tropospheric OH burden and CH<sub>4</sub> lifetime mainly through changes in biomass burning from CO (Nicely et al., 2020; Nguyen et al, 2020) and in NO emission from lightning (Murray et al., 2013; Turner et al., 2018). The ENSO signal is weak during the early 2000s, resulting in small interannual variations of tropospheric OH burden (Zhao et al., 2019). The mechanisms of OH variations related to ENSO and their impacts on the CH<sub>4</sub> budget need to be explored by inversions, but over a longer time period than this study (e.g. 1980-2010, Zhao et al., 2020).”**

## 2.2 Oversight of previous work and faith in the CCMI models

The authors seem to have quite a bit of faith in the CCMI models, more than this reviewer finds to be justified. There are quite a few known shortcomings of the models. For example, the models don't even get the ratio of the N/S gradient in OH correct. Yet the authors are quick to criticize MCF-constrained [OH] fields with seemingly no validation of their own OH fields (e.g., Lines 595-600). Is their analysis consistent with MCF? The authors seem to be arguing that these model derived forward simulations of OH are more reliable than reconstructions. The strongest claims made in this paper seem to be those that are critical of previous work estimating OH (e.g., Rigby and Turner). For example, Lines 595-600, the abstract is dismissive of box modeling results: ‘previous research mostly relied on box modeling inversions with a very simplified atmospheric transport’. The latter line in the abstract isn't even correct as there has been quite a bit of non-box model work the authors seem to discount or miss: McNorton et al., ACP (2016; <https://doi.org/10.5194/acp-16-7943-2016>), Gaubert et al., GRL (2017;

<https://doi.org/10.1002/2017GL074987>), Rigby et al., PNAS (2017; <https://doi.org/10.1073/pnas.1616426114>), Turner et al., PNAS (2017; <https://doi.org/10.1073/pnas.1616020114>), McNorton et al., ACP (2018; <https://doi.org/10.5194/acp-18-18149-2018>), Maasakkers et al., ACP (2019; <https://doi.org/10.5194/acp-19-7859-2019>), Naus et al., ACP (2018; <https://doi.org/10.5194/acp-19-407-2019>), Nguyen et al., (2020; <https://doi.org/10.1029/2019GL085706>), and He et al., ACP (2020; <https://doi.org/10.5194/acp-20-805-2020>). About half of these papers use 3-D atmospheric transport models and some even include fully-coupled chemistry (e.g., He et al., 2020), which is more comprehensive than the models used by the authors. The authors should do a more complete reading of the literature as they don't cite Holmes et al., ACP (2013), Murray et al., ACP (2014), or any of Michael Prather's papers.

## **Response:**

### **About CCMI models and proxy methods.**

**To date, we have mostly two approaches to estimate regional and global [OH], one using direct atmospheric chemistry modeling and one using proxy tracers, the main one being MCF. We do not have a specific faith in CCMI models (neither we deny the interest of MCF) but here, we choose to investigate the first approach using chemistry models, taking benefit of an important collaborative effort of this scientific community (CCMI experiments) to compare and, in fine, improve their models. Each method has its caveats and, following the comment of the reviewer, we try to balance more things between the two approaches in the updated version of the manuscript.**

**We added in the introduction(L104-106): “However, the OH fields simulated by atmospheric chemistry models show some uncertainties in both global burden and spatial-temporal variations (Naik et al., 2013; Zhao et al., 2019)”**

For the N/S ratio > 1 simulated by CCMI models, we reported their ranges, with a clarification in the text (L176-179):

” The inter-hemispheric OH ratios range from 1.0 to 1.5, larger than ones derived from MCF inversions (e.g. Bousquet et al., 2005; Patra et al., 2014), partly explained by the underestimation of CO in the northern hemisphere by atmospheric chemistry models (Naik et al., 2013).”

For lines 595-600, we just wanted to mention that the OH trend simulated by CCMI models (positive) is different than that from MCF inversions, which mainly show a decrease of [OH] after the early 2000s. It is hard to say which one is correct since both of the methods have their caveats regarding trends. For the increasing trend simulated by CCMI models, we have discussed the impact on CH<sub>4</sub> budget in the manuscript by writing with caution:” if the CCMI models represent the OH trend properly, a higher increasing trend of CH<sub>4</sub> emissions is needed to match the CH<sub>4</sub> observations (compared to the CH<sub>4</sub> emission trend derived using constant OH).”. We do not argue that CCMI models simulate a more realistic OH trend than two-box model inversions and/or proxy-based methods.

For the abstract, we removed “previous research mostly relied on box modeling inversions with a very simplified atmospheric transport”.

### About missing literature

For previous studies that quantify the impact of OH variations on the top-down estimate of CH<sub>4</sub> by 3D models, we acknowledge the missing references and thank the reviewer to have provided them. We added in the introduction (L105-L112):

“The role of OH variations on the top-down estimates of CH<sub>4</sub> emissions has been evaluated using

two box-model inversions with surface observations (e.g. Rigby et al., 2017; Turner et al., 2017, Naus et al., 2019) and 3D models that optimize CH<sub>4</sub> emissions together with [OH] by assimilating surface observations (Bousquet et al., 2006) or satellite data (Cressot et al., 2014, McNorton et al., 2018; Zhang et al., 2018; Maasakkers et al., 2019). The proxy-based constraints usually optimize [OH] on a global or latitudinal scale, the impact of OH vertical and horizontal distributions being less quantified to date. Also, proxy methods do not allow to access underlying processes as direct chemistry modeling (Zhao et al., 2019). ”

He et al. (2020) estimated the global CH<sub>4</sub> budget by forward-model simulations and mass balance method and estimated that a 1 % change in OH levels could lead to an annual mean difference of ~ 4 Tg yr<sup>-1</sup> in the optimized emissions, consistent with our top-down estimates. We cited in Section 3.1.1 (L334-336):

“Where a  $1 \times 10^5$  molec cm<sup>-3</sup> (1%) increase in [OH]<sub>GM-CH<sub>4</sub></sub> will increase the top-down estimated CH<sub>4</sub> emissions (EMIS<sub>CH<sub>4</sub></sub>) by 40.4 Tg yr<sup>-1</sup>, consistent with that given by He et al. (2020) using full-chemistry modeling and a mass balance approach.”

Holmes et al. ACP (2013), Murray et al. ACP (2014), Gaubert et al. (2017), Nguyen et al. (2020) analyzed the factors controlling OH variability, we cited them in the conclusions and discussion (L692-L698):

”The trend and interannual variations of tropospheric OH burden are determined by both precursor emissions from anthropogenic and natural sources and climate change (Murray et al., 2014; Holmes et al., 2013). Based on satellite observations, Gauber et al. (2017) estimated that ~20% decrease in atmospheric CO concentrations during 2002-2013 led to an ~8% increase in atmospheric [OH]. The El Niño-Southern Oscillation (ENSO) has been proven to impact the tropospheric OH burden and CH<sub>4</sub> lifetime mainly through changes in biomass burning from CO

(Nicely et al., 2020; Nguyen et al, 2020) and in NO emission from lightning (Murray et al., 2013; Turner et al., 2018).”

We also cited Prather et al. (2012) and Prather et al. (2017):

L85: “resulting in a chemical lifetime of ~9 years for tropospheric CH<sub>4</sub> (Prather et al., 2012; Naik et al., 2013).”

L86-L88: “However, accurate estimation of [OH] magnitude, distributions, and year-to-year variations needed for CH<sub>4</sub> emission optimizations are still pending (Prather et al., 2017; Turner et al., 2019).”

And in the conclusions and discussion (L729-L731):

“In addition, as suggested by Prather et al. (2017), the OH inversion would benefit from including in their prior data the responses of [OH] to variations of the precursor emissions (e.g. biomass burning and lightning) using the uncertainties estimated by 3D models.”

We added the following references:

McNorton, J., Wilson, C., Gloor, M., Parker, R. J., Boesch, H., Feng, W., Hossaini, R., and Chipperfield, M. P.: Attribution of recent increases in atmospheric methane through 3-D inverse modelling, *Atmos. Chem. Phys.*, 18, 18149-18168, 10.5194/acp-18-18149-2018, 2018.

Holmes, C. D., Prather, M. J., Søvde, O. A., and Myhre, G.: Future methane, hydroxyl, and their uncertainties: key climate and emission parameters for future predictions, *Atmospheric Chemistry and Physics*, 13, 285-302, 10.5194/acp-13-285-2013, 2013.

Gaubert, B., Worden, H. M., Arellano, A. F. J., Emmons, L. K., Tilmes, S., Barré J., Martínez Alonso, S., Vitt, F., Anderson, J. L., Alkemade, F., Houweling, S., and Edwards, D. P.: Chemical

Feedback From Decreasing Carbon Monoxide Emissions, *Geophysical Research Letters*, 44, 9985-9995, 10.1002/2017gl074987, 2017.

Nguyen, N. H., Turner, A. J., Yin, Y., Prather, M. J., and Frankenberg, C.: Effects of Chemical Feedbacks on Decadal Methane Emissions Estimates, *Geophysical Research Letters*, 47, e2019GL085706, 10.1029/2019gl085706, 2020.

He, J., Naik, V., Horowitz, L. W., Dlugokencky, E., and Thoning, K.: Investigation of the global methane budget over 1980–2017 using GFDL-AM4.1, *Atmos. Chem. Phys.*, 20, 805-827, 10.5194/acp-20-805-2020, 2020.

Murray, L. T., Logan, J. A., and Jacob, D. J.: Interannual variability in tropical tropospheric ozone and OH: The role of lightning, *Journal of Geophysical Research: Atmospheres*, 118, 11,468-411,480, 10.1002/jgrd.50857, 2013.

Murray, L. T., Mickley, L. J., Kaplan, J. O., Sofen, E. D., Pfeiffer, M., and Alexander, B.: Factors controlling variability in the oxidative capacity of the troposphere since the Last Glacial Maximum, *Atmospheric Chemistry and Physics*, 14, 3589-3622, 10.5194/acp-14-3589-2014, 2014.

Prather, M. J., Holmes, C. D., and Hsu, J.: Reactive greenhouse gas scenarios: Systematic exploration of uncertainties and the role of atmospheric chemistry, *Geophysical Research Letters*, 39, L09803, doi:10.1029/2012GL051440, 2012.

Prather, M. J., and Holmes, C. D.: Overexplaining or underexplaining methane's role in climate change, *Proceedings of the National Academy of Sciences*, 114, 5324-5326, 10.1073/pnas.1704884114, 2017.

Nicely, J. M., Duncan, B. N., Hanisco, T. F., Wolfe, G. M., Salawitch, R. J., Deushi, M., Haslerud, A. S., Jöckel, P., Josse, B., Kinnison, D. E., Klekociuk, A., Manyin, M. E., Maréchal, V., Morgenstern, O., Murray, L. T., Myhre, G., Oman, L. D., Pitari, G., Pozzer, A., Quaglia, I., Revell, L. E., Rozanov, E., Stenke, A., Stone, K., Strahan, S., Tilmes, S., Tost, H., Westervelt, D. M., and Zeng, G.: A machine learning examination of hydroxyl radical differences among model simulations for CCMI-

1, *Atmos. Chem. Phys.*, 20, 1341-1361, 10.5194/acp-20-1341-2020, 2020.

Zhao, Y., Saunio, M., Bousquet, P., Lin, X., Berchet, A., Hegglin, M. I., Canadell, J. G., Jackson, R. B., Deushi, M., Jöckel, P., Kinnison, D., Kirner, O., Strode, S., Tilmes, S., Dlugokencky, E. J., and Zheng, B.: On the role of trend and variability of hydroxyl radical (OH) in the global methane budget, *Atmos. Chem. Phys. Discuss.*, 2020, 1-28, 10.5194/acp-2020-308, 2020.

**Other references were already cited in the previous version of the paper.**

2.3 Very difficult to follow The paper is filled with jargon and abbreviations. For example, nearly half of the text in Lines 440-452 are acronyms or parenthetical expressions interjecting things. This was very hard to follow as a reader.

**Response: the jargon and abbreviations are mainly used in the 3.2, we reduced the jargon and abbreviations used in this section and organize sentences in the text.**

*Reply to SCI: ' Important evidence to importance of OH but it can have more impact' '*

**Comments:** This study provides important evidence to the importance of improving our estimates of the tropospheric OH sink in order to accurately quantify the CH<sub>4</sub> budget. However, I believe that there are three main aspects of this study that could make this study have a much stronger impact:

**Response: We thank Tonatiuh Guillermo Nuñez Ramirez for the helpful comments. Please see our itemized responses below.**

**Comments:** 1. The study found the largest absolute OH induced differences for Inv1 over northern South America, South Asia and China and at gridcell level over South America, Central Africa, East and South Asia, and mainly for wetlands, and agriculture and waste. While, it is already explained that the distribution of sampling stations is one of the reasons for this. This and further reasons for the larger uncertainty in the Tropics were discussed in detail in Bousquet et al., 2011 (another paper from this group which I think should be referenced at that point in the paper). Furthermore, there are not only less sensitivity to observations in the Tropics, but also larger uncertainty in the fluxes. As a consequence, the inversion fits in everything in the Tropics which is too costly to accommodate elsewhere. Unfortunately, the Tropics is also the region where most of the OH reaction occurs. Therefore, it is very difficult to make conclusions on how the estimation of Tropical fluxes is affected by the OH assumptions on a regional level. I believe the study is missing either one more scenario where the uncertainties for each source are uniform globally, e.g. 5 nmol m<sup>-2</sup> s<sup>-1</sup> for wetlands (if there are wetland emissions in the gridcell), and/or include the analysis of the uncertainty reduction and posterior correlations, to determine how well resolved are these regions.

**Response: We discussed the impact of the distribution of the sampling stations in the text (L407-415):**

**”The uncertainties in the top-down estimated regional emissions are not only due to inter-model**

differences of the regional OH fields but also rely on the distribution of the surface observations used in the inversions. Over the regions with large prior emissions but less constrained by observations (e.g. South America, South Asia, and China), our OH analysis leads to larger uncertainties than regions that are well constrained by observations (e.g. the North America and Canada) (Fig. S3). The results may indicate that on the regional scale, the top-down estimated CH<sub>4</sub> emissions and the uncertainties lead by OH are specific to the observation system retained. If more surface observations (e.g. in the southern hemisphere) or satellite columns with a more even global coverage were included in our inversions, spatial patterns of the top-down estimated CH<sub>4</sub> emissions and their uncertainties (as shown by Fig.3) could be different.”

We acknowledge the fact that more scenarios could provide additional conclusions but this would necessitate extensive additional work and the paper is already long. Here this study aims to quantify the uncertainties in the current top-down due to uncertainties in OH. Analysis of how the top-down inversion can resolve the regional emissions by testing the uncertainty reduction and posterior correlations can be a separate study in our further study. However, we thank you for the suggestion and keep the idea for future works.

**Comments: 2.** The main goal of using an inversion is to find the fluxes that best explain the observations. However, we do not get to see how well the observations are fitted by the inversions with the different OH fields. Therefore, we cannot evaluate which features of the different OH distributions are realistic. By knowing for example the spatial distribution of the residuals, or of the correlations between posterior mixing ratio and observations, we can evaluate if certain spatial patterns are realistic. Also the use of aircraft profiles for validation, e.g. over the Amazon (Miller et al., 2007, Beck et al., 2012, Gatti et al., 2015, Basso et al., 2016), Asia (Brenninkmeijer et al., 2007, Baker et al., 2012, Schuck et al., 2010) or across latitudinal transects (e.g. Wofsy, 2011 and Schuck et al., 2012) could provide information on the

realism of the vertical distribution. During the period of the simulation, there were two satellites sensors available SCIAMACHY and IASI with distinctly different sensitivities. SCIAMACHY is more sensitive to the surface, while IASI to the upper troposphere. Using this, it may be possible to say something about how realistic is both the horizontal and vertical distribution.

**Response:**

**In the updated version, we evaluate the inversions using aircraft observations. Usually, one can use the surface observations to evaluate the inversions using satellite data but we do not use satellite data to evaluate the inversions using surface observations. Comparison can still be made but (i) the observations from IASI do not provide the averaging kernel, thus they cannot directly compare with model simulations, and (ii) SCIAMACHY CH<sub>4</sub> data experience significant to large systematic errors, limiting strongly the interest of comparison.**

**We added in the text (L284-L296):**

**“We evaluate the optimized CH<sub>4</sub> emissions by comparing the simulated CH<sub>4</sub> mixing ratios using prior and posterior CH<sub>4</sub> emissions with independent measurements from the NOAA/ESRL Aircraft Project. The location of the observation site (Table S1) and the vertical profile of the model bias in CH<sub>4</sub> mixing ratios compared with the aircraft observations (model minus observations) are shown in the supplement (Fig. S4a for Inv1 and Fig. S4b for Inv2). The comparisons with independent aircraft observations confirm the improvement of model-simulated CH<sub>4</sub> mixing ratios when using posterior emissions. All of the inversions in Inv1 and Inv2 reach small biases when compared with aircraft observations (right panel of Fig.S4a and Fig.S4b), which means that it is hard to distinguish which OH spatial and vertical distributions are more realistic in terms of quality of fit to these aircraft CH<sub>4</sub> observations. For Inv1, the root mean square errors ( $RMSE = \frac{\sqrt{\sum(model-observation)^2}}{n\_obs}$ , n\_obs is the number of observations) are reduced from up to more than 100ppbv (prior) emissions**

to ~10ppbv (posterior). For Inv2, although the CH<sub>4</sub> mixing ratios simulated using prior emissions already match well with aircraft observations (MSE=8-17ppbv), the posterior emissions still reduce the RMSE by up to 10ppbv.”

We added Table S1 and Figure S4a and Figure 4b in the supplement:

**Table S1. Location of the NOAA ESRL aircraft sites.**

<b>STATION ID</b>	<b>SITE LOCATION</b>	<b>BOTTOM ALT(m)</b>	<b>TOP ALT(m)</b>	<b>latitude</b>	<b>longitude</b>
CAR	Briggsdale, Co	1658	11879	40° 22' N	104° 17' W
HAA	Molokai Island, HI	305	8104	21° 14' N	158° 57' W
HFM	Harvard Forest, Ma	582	8063	42° 32' N	72° 10' W
PFA	Poker Flat, AK	131	7604	65° 04' N	147° 17' W

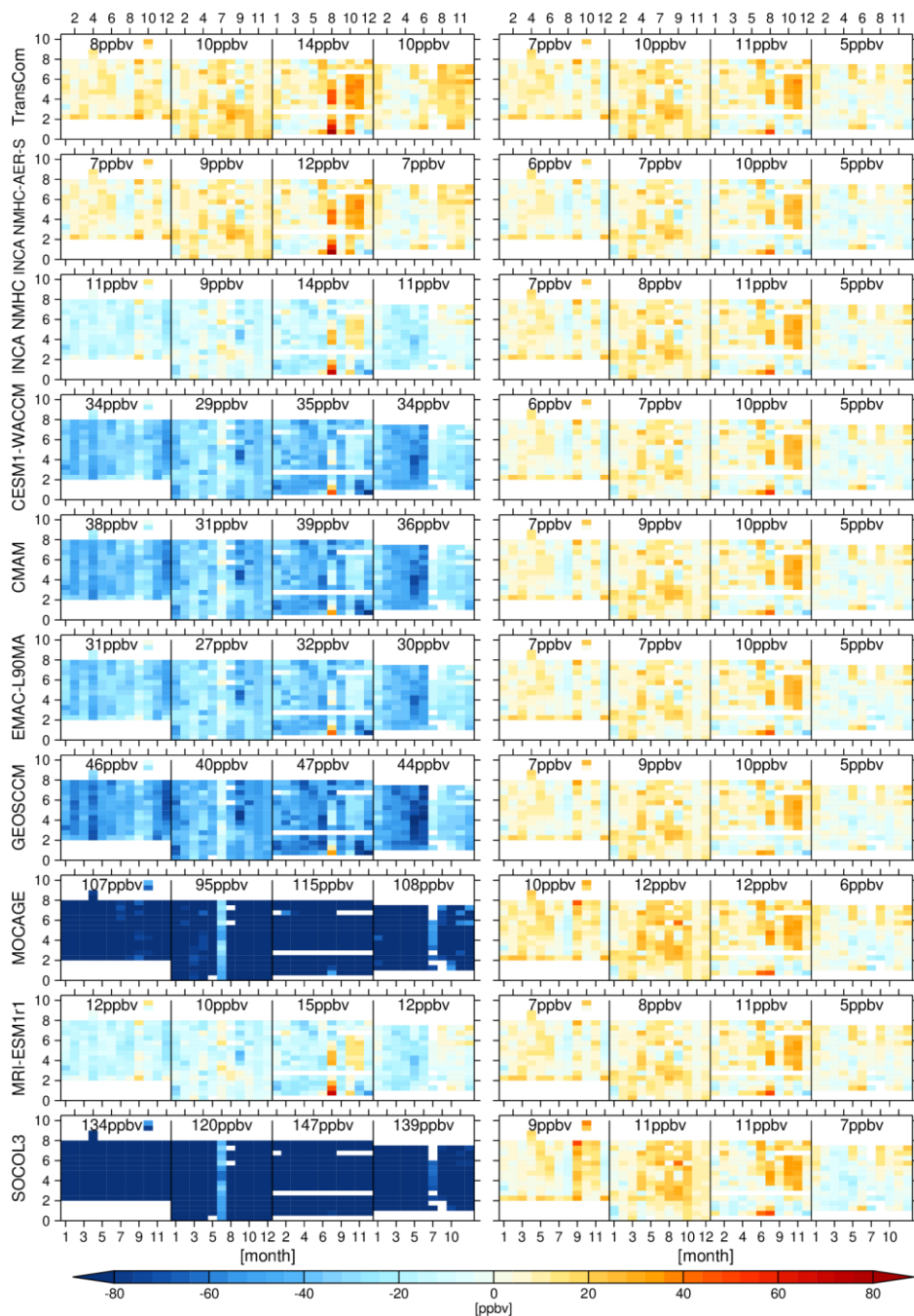


**Figure S4a.** The vertical profiles of the bias in LMDz simulated monthly CH<sub>4</sub> mixing ratios compare with measurements from the NOAA/ESRL Aircraft Project (model — observations) during 2000/7-2002/6. The left panels show the bias simulated by prior emissions with 10 original OH fields and the right panels show the bias simulated by corresponding posterior emissions from Inv1. The root mean square errors

(RMSE =  $\frac{\sqrt{\sum(model-observation)^2}}{n_{obs}}$ ) are shown inset.

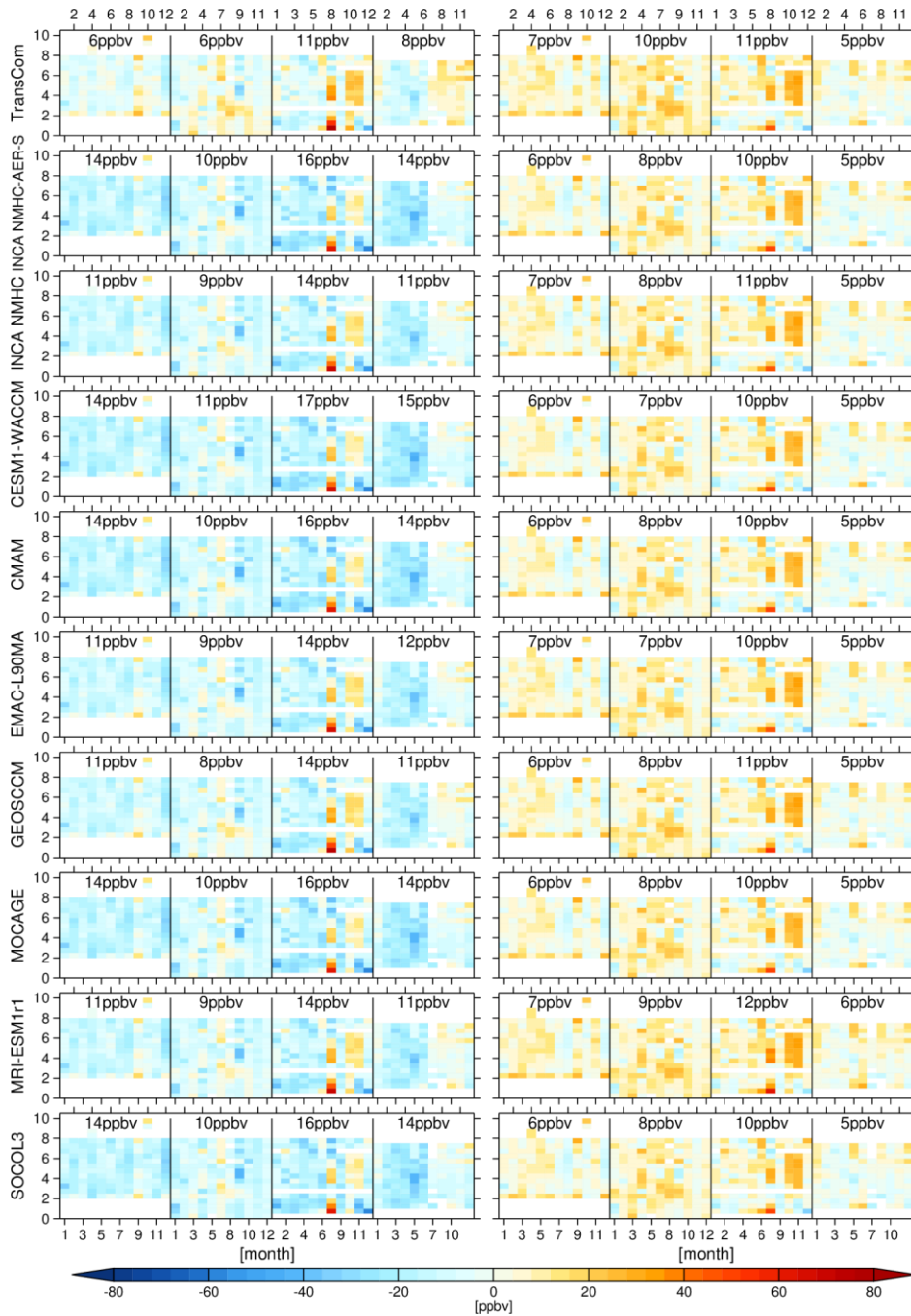


**Figure S4b.** The same as figure S3a but for Inv2.

**Comments:** 3. Link to the validation, there is little discussion on the features of the OH fields provided by the models. For example, Patra et al., (2015) determine that observations of CH<sub>3</sub>CCl<sub>3</sub> support a N/S gradient of 1, so more should be done to explain how probable bias in the modeled OH distributions affects the CH<sub>4</sub> estimations. Also many of the different features in the spatial distributions OH are caused by known biases in the climate chemistry models, e.g. the NMVOC levels, the CO burden, CO biases, O<sub>3</sub> biases (e.g. Naik et al. 2013, Shindell et al., 2006). Here, it would be very interesting to see, for example, if there is a relationship between the N/S ratio of the OH distributions and the N/S ratio of the posterior fluxes (similar to figure 2). Also why are SOCOL3 and MOCAGE such outliers?

**Response:** We have evaluated the impact of the uncertainties in OH spatial distribution by conducting Inv2. For the relationship between the N/S ratio of the OH and N/S ratio of the posterior fluxes, we have stated in the text (L369-371):” The TransCom OH field, for which OH N/S ratio is 1.0, leads to an inter-hemispheric CH<sub>4</sub> emission difference of 205Tg yr<sup>-1</sup>, which is 35Tg yr<sup>-1</sup> (27Tg yr<sup>-1</sup>) smaller than the mean (minimum) inter-hemispheric difference calculated using other OH fields with OH N/S ratio of 1.2-1.3.” We don’t think it will be helpful if we further estimate the correlation between the N/S ratio of OH and fluxes because, among the 8 OH fields analyzed here (exclude MOCAGE and SOCOL3), only one has N/S ratio of 1, five having N/S ratio of 1.2, and two of 1.3.

The explanation of SOCOL3 and MOCAGE simulating high [OH] can be found in Zhao et al. (2019) and we added in section 3.1.1 (L310-L314):

” The high [OH]<sub>GM-CH<sub>4</sub></sub> simulated by SOCOL3 and MOCAGE are mainly due to high surface and mid-tropospheric NO mixing ratio simulated by these two models (Zhao et al., 2019). As analyzed in Zhao et al. (2019), the lack of N<sub>2</sub>O<sub>5</sub> heterogeneous hydrolysis (by both SOCOL3 and MOCAGE) and the overestimation of tropospheric NO production by NO<sub>2</sub> photolysis (by SOCOL3) are the

**major factors behind the overestimation of NO and OH.”**

**Comments:** We are shown inversions with and without interannual variability in the OH fields. However, due to the increase of tropospheric temperatures, even in the simulations with fixed OH or the fields distributed in the TRANSCOM-CH<sub>4</sub> experiment, the lifetime of CH<sub>4</sub> will decrease. This effect is not quantified in the paper unless I missed it.

**Response: Indeed, temperature changes will impact the CH<sub>4</sub> lifetime but we do not test the impact of this effect here.**

**Comments:** As stated in the study, the transport model uncertainty is very large. This means that the distribution of CH<sub>4</sub> is model dependent. Therefore, there could be a large uncertainty in the global OH means weighted by the CH<sub>4</sub> reaction. I believe an air mass or volume weighted OH means should be at least provided in the supplement and that the comparison with box models or with other models should be done with air mass or volume weighted means, including the relationship in figure 2.

**Response: The air mass-weighted [OH] is already given in table 1 and volume-weighted OH was given by Zhao et al. (2019).**

**We added in section 2.1 (L170):” The volume-weighted [OH] was given by Zhao et al. (2019).”**

**For the relationship in Figure 2, the air mass-weighted and volume-weighted [OH] do not show a linear relationship with optimized CH<sub>4</sub> emissions since some OH field shows distinct vertical variations. For example, the air mass and volume-weighted [OH] simulated by CMAM model ( $11.3 \times 10^5$  molec cm<sup>-3</sup> and  $10.4 \times 10^5$  molec cm<sup>-3</sup>) is smaller than simulated by EMAC-L90MA model ( $11.5 \times 10^5$  molec cm<sup>-3</sup> and  $11.1 \times 10^5$  molec cm<sup>-3</sup>), but the top-down inversions using CMAM OH field estimated larger CH<sub>4</sub> emissions ( $599\text{Tg yr}^{-1}$ ) than that using EMAC-L90MA OH fields ( $589\text{Tg yr}^{-1}$ ).**

**Comments:** On which basis did you choose only 7 of the 20 CCMi simulations?

**Response:** The same reasons explained in Zhao et al. (2019) as we explained it in section 2.1.

**Comments:** You mentioned the TRANSCOM-2011 project. However, this was actually known as the TRANSCOM-CH4 (Patra et al., 2011), since there have been several TRANSCOM projects mainly with CO<sub>2</sub>. It might be useful to mention, that in Patra et al., (2011), the OH fields from Spivakovsky (2000).

**Response:** We corrected TRANSCOM-2011 to TRANSCOM-CH4.

**We have already mentioned this in Sect 2.1.1 (L161-L163):**

**“We also include the climatological OH field used in the TransCom simulations (Patra et al., 2011), which uses the semi-empirical, observation-based OH field computed by Spivakovsky et al. (2000) in the troposphere”**

**Comments:** Table 1 and Table 2 are missing the units

**Response:** We added the units, thank you very much.

**Comments:** Could you specify which convection parameterization is used? In Locatelli et al., (2015) three parameterizations are used.

**Response:** We added in the text(L226):

**“The deep convection is parametrized based on the Tiedtke (1989) scheme.”**

**We added in the reference: “Tiedtke, M.: A Comprehensive Mass Flux Scheme for Cumulus Parameterization in Large-Scale Models, Monthly Weather Review, 117, 1779-1800, 10.1175/1520-0493(1989)117<1779:acmfsf>2.0.co;2, 1989.”**

**Comments:** I think that at least in the supplements you should include the maps of the mean differences

between the scenarios, e.g. Echangeall;Echange ixoh;Echangevaroh:

**Response:** Thank you very much for the suggestion. Here we mainly analyzed the regional emission changes for the large emitting regions follow Saunio et al. (2016; 2017) and Locatelli et al. (2013). The differences in emission changes on the grid-scale cannot be well resolved by the global inversions with limited surface observations so it is not analyzed here and we prefer to only provide results aggregated at the regional scale. Analysis of the impact of OH top-down emission changes on grid-scale belongs to future studies doing regional inversions using more dense observation networks (e.g. satellite).

**Comments:** In figures 4 and 5, would it be possible to show the a priori uncertainties as error bars? In general I find the double axes confusing and maybe a single axis with absolute emissions would be better.

**Response:** Thank you very much for the suggestion. The prior uncertainties are 100% of the prior emissions (see Section 2.2). So it is the same as the prior emissions which limit the interest to show them in the figure.

We agree that showing the absolute value will be easier to understand. But the aim of Fig. 4 and Fig.5 is to show the uncertainties due to OH. Showing absolute emissions (0-100Tg yr<sup>-1</sup>) will make it difficult to recognize the spread among different inversions (<20Tg yr<sup>-1</sup> or even <5Tg yr<sup>-1</sup>), which is the purpose of this figure.

# **Influences of hydroxyl radicals (OH) on top-down estimates of the global and regional methane budgets**

5 Yuanhong Zhao<sup>1</sup>, Marielle Saunois<sup>1</sup>, Philippe Bousquet<sup>1</sup>, Xin Lin<sup>1,a</sup>, Antoine Berchet<sup>1</sup>, Michaela I. Hegglin<sup>2</sup>, Josep G. Canadell<sup>3</sup>, Robert B. Jackson<sup>4</sup>, Edward J. Dlugokencky<sup>5</sup>, Ray L. Langenfelds<sup>6</sup>, Michel Ramonet<sup>1</sup>, Doug Worthy<sup>7</sup>, and Bo Zheng<sup>1</sup>

<sup>1</sup> Laboratoire des Sciences du Climat et de l'Environnement, LSCE-IPSL (CEA-CNRS-UVSQ), Université Paris-Saclay, 91191 Gif-sur-Yvette, France

10 <sup>2</sup> Department of Meteorology, University of Reading, Reading, RG6 6LA, UK

<sup>3</sup> Global Carbon Project, CSIRO Oceans and Atmosphere, Canberra, Australian Capital Territory 2601, Australia

<sup>4</sup> Earth System Science Department, Woods Institute for the Environment, and Precourt Institute for Energy, Stanford University, Stanford, CA 94305, USA

15 <sup>5</sup> NOAA ESRL, 325 Broadway, Boulder, CO 80305, USA

<sup>6</sup> Climate Science Centre, CSIRO Oceans and Atmosphere, Aspendale, Victoria 3195, Australia

<sup>7</sup> Environment and Climate Change Canada, Toronto, M3H 5T4, Canada

<sup>a</sup> now at: Climate and Space Sciences and Engineering, University of Michigan, Ann Arbor, MI 48109, USA

20

## Abstract

The hydroxyl radical (OH), which is the dominant sink of methane (CH<sub>4</sub>), plays a key role to close the global methane budget. Current top-down estimates of the global and regional CH<sub>4</sub> budget using 3D models usually apply prescribed OH fields and attribute model-observation mismatches almost exclusively to CH<sub>4</sub> emissions, leaving the uncertainties due to prescribed OH field less quantified. Here, using a variational Bayesian inversion framework and the 3D chemical transport model LMDz, combined with 10 different OH fields derived from chemistry-climate models (CCMI experiment), we evaluate the influence of OH burden, spatial distribution, and temporal variations on the global and regional CH<sub>4</sub> budget. The global tropospheric mean CH<sub>4</sub>-reaction-weighted [OH] ([OH]<sub>GM-CH<sub>4</sub></sub>) ranges 10.3-16.3 × 10<sup>5</sup> molec cm<sup>-3</sup> across 10 OH fields during the early 2000s, resulting in inversion-based global CH<sub>4</sub> emissions between 518 and 757 Tg yr<sup>-1</sup>. The uncertainties in CH<sub>4</sub> inversions induced by the different OH fields are similar to the CH<sub>4</sub> emission range estimated by previous bottom-up syntheses and larger than the range reported by the top-down studies. The uncertainties in emissions induced by OH are largest over South America, corresponding to large inter-model differences of [OH] in this region. From the early to the late 2000s, the optimized CH<sub>4</sub> emissions increased by 21.9 ± 5.7 Tg yr<sup>-1</sup> (16.6-30.0 Tg yr<sup>-1</sup>), of which ~25% (on average) offsets the 0.7% (on average) increase in OH burden. If the CCMI models represent the OH trend properly over the 2000s, our results show that a higher increasing trend of CH<sub>4</sub> emissions is needed to match the CH<sub>4</sub> observations compared to the CH<sub>4</sub> emission trend derived using constant OH. This study strengthens the importance to reach a better representation of OH burden and of OH spatial and temporal distributions to reduce the uncertainties on the global and regional CH<sub>4</sub> budgets.

## 1 Introduction

45 Methane (CH<sub>4</sub>) plays an important role in both climate change and air quality as a major greenhouse gas and tropospheric ozone precursor (Ciais et al., 2013). CH<sub>4</sub> is emitted from various anthropogenic sources including agriculture, waste, fossil fuel, and biomass burning, as well as natural sources including wetlands and other freshwater systems, geological sources, termites, and wild animals. CH<sub>4</sub> is removed from the atmosphere mainly by reaction with hydroxyl radical (OH) (Saunois et al. 2016, 2017).  
50 Tropospheric CH<sub>4</sub> levels have more than doubled between the 1850s and present-day (Etheridge et al., 1998) in response to anthropogenic emissions and climate variabilities, leading to about 0.62 W m<sup>2</sup> radiative forcing (Etminan et al., 2016) and increases in tropospheric ozone levels of ~5 ppbv (Fiore et al., 2008). The global CH<sub>4</sub> atmospheric mixing ratio stabilized in the early 2000s but resumed growing at a rate of ~5ppbv yr<sup>-1</sup> or more since 2007 (Dlugokencky, NOAA/ESRL, 2019).

55

Explaining the CH<sub>4</sub> stabilization and renewed growth requires an accurate estimation of the CH<sub>4</sub> budget and its evolution, as the source-sink imbalance that is responsible for the contemporary CH<sub>4</sub> yearly growth only accounts for 3% of the total CH<sub>4</sub> burden (Turner et al., 2019). To reconcile the uncertainties in the current estimation of CH<sub>4</sub> emissions from various sources, the Global Carbon Project integrates top-down  
60 and bottom-up approaches (Kirschke et al. 2013; Saunois et al., 2016; 2017; 2019). However, gaps remain in global and regional CH<sub>4</sub> emissions estimated by top-down and bottom-up approaches, as well as within each approach (Kirschke et al. 2013; Saunois et al., 2016; Bloom et al., 2017). The top-down method, which optimizes emissions by assimilating observations in an atmospheric inversion system, is expected to reduce uncertainties of bottom-up estimates. Among the remaining causes of uncertainties in the global  
65 methane budget, the representation of CH<sub>4</sub> sinks, mainly from OH oxidation, is one of the largest, as seen by process-based models for atmospheric chemistry (Saunois et al., 2017).

OH is the most important tropospheric oxidizing agent determining the lifetime of many pollutants and

greenhouse gases including CH<sub>4</sub> (Levy, 1971). A small perturbation of OH can result in significant changes in the budget of atmospheric CH<sub>4</sub> (Turner et al., 2019). At the global scale, tropospheric OH is mainly produced by the reaction of excited oxygen atoms (O(<sup>1</sup>D)) with water vapor (primary production) but also by the reaction of nitrogen oxide (NO) and ozone (O<sub>3</sub>) with hydroperoxyl radicals (HO<sub>2</sub>) and organic peroxy radicals (RO<sub>2</sub>) (secondary production). At regional scales, photolysis of hydrogen peroxide and oxidized VOC photolysis can be important depending on the chemical environment (Lelieveld et al. 2016). OH is rapidly removed by carbon monoxide (CO), methane (CH<sub>4</sub>), and non-methane volatile organic compounds (NMVOCs) (Logan et al., 1981; Lelieveld et al., 2004). Tropospheric OH has a very short lifetime of a few seconds (Logan et al., 1981; Lelieveld et al., 2004), hindering estimates of global OH concentrations ([OH]) through direct measurements and limiting our ability to estimate the global CH<sub>4</sub> sink.

Global tropospheric [OH] is approximately  $1 \times 10^6$  molec cm<sup>-3</sup> as calculated by atmospheric chemistry models (Naik et al., 2013; Voulgarakis et al., 2013, Zhao et al., 2019) and inversions of 1-1,1-trichloroethane (methyl chloroform, MCF) (Prinn et al., 2001; Bousquet et al., 2005; Montzka et al., 2011; Cressot et al., 2014), resulting in a chemical lifetime of ~9 years for tropospheric CH<sub>4</sub> (Prather et al., 2012; Naik et al., 2013). However, accurate estimation of [OH] magnitude, distributions, and year-to-year variations needed for CH<sub>4</sub> emission optimizations are still pending (Prather et al., 2017; Turner et al., 2019). For global tropospheric [OH], both MCF inversions and atmospheric chemistry model inter-comparisons give a 10%-15% uncertainty (Prinn et al., 2001; Bousquet et al., 2005; Naik et al., 2013; Zhao et al., 2019). For [OH] spatial distributions, MCF-based inversions generally infer similar mean [OH] over both hemispheres (Bousquet et al., 2005; Patra et al., 2014), while atmospheric chemistry models generally give [OH] Northern hemisphere to Southern hemisphere (N/S) ratios above 1 (e.g. Naik et al., 2013; Zhao et al., 2019). For [OH] year-to-year variations, some studies have estimated magnitudes significant enough to help explain part of the stagnation in atmospheric CH<sub>4</sub> concentrations during the

early 2000s (Rigby et al., 2008; McNorton et al., 2016; Dalsøren et al., 2016; Rigby et al., 2017; Turner  
95 et al., 2017), whereas others show smaller trends and inter-annual variations of [OH] (Montzka et al., 2011;  
Naik et al., 2013; Voulgarakis et al., 2013; Zhao et al., 2019). In a recent study, Zhao et al. (2019)  
simulated atmospheric CH<sub>4</sub> with an ensemble of OH fields and showed that uncertainties in [OH]  
variations could explain up to 54% of model-observation discrepancies in surface CH<sub>4</sub> mixing ratio  
changes from 2000 to 2016.

100

Current top-down estimates of the global CH<sub>4</sub> budget usually apply prescribed and constant [OH]  
simulated by atmospheric chemistry models and attribute model-observation mismatches exclusively to  
CH<sub>4</sub> emissions (Saunois et al., 2017). However, the OH fields simulated by atmospheric chemistry models  
show some uncertainties in both global burden and spatial-temporal variations (Naik et al., 2013; Zhao et  
105 al., 2019). The role of OH variations on the top-down estimates of CH<sub>4</sub> emissions has been evaluated  
using two box-model inversions with surface observations (e.g. Rigby et al., 2017; Turner et al., 2017,  
Naus et al., 2019) and 3D models that optimize CH<sub>4</sub> emissions together with [OH] by assimilating surface  
observations (Bousquet et al., 2006) or satellite data (Cressot et al., 2014, McNorton et al., 2018; Zhang  
et al., 2018; Maasakkers et al., 2019). The proxy-based constraints usually optimize [OH] on a global or  
110 latitudinal scale, the impact of OH vertical and horizontal distributions being less quantified to date. Also,  
proxy methods do not allow to access underlying processes as direct chemistry modeling (Zhao et al.,  
2019). This paper follows the work of Zhao et al. (2019), where we analyzed in details 10 OH fields  
derived from atmospheric chemistry models considering different chemistry, emissions, and dynamics  
(Patra et al., 2011; Szopa et al., 2013; Hegglin and Lamarque, 2015; Morgenstern et al., 2017; Zhao et al.,  
115 2019; Terrenoire et al., 2019). We now aim to build on this previous paper to estimate the impact of these  
OH fields on methane emissions as inferred by an atmospheric 4D variational inversion system. To do so,  
we use each of the OH fields in the 4D variational inversion system PYVAR-LMDz based on LMDZ-  
SACS (Laboratoire de Mééorologie Dynamique model with Zooming capability-Simplified Atmospheric

Chemistry System) 3D chemical transport model to evaluate the influence of OH distributions and variations on the top-down estimated global and regional CH<sub>4</sub> budget. Section 2 briefly describes the OH fields and their characteristics and underlying processes (see also Zhao et al., 2019 for more details), the inversion method, and the setups of inversion experiments. Section 3 illustrates the influence of OH on the top-down estimation of CH<sub>4</sub> budgets and variations, specifically: i) global, regional, and sectoral CH<sub>4</sub> emissions (Section 3.1), ii) emission changes between the early 2000s and late 2000s (Section 3.2), and iii) year-to-year variations in methane emissions (Section 3.3). Section 4 summarizes the results and discusses the impact of OH on the current CH<sub>4</sub> budget.

## 2 Method

### 2.1 OH fields

In this study, we test the 10 OH fields presented in by Zhao et al. (2019), including 7 OH fields simulated by chemistry-transport and chemistry-climate models from Phase 1 of the Chemistry-Climate Model Initiative (CCMI) (Hegglin and Lamarque, 2015; Morgenstern et al., 2017), 2 OH fields simulated by the Interaction with Chemistry and Aerosols (INCA) model coupled to the general circulation model of the Laboratoire de Météorologie Dynamique (LMD) model (Hauglustaine et al., 2004; Szopa et al., 2013), and 1 OH field from the TRANSCOM-CH<sub>4</sub> inter-comparison exercise (Patra et al., 2011)(Table 1).

The CCMI project conducted simulations with 20 state-of-the-art atmospheric chemistry-climate and chemistry-transport models to evaluate the model's projections of atmospheric composition (Hegglin and Lamarque, 2015; Morgenstern et al., 2017). To force atmospheric inversions during 2000-2010, we use OH fields from 7 of the 20 CCMI model simulations of REF-C1 experiments (Table 1), which were driven by observed sea surface temperatures and state-of-the-art historical forcings (covering 1960-2010). For the inversions after 2010 (only with the CESM1-WACCM model, see Section 2.3), we apply inter-annual variations of OH generated from REF-C2 experiments, which were driven by sea surface conditions

calculated by the online-coupled ocean and sea ice modules. Although all of the CCMi models use the  
145 same anthropogenic emission inventories, the simulated OH fields show different spatial and vertical  
distributions. The inter-model differences of OH burden and vertical distributions are mainly attributed  
to differences in chemical mechanisms related to NO production and loss. The differences in [OH] spatial  
distributions are due to applying different natural emissions: for example, primary biogenic VOC  
emissions and NO emissions from soil and lightning (Zhao et al., 2019). As a result, the regions dominated  
150 by natural emissions (e.g. South America, central Africa) show the largest inter-model differences in [OH]  
(Fig.S1). The CCMi models consistently simulated positive OH trend during 2000-2010, mainly due to  
more OH production by NO than loss by CO over the East and Southeast Asia and positive trend of water  
vapor over the tropical regions (Zhao et al., 2019; Nicely et al., 2020). More details can be found in Zhao  
et al. (2019) and the herein cited literature.

155  
The two INCA OH fields, INCA NMHC-AER-S and INCA NMHC are simulated by two different  
versions of the INCA (Interaction with Chemistry and Aerosols) chemical model coupled to LMDz  
(Szopa et al., 2013; Terrenoire et al., 2019). The main difference between the two simulations is that INCA  
NMHC-AER-S includes both gas-phase and aerosol chemistry in the whole atmosphere while INCA  
160 NMHC only includes gas-phase chemistry in the troposphere (Szopa et al., 2013; Terrenoire et al., 2019).  
We also include the climatological OH field used in the TransCom simulations (Patra et al., 2011), which  
uses the semi-empirical, observation-based OH field computed by Spivakovsky et al. (2000) in the  
troposphere.

165 Table 1 summarizes the global tropospheric mean CH<sub>4</sub>-reaction-weighted [OH] ([OH]<sub>GM-CH<sub>4</sub></sub>, [OH]  
weighted by reaction rate of OH with CH<sub>4</sub> ( $K_{OH+CH_4}$ ) × dry air mass, Lawrence et al., 2001) and dry air  
mass-weighted [OH] ([OH]<sub>GM-M</sub>), as well as inter-hemispheric ratios (N/S ratios) calculated with [OH]<sub>GM-  
CH<sub>4</sub></sub> for the 10 OH fields used in this study. The tropopause height is assumed at 200hPa following Naik

et al. (2013) and the 3D temperature field used to compute  $[\text{OH}]_{\text{GM-CH}_4}$  is from ERA Interim re-analysis meteorology data (Dee et al, 2011). The volume-weighted  $[\text{OH}]$  was given by Zhao et al. (2019). The  $[\text{OH}]_{\text{GM-CH}_4}$  is a better indicator of the global atmospheric oxidizing efficiency for  $\text{CH}_4$  than  $[\text{OH}]_{\text{GM-M}}$  since the latter is insensitive to the  $\text{CH}_4+\text{OH}$  reaction rate increased with temperature (Lawrence et al., 2001). Both the mean value ( $12.3 \pm 3.8 \times 10^5 \text{ molec cm}^{-3}$ ) and absolute range ( $10.3\text{-}16.3 \times 10^5 \text{ molec cm}^{-3}$ ) of  $[\text{OH}]_{\text{GM-CH}_4}$  calculated for the 10 OH fields are larger than those of  $[\text{OH}]_{\text{GM-M}}$  ( $11.4 \pm 2.8 \times 10^5 \text{ molec cm}^{-3}$  and  $9.4\text{-}14.4 \times 10^5 \text{ molec cm}^{-3}$ , respectively). This is mainly because MOCAGE and SOCOL3 OH fields show much higher  $[\text{OH}]$  near the surface than in the upper troposphere (Zhao et al., 2019). The inter-hemispheric OH ratios range from 1.0 to 1.5, larger than ones derived from MCF inversions (e.g. Bousquet et al., 2005; Patra et al., 2014), partly explained by the underestimation of CO in the northern hemisphere by atmospheric chemistry models (Naik et al., 2013). A comprehensive analysis of spatial and vertical distributions of these OH fields was presented in Zhao et al. (2019).

## 2.2 Inverse method

We conduct an ensemble of variational inversions of  $\text{CH}_4$  budget that rely on Bayes' theorem (Chevallier et al., 2005) with the same set of atmospheric observations of  $\text{CH}_4$  mixing ratios but different prescribed monthly mean OH fields as described in Sect. 2.1. A variational data assimilation system optimizes  $\text{CH}_4$  emissions and sinks by minimizing the cost function  $J$ , defined as:

$$J(\mathbf{x}) = \frac{1}{2}(\mathbf{x} - \mathbf{x}^b)^T \mathbf{B}^{-1}(\mathbf{x} - \mathbf{x}^b) + \frac{1}{2}(\mathbf{H}(\mathbf{x}) - \mathbf{y})^T \mathbf{R}^{-1}(\mathbf{H}(\mathbf{x}) - \mathbf{y}) \quad (1)$$

where  $\mathbf{x}$  is the control vector that includes total  $\text{CH}_4$  emissions per 10 days at the model resolution of  $3.75^\circ$  (in longitude)  $\times 1.85^\circ$  (in latitude) and initial conditions at longitudinal and latitudinal bands of  $20^\circ \times 15^\circ$ ,  $\mathbf{x}^b$  is the prior of the control vector  $\mathbf{x}$ ;  $\mathbf{y}$  is the observation vector of observed  $\text{CH}_4$  mixing ratios, here at the surface; and  $\mathbf{H}(\mathbf{x})$  represents the sensitivity of simulated  $\text{CH}_4$  to emissions, for comparison with  $\mathbf{y}$ .  $\mathbf{B}$  and  $\mathbf{R}$  represent the prior and observation error covariance matrix, respectively. The cost

function  $J$  is minimized iteratively by the M1QN3 algorithm (Gilbert and Lemaréchal, 1989). We do not include sinks in the control vector  $\mathbf{x}$  but prescribe the different OH fields mentioned above.

195

Prior knowledge ( $\mathbf{x}^b$ ) on CH<sub>4</sub> emissions is provided by the Global Carbon Project (GCP, Saunoy et al., 2019). The GCP emission inventory includes time-varying anthropogenic and fire emissions and climatology of the natural emissions. Global total CH<sub>4</sub> emissions of the GCP inventory are 511Tg yr<sup>-1</sup> in 2000, increased to 562Tg yr<sup>-1</sup> in 2010, and 581Tg yr<sup>-1</sup> in 2016 (with soil uptake excluded). The soil uptake of CH<sub>4</sub> is estimated to be 38Tg yr<sup>-1</sup> with seasonal variations. Averaged over 2000-2016, the anthropogenic sources (including biofuel emissions, agriculture, and waste) and wetlands contribute 56% and 32% of total CH<sub>4</sub> emissions, respectively (Fig. S2). The prior information of emissions by sector in each grid cell is used to separate the total optimized CH<sub>4</sub> emissions into four broad categories: wetlands, agriculture and waste, fossil fuel, and other natural sources (biomass burning, termite, geological, and ocean emissions). The spatial distributions of the prior emissions from the four categories averaged over 2000-2016 are shown in Fig. S2. A detailed description of the GCP emission inventory can be found in Zhao et al. (2019) and Saunoy et al. (2019). The prior error of CH<sub>4</sub> fluxes is set to 100% of  $\mathbf{x}^b$ , and the error correlation is calculated with a correlation length of 500km over land and 1000km over the oceans for CH<sub>4</sub> fluxes.

200

210

The vector of observations ( $\mathbf{y}$ ) is generated from surface measurements of the World Data Centre for Greenhouse Gases (WDCGG, <https://gaw.kishou.go.jp/>) through the WMO Global Atmospheric Watch (WMO-GAW) program. The surface measurements include both continuous time series of hourly afternoon observations and flask data. In total, 97 sites are included here, covering different time periods, including 68 sites from the Earth System Research Laboratory from the U.S. National Oceanic and Atmospheric Administration (NOAA/ESRL, Dlugokencky et al. (1994)), 14 sites from the Laboratoire des Sciences du Climat et de l'Environnement (LSCE), 8 sites from Environment and Climate Change Canada (ECCC), 4 sites from the Commonwealth Scientific and Industrial Research Organisation (CSIRO,

215

Francey et al. (1999)), and 3 from the Japan Meteorological Agency (JMA: <http://www.jma.go.jp/jma/indexe.html>). The location of the sites is shown in Fig. S3.

220

Atmospheric CH<sub>4</sub> sensitivities to fluxes ( $H(x)$ ) are simulated by LMDz5B, an offline version of the LMDz atmospheric model (Locatelli et al., 2015), which has been widely used for CH<sub>4</sub> studies (e.g. Bousquet et al., 2005; Pison et al., 2009; Lin et al., 2018; Zhao et al., 2019). LMDz5B is associated with the simplified chemistry module SACS (Pison et al., 2009), which calculates the CH<sub>4</sub> chemical sink using prescribed 4D OH and O(<sup>1</sup>D) fields. The CH<sub>4</sub> sink by reaction with chlorine is not considered in our LMDz model simulations. The deep convection is parametrized based on the Tiedtke (1989) scheme. Air mass fluxes simulated by the general circulation model LMDz with temperature and wind nudged to ERA Interim re-analysis meteorology data (Dee et al, 2011) are used to force the transport of chemical tracers in LMDz5B every 3 hours.

230

### 2.3 Model experiments

As shown in Fig. 1, we performed six groups of inversions (Inv1 to Inv6, 34 inversions in total). The impacts of OH on the top-down estimation of CH<sub>4</sub> emissions are comprehensively analyzed by comparing the inversion results within one group or between two different groups. We analyze the overall impacts of differences in OH burden, spatial distribution, and temporal change on CH<sub>4</sub> emissions (colored boxes on the right in Fig. 1), and separate the impacts of OH spatial distribution and temporal variations (colored boxes on the left in Fig. 1). The results are presented and discussed in three sections as shown in different colors in Fig. 1.

235

240

We perform four groups of 3-year CH<sub>4</sub> inversion experiments using 6 to 10 OH fields (Inv1 to Inv4, Fig. 1), and two groups of 17-year CH<sub>4</sub> inversions from 2000 to 2016 (Inv5 and Inv6, Fig. 1) using only CESM1-WACCM OH fields. For the short-term inversions, the first and last six months are treated as

spin-up and spin-down periods and discarded from the following analyses (to avoid edge effect). Thus, we only analyze the results over 2000/07-2002/06 (i.e. the early 2000s) for Inv1 and Inv2 and 2007/07-2009/06 (i.e. the late 2000s) for Inv3 and Inv4. The early 2000s and the late 2000s represent the time periods with stagnant and resumed growth of atmospheric CH<sub>4</sub> mixing ratios, respectively. For the long-term inversions, we take a one-year spin-up and spin-down and analyze the 15-year results from 2001 to 2015.

The aim of Inv1, conducted for 2000-2002 with 10 OH fields, is to quantify the influence of both OH global burden and spatial distributions on top-down estimates of global, regional, and sectoral CH<sub>4</sub> emissions (the brown box with the solid line, Fig. 1). Because of the long lifetime of CH<sub>4</sub> relative to OH, the top-down estimates of regional CH<sub>4</sub> emissions can be influenced by both global total OH burden and OH spatial and seasonal distributions. To separate the influence of OH spatial distributions (including their seasonal variations) from that of the global annual mean [OH], we conduct Inv2, where all the prescribed OH fields are globally scaled to the global [OH]<sub>GM-CH<sub>4</sub></sub> value of the INCA NMHC OH field in 2000 to get the same loss of CH<sub>4</sub> by OH (scaled OH fields). As such, Inv2 provides the uncertainty range of CH<sub>4</sub> emissions induced by OH spatial distribution in both horizontal and vertical directions as well as seasonal variations when assuming that the global total burden of OH can be precisely constrained (the brown box with the dashed line, Fig. 1). Thus, Inv1 (the inversions using original OH fields) and Inv2 (the inversions using scaled OH fields) yield upper (uncertainties from both global OH burden and spatial distributions) and lower (uncertainties only from OH spatial and seasonal distributions) limits of influences of OH on regional CH<sub>4</sub> emissions, respectively.

To quantify the influence of OH on CH<sub>4</sub> interannual emission changes, we also conduct Inv3 and Inv4 over 2007-2009, with 6 scaled OH fields (instead of 10 to limit computational time). While both of the inversions are done for 2007-2009 (Inv3 and Inv4), the OH variations during 2007-2009 (Inv3) and 2000-

2002 (Inv4) are used for the two inversions, respectively. Therefore, the difference Inv3—Inv2 reveal the impact of OH on CH<sub>4</sub> emission changes between the early and late 2000s (the yellow box with solid lines of Fig. 1), Inv3—Inv4 separates the impact of OH interannual variations, and the difference Inv4—Inv2 allows assessing the uncertainties of optimized CH<sub>4</sub> emission changes due to different OH spatial and seasonal distributions (the yellow boxes with dashed lines in Fig. 1).

Finally, we test the impact of OH year-to-year variations and trends on CH<sub>4</sub> emissions over 2001-2015 by running two long-term inversions (Inv5 and Inv6) with the OH fields simulated by CESM-WACCM only (the green box with dashed lines in Fig. 1). Inv5 is forced by the OH fields with both year-to-year variations and trends, while Inv6 is forced by the OH fields for the year 2000. For each group, only one experiment was done for computational reasons. We chose OH fields simulated by CESM1-WACCM because it shows the largest year-to-year OH variations and a positive trend of 0.35% yr<sup>-1</sup> during 2000-2010 among the CCMI OH fields (Zhao et al., 2019). Therefore, inversions using CESM1-WACCM OH are expected to yield an upper limit of the influence of OH variations on CH<sub>4</sub> emissions as seen from atmospheric chemistry models.

We evaluate the optimized CH<sub>4</sub> emissions by comparing the simulated CH<sub>4</sub> mixing ratios using prior and posterior CH<sub>4</sub> emissions with independent measurements from the NOAA/ESRL Aircraft Project. The location of the observation site (Table S1) and the vertical profile of the model bias in CH<sub>4</sub> mixing ratios compared with the aircraft observations (model minus observations) are shown in the supplement (Fig. S4a for Inv1 and Fig. S4b for Inv2). The comparisons with independent aircraft observations confirm the improvement of model-simulated CH<sub>4</sub> mixing ratios when using posterior emissions. All of the inversions in Inv1 and Inv2 reach small biases when compared with aircraft observations (right panel of Fig.S4a and Fig.S4b), which means that it is hard to distinguish which OH spatial and vertical distributions are more realistic in terms of quality of fit to these aircraft CH<sub>4</sub> observations. For Inv1, the root mean square errors

( $RMSE = \frac{\sqrt{\sum(model-observation)^2}}{n_{obs}}$ ,  $n_{obs}$  is the number of observations) are reduced from up to more than 100ppbv (prior) emissions to ~10ppbv (posterior). For Inv2, although the CH<sub>4</sub> mixing ratios simulated using prior emissions already match well with aircraft observations (MSE=8-17ppbv), the posterior emissions still reduce the RMSE by up to 10ppbv.

In the following sections, to quantify uncertainties in top-down estimations of CH<sub>4</sub> emissions due to OH, we calculate OH-induced CH<sub>4</sub> emission differences and uncertainties as the standard deviation and the maximum minus minimum values of the inversion results, respectively.

### 3 Results

#### 3.1 The impacts of OH burden and spatial distributions on CH<sub>4</sub> emissions in 2000-2002

##### 3.1.1 Global total CH<sub>4</sub> emissions

Based on the ensemble of the 10 different OH fields listed in Table 1, global total emissions inverted by our system in Inv1 vary from 518 to 757Tg CH<sub>4</sub> yr<sup>-1</sup> during the early 2000s (2000/07-2002/06). The highest CH<sub>4</sub> emissions exceeding 700Tg yr<sup>-1</sup> are calculated using MOCAGE and SOCOL3 OH fields, for which  $[OH]_{GM-CH_4}$  ( $15.0 \times 10^5$  and  $16.3 \times 10^5$  molec cm<sup>-3</sup>) are much higher than those of other OH fields ( $10.3-12.6 \times 10^5$  molec cm<sup>-3</sup>), leading to a larger CH<sub>4</sub> sink, and as a consequence larger CH<sub>4</sub> emissions due to the mass balance constraint of atmospheric inversions. The high  $[OH]_{GM-CH_4}$  simulated by SOCOL3 and MOCAGE are mainly due to high surface and mid-tropospheric NO mixing ratio simulated by these two models (Zhao et al., 2019). As analyzed in Zhao et al. (2019), the lack of N<sub>2</sub>O<sub>5</sub> heterogeneous hydrolysis (by both SOCOL3 and MOCAGE) and the overestimation of tropospheric NO production by NO<sub>2</sub> photolysis (by SOCOL3) are the major factors behind the overestimation of NO and OH.

The minimum-maximum range of the CH<sub>4</sub> emissions estimated by the 10 OH fields is almost similar to

the range estimated by previous bottom-up studies (542-852Tg yr<sup>-1</sup> given by Kirschke et al., 2013 and 583-861Tg yr<sup>-1</sup> given by Saunois et al, 2016) from GCP syntheses and much larger than that reported by an ensemble of top-down studies for 2000-2009 in Kirschke et al. (2013) (526-569Tg yr<sup>-1</sup>), Saunois et al. (2016) (535-566Tg yr<sup>-1</sup>) or the recent Saunois et al. (2019) (522-559 Tg yr<sup>-1</sup>). (Table 2 and Fig. 2). In the three top-down model ensembles, most of the inversion systems use TransCom OH fields, and the reported differences are mainly from different model transport and set-up of the inversion systems (e.g. the observations used in the inversions). Excluding the two outliers (MOCAGE and SOCOL-3) in Inv1, we find an uncertainty of about 17% in global methane emissions (518 to 611Tg yr<sup>-1</sup>) due to OH global burden and distributions, while transport model errors lead to only 5% of the uncertainty of the global methane budget (Table 3, Locatelli et al. (2013)). Our results indicate that considering different OH fields within top-down CH<sub>4</sub> inversions would lead to larger uncertainty on the top-down CH<sub>4</sub> budget.

Plotting top-down estimated CH<sub>4</sub> emissions against [OH]<sub>GM-CH<sub>4</sub></sub>, which directly reflects the global OH oxidizing efficiency with respect to CH<sub>4</sub> (Lawrence et al., 2001), reveals that the global total CH<sub>4</sub> emissions vary linearly with [OH]<sub>GM-CH<sub>4</sub></sub> ( $r^2 > 0.99$ , Fig. 2, right panel). The top-down estimation of global total CH<sub>4</sub> emissions (EMIS<sub>CH<sub>4</sub></sub>) can be approximately calculated as:

$$\text{EMIS}_{\text{CH}_4} = 40.4 \times [\text{OH}]_{\text{GM-CH}_4} + 66.7 \quad (1)$$

Where a  $1 \times 10^5$  molec cm<sup>-3</sup> (1%) increase in [OH]<sub>GM-CH<sub>4</sub></sub> will increase the top-down estimated CH<sub>4</sub> emissions (EMIS<sub>CH<sub>4</sub></sub>) by 40.4 Tg yr<sup>-1</sup>, consistent with that given by He et al. (2020) using full-chemistry modeling and a mass balance approach. Other CH<sub>4</sub> sinks including soil uptake and oxidation by O<sup>1</sup>(D), which are prescribed in this study, remove 66.7Tg yr<sup>-1</sup> CH<sub>4</sub>. If uncertainties in all the CH<sub>4</sub> sinks were also considered, the correlation between optimized CH<sub>4</sub> emissions and the [OH]<sub>GM-CH<sub>4</sub></sub> would be reduced.

Using box-model inversions, previous studies calculated that a 4% ( $0.4 \times 10^5$  molec cm<sup>-3</sup>) decrease in [OH]<sub>GM</sub> is equivalent to an increase of 22Tg yr<sup>-1</sup> CH<sub>4</sub> emissions (Rigby et al., 2017; Turner et al., 2017,

2019). If we apply the same  $[\text{OH}]_{\text{GM}}$  changes in Eq.1 ( $0.4 \times 10^5 \text{ molec cm}^{-3}$ ), the equivalent emissions change is  $16 \text{ Tg yr}^{-1}$ , about 25% smaller than that given by Turner et al., (2017). This difference probably results from the different hemispheric mean reaction rates of  $\text{OH} + \text{CH}_4$  applied in box models, but could also be due to different treatments of inter-hemispheric transport and stratospheric  $\text{CH}_4$  loss in global 3D transport models compared to simplified box-models (Naus et al., 2019).

With the OH fields scaled to the same  $[\text{OH}]_{\text{GM-CH}_4}$  ( $11.1 \times 10^5 \text{ molec cm}^{-3}$ ), the Inv2 simulations (assuming a global total OH burden well constrained) estimated global  $\text{CH}_4$  emissions of  $551 \pm 2 \text{ Tg yr}^{-1}$  (Table 3), as expected by the scaling. Differences in OH spatial distributions only lead to negligible uncertainty in global total  $\text{CH}_4$  emissions estimated by top-down inversions.

### 3.1.2 Regional $\text{CH}_4$ emissions

#### Inv1 and Inv2

Since MOCAGE and SOCOL3 OH fields show much higher  $[\text{OH}]_{\text{GM}}$  than constrained by MCF observations ( $\sim 10 \times 10^5 \text{ molec cm}^{-3}$ , e.g. Prinn et al., 2001; Bousquet et al., 2005) and give much higher estimates of  $\text{CH}_4$  emissions ( $> 700 \text{ Tg yr}^{-1}$ ) than other OH fields, we exclude inversion results with these two OH fields from the following analyses.

In response to both global total OH burden and inter-hemispheric OH ratios (Table 1),  $\text{CH}_4$  emissions over northern and southern hemispheres calculated by Inv1 (Table 2) vary from  $368$  to  $424 \text{ Tg yr}^{-1}$  ( $401 \pm 21 \text{ Tg yr}^{-1}$ ) and  $138$  to  $187 \text{ Tg yr}^{-1}$  ( $166 \pm 15 \text{ Tg yr}^{-1}$ ), respectively; resulting in a range in inter-hemispheric  $\text{CH}_4$  emission difference (NH–SH) of  $206$ – $254 \text{ Tg yr}^{-1}$  ( $236 \pm 14 \text{ Tg yr}^{-1}$ ). When scaling all OH fields to the same loss for Inv2, the standard deviations of hemispheric  $\text{CH}_4$  emissions are reduced to  $7 \text{ Tg CH}_4 \text{ yr}^{-1}$  for both hemispheres (Table 2), much smaller than those derived in Inv1 ( $21 \text{ Tg yr}^{-1}$  and  $15 \text{ Tg yr}^{-1}$  over the northern and southern hemisphere, respectively). However, the  $\text{CH}_4$  emission inter-hemispheric

difference calculated by Inv2 remains at  $236 \pm 14 \text{Tg yr}^{-1}$ , similar to that calculated by Inv1, which indicates that the hemispheric  $\text{CH}_4$  emissions differences are mainly determined by OH spatial distributions. Without the TransCom OH simulation, the inter-hemispheric  $\text{CH}_4$  emission difference ranges between 232 and  $246 \text{Tg yr}^{-1}$ . The TransCom OH field, for which OH N/S ratio is 1.0, leads to an inter-hemispheric  $\text{CH}_4$  emission difference of  $205 \text{Tg yr}^{-1}$ ,  $35 \text{Tg yr}^{-1}$  ( $27 \text{Tg yr}^{-1}$ ) smaller than the mean (minimum) inter-hemispheric difference calculated using other OH fields (OH N/S ratio = 1.2-1.3). Previous studies show that differences in atmospheric transport models can lead to  $\pm 28 \text{Tg yr}^{-1}$  uncertainties in the top-down calculation of the inter-hemispheric  $\text{CH}_4$  emission difference, using a single OH field – TransCom (Locatelli et al., 2013). Here, using a single atmospheric transport model, but different OH fields, we find a  $\pm 14 \text{Tg yr}^{-1}$  uncertainty, about half of the atmospheric transport model uncertainty. Combining the two studies, one could expect more than  $30 \text{Tg yr}^{-1}$  uncertainty in top-down estimates of the inter-hemispheric  $\text{CH}_4$  emission difference, based on different atmospheric models and different OH fields.

Fig. 3 shows the optimized and prior  $\text{CH}_4$  emissions calculated by Inv1 (top) and Inv2 (bottom) over latitudinal intervals (left panels) and large emitting regions (right panels). Compared with prior emissions, nearly all the optimized latitudinal and regional emissions show the same increment direction from prior emissions, but the magnitudes of the increment largely vary. The  $\text{CH}_4$  emissions calculated by Inv1 amount to i)  $147 \pm 14 \text{Tg yr}^{-1}$  and are  $1-47 \text{Tg yr}^{-1}$  higher than the prior estimate over the southern tropical regions ( $30^\circ \text{S}-0^\circ$ ), ii)  $199 \pm 14 \text{Tg yr}^{-1}$  and are  $6-45 \text{Tg yr}^{-1}$  higher than the prior estimate over the northern tropical regions ( $0^\circ-30^\circ \text{N}$ ), and iii)  $174 \pm 8 \text{Tg yr}^{-1}$  and are  $1-26 \text{Tg yr}^{-1}$  lower than the prior estimate over the northern mid-latitude regions ( $30^\circ \text{N}-60^\circ \text{N}$ ) (Table 3). The uncertainties in global OH burden and distributions lead to larger uncertainty (maximum – minimum) in top-down estimated  $\text{CH}_4$  emissions over the tropics (>20% of multi-inversion mean) and smaller uncertainty over the northern mid-latitude regions (14%) compare with that lead by transport model errors and different observations given by

Saunois et al. (2016) (13% over tropics and 20% over northern mid-latitude regions) (Table 3).

Over the large emitting regions Europe (EU), Canada (CAN), and China (CHN), optimized emissions are lower than the prior. The emissions calculated by Inv1 show the largest absolute OH induced differences over South America (SA,  $73 \pm 9 \text{Tg yr}^{-1}$ ), South Asia (SAS,  $59 \pm 6 \text{Tg yr}^{-1}$ ), and China ( $42 \pm 5 \text{Tg yr}^{-1}$ ) (Fig. 3, right panels and Table 3), of which the uncertainty (maximum—minimum) account for more than 20% of the multi-inversion mean emission over the corresponding regions (Table 3). Over high-latitude regions (Canada, Europe, and Russia), OH lead to small uncertainty ranges ( $< 10 \text{Tg yr}^{-1}$ ). At the model grid-scale, the uncertainty range due to OH can be much larger than the regional mean (middle panel of Fig. 3), for example, larger than 50% of the multi-inversion mean emissions over South America and East Asia. As shown in Table 3, at regional scales, the uncertainty (maximum—minimum) in top-down estimated  $\text{CH}_4$  emissions due to different OH global burden and distributions over Asia and South America ( $\sim 37\%$  of multi-inversion mean) are of the same order than those lead by transport errors (25% and 48%) or given by Saunois et al. (2016) ( $\sim 40\%$ ). Over other regions, using different OH fields lead to smaller uncertainties (11%-18%) compared to other causes of errors (23%-70%) (Table 3).

The uncertainties in the top-down estimated regional emissions are not only due to inter-model differences of the regional OH fields but also rely on the distribution of the surface observations used in the inversions. Over the regions with large prior emissions but less constrained by observations (e.g. South America, South Asia, and China), our OH analysis leads to larger uncertainties than regions that are well constrained by observations (e.g. the North America and Canada) (Fig. S3). The results may indicate that on the regional scale, the top-down estimated  $\text{CH}_4$  emissions and the uncertainties lead by OH are specific to the observation system retained. If more surface observations (e.g. in the southern hemisphere) or satellite columns with a more even global coverage were included in our inversions, spatial patterns of the top-down estimated  $\text{CH}_4$  emissions and their uncertainties (as shown by Fig.3) could be different.

## Comparing Inv1 and Inv2

We now compare the inversion results using the original OH fields (Inv1) with those using scaled OH fields (Inv2) to estimate how much the optimized regional CH<sub>4</sub> emission differences of Inv1 are dominated by OH spatial and seasonal distributions versus the global OH burden. Applying one single global scaling factor per model reduces the inter-model differences of original OH fields by 33%, 67%, and 33% in the southern tropics(0 °-30 °S), northern tropics(0 °-30 °N), and northern mid and high latitudes (30 °-90 °N) (Table S2). This scaling results in 57%, 93%, and 22% reduction of OH induced latitudinal CH<sub>4</sub> emission differences, respectively for the southern tropics(0 °-30 °S), northern tropics(0 °-30 °N), and northern mid and high latitudes (30 °-90 °N) (Fig. 3, left panels comparing standard deviations of Inv1 and Inv2). At the regional scale (Fig. 3, right panel and Table 3), the OH spatial distribution-induced CH<sub>4</sub> emission differences (standard deviation of Inv2) account for 50% of the differences due to both OH burden and spatial distributions (standard deviation of Inv1) over northern mid-latitude regions (China, North America) and South America. Over northern tropical regions (Southern Asia and Southeast Asia), the OH spatial distribution induces negligible CH<sub>4</sub> emission differences.

The comparison of Inv1 and Inv2 reveals that methane emissions in tropical regions are less sensitive to OH spatial distribution than mid- and high-latitude regions in our framework. One possible explanation could be the location of monitoring sites. Over tropical regions, CH<sub>4</sub> emissions are less constrained (with few to none observation sites near source regions) than in the northern extra-tropics, where several monitoring sites located at or near the regions with high CH<sub>4</sub> emission rates and high OH uncertainties (e.g. North America, Europe, and downwind of East Asia). Thus, CH<sub>4</sub> emissions over the tropical regions mainly contribute to match the global total CH<sub>4</sub> sinks (instead of the sinks over the tropical regions only) estimated by inversion systems. When all OH fields are scaled to the same CH<sub>4</sub> losses (Inv2), differences of emissions over the tropical regions are therefore largely reduced.

### 3.1.3 Global and regional CH<sub>4</sub> emissions per source category

Fig. 4 compares optimized and prior global total CH<sub>4</sub> emissions and the difference between the prior and optimized CH<sub>4</sub> emissions for four broad source categories: wetlands, agriculture and waste (named Agri-waste), fossil fuels, and other natural sources. We attribute the optimized emissions to different source sectors depending on the relative strength of individual prior sources in each grid-cell. With original OH fields, Inv1 calculates CH<sub>4</sub> emissions of 203 ± 15 Tg yr<sup>-1</sup> for wetlands, 209 ± 12 Tg yr<sup>-1</sup> for Agri-waste, 89 ± 4 Tg yr<sup>-1</sup> for fossil fuel, and 66 ± 3 Tg yr<sup>-1</sup> for other natural sources. Optimized emissions of the four sectors are 23 ± 15 Tg yr<sup>-1</sup> (-2-42 Tg yr<sup>-1</sup>), 13 ± 12 Tg yr<sup>-1</sup> (-3-29 Tg yr<sup>-1</sup>), 5 ± 4 Tg yr<sup>-1</sup> (-1-9 Tg yr<sup>-1</sup>), and 4 ± 3 Tg yr<sup>-1</sup> (0.1-8 Tg yr<sup>-1</sup>) higher than the prior emissions, respectively. Although Inv2 is conducted with scaled OH fields and all inversions calculate similar global total CH<sub>4</sub> emissions (551 ± 2 Tg yr<sup>-1</sup>), optimized CH<sub>4</sub> emissions still show some uncertainties due to OH (as standard deviation) (3 Tg yr<sup>-1</sup> for wetland emissions and 2 Tg yr<sup>-1</sup> for agriculture and waste, yellow boxplots in Fig. 4), in response to different OH spatial distributions.

We have further calculated CH<sub>4</sub> emissions per source category and per region estimated by Inv1 (Fig. 5), to explore the contribution of each region to the OH-induced sectoral emission uncertainties. Wetland CH<sub>4</sub> emissions mainly dominate emissions over Northern South America, Africa, South and East Asia, and Canada. Northern South America (53 ± 7 Tg yr<sup>-1</sup>) and Africa (30 ± 2 Tg yr<sup>-1</sup>) contribute most of the global total OH induced wetland emission differences and are 1-22 Tg yr<sup>-1</sup> and 1-8 Tg yr<sup>-1</sup> higher than prior emissions, respectively. In contrast to the higher wetland emissions than prior ones over tropical regions, optimized boreal wetland emissions (in Canada) are 6-9 Tg yr<sup>-1</sup> lower than prior emissions, consistent with lower top-down estimations than the prior given by Saunio et al. (2016). Agriculture and waste emissions are most intensive over China (25 ± 3 Tg yr<sup>-1</sup>) and South Asia (SAS) (39 ± 3 Tg yr<sup>-1</sup>). The optimized inventories show lower agriculture and waste emissions over China (0.6-10 Tg yr<sup>-1</sup>) and Europe (1-3 Tg

yr<sup>-1</sup>) and much higher emissions over SAS (4-13Tg yr<sup>-1</sup>) compared with the prior emission inventory. The OH induced differences in fossil fuel emissions are found mainly in China and Africa, which are 0.8-5Tg yr<sup>-1</sup> lower and 0.6-3Tg higher than prior emissions, respectively. In agreement with the previous regional discussion, scaling the OH (Inv2) highly reduces the uncertainties attributable to different OH over the tropical regions but not for the mid-high latitude regions. In Inv2, the largest CH<sub>4</sub> emission differences due to different OH spatial distribution are found for wetland emissions in South America ( $60 \pm 4$ Tg yr<sup>-1</sup>), agriculture and waste emissions in South Asia ( $17 \pm 1$ Tg yr<sup>-1</sup>) and China ( $24 \pm 2$ Tg yr<sup>-1</sup>), and fossil fuel emissions in China ( $8 \pm 0.7$ Tg yr<sup>-1</sup>) and Russia ( $9 \pm 0.4$ Tg yr<sup>-1</sup>).

Previous studies have highlighted that anthropogenic emissions over China are largely overestimated by bottom-up emissions inventories compared with top-down estimates (Kirschke et al., 2013; Tohjima et al., 2014; Saunio et al., 2016). In our study, total anthropogenic emissions (agriculture, waste, and fossil fuel) over China are 1-15Tg yr<sup>-1</sup> lower than the prior bottom-up inventory as calculated by Inv1, and 7-14Tg yr<sup>-1</sup> as calculated by Inv2, with the lowest emissions calculated with the TransCom OH field (for both Inv1 and Inv2). The TransCom OH field is the one most widely used in current top-down CH<sub>4</sub> emission estimations but shows much lower [OH] over China than other OH fields (Zhao et al., 2019), which may be due to the use of the same NO<sub>x</sub> profile over East Asia as for remote regions based on the observations of 1990s when constructing the TransCom OH field (Spivakovsky et al., 2000). Thus, the large reduction of top-down estimated anthropogenic CH<sub>4</sub> emissions over China as compared to the prior emissions may be partly due to an underestimation of [OH] over China in the TransCom field.

### **3.2 Impact of OH on CH<sub>4</sub> emission changes between 2000-2002 and 2007-2009**

As shown in Table 4, the global mean [OH] simulated by CCMi models increased by 0.7%-1.8% from 2000-2002 to 2007-2009, in response to anthropogenic emissions and climate change (Zhao et al., 2019), whereas the INCA-NMHC model-simulated global [OH] shows a slight decrease of 0.5%. The TransCom

OH field, being constant over time, shows no change. The increase in global mean [OH] mainly results from the combination of a higher increase in the tropics compared to the northern extra-tropics and a slight decrease in the southern extra-tropics. As a result, the changes in OH between the two periods show different patterns between regions. We have conducted inversions for 2007-2009 with scaled OH fields (Inv3) to explore how uncertainties in OH (both spatial and seasonal distribution and interannual changes) can influence the top-down estimates of temporal CH<sub>4</sub> emission changes from the early 2000s (2000/07-2002/06, Inv2) to the late 2000s (2007/07-2009/06, Inv3) (Inv3 – Inv2). We have also performed Inv4 for 2007-2009 but using OH fields of 2000-2002 to separate the contribution of OH from different time periods (Inv3 – Inv4).

500

### 3.2.1 Global total emission changes between 2000-2002 and 2007-2009

**Total emission changes.** From the early 2000s (Inv2) to the late 2000s (Inv3), the top-down estimated CH<sub>4</sub> emissions increased by  $21.9 \pm 5.7 \text{ Tg yr}^{-1}$  ( $16.6\text{-}30.0 \text{ Tg yr}^{-1}$ , Table 5). The largest CH<sub>4</sub> increase of  $30.0 \text{ Tg yr}^{-1}$  is estimated with CESM1-WACCM OH fields (for which OH increased by 1.8% from 2000-2002 to 2007-2009),  $13.4 \text{ Tg yr}^{-1}$  higher than the smallest increase of  $16.6 \text{ yr}^{-1}$  estimated with the INCA NMHC OH field (for which OH decreased by 0.5% from 2000-2002 to 2007-2009). In Saunois et al. (2017), the minimum-maximum uncertainty range of emission changes between 2002-2006 and 2008-2012 was  $16 \text{ Tg yr}^{-1}$ . This means that the uncertainty attributable to uncertainty in OH fields ( $13.4 \text{ Tg yr}^{-1}$ ), is comparable to the minimum-maximum uncertainty resulting from using different atmospheric chemistry transport models and observations (surface and satellite), but mostly constant OH over time ( $16 \text{ Tg yr}^{-1}$ , Saunois et al., 2017).

510

**Spatial versus temporal OH effects.** Only changing OH from 2000-2002 (Inv4) to 2007-2009 (Inv3), top-down estimated CH<sub>4</sub> emissions due to OH interannual changes are  $+5.1 \pm 6.4 \text{ Tg yr}^{-1}$  ( $-2.7\text{-}13.5 \text{ Tg yr}^{-1}$

515 <sup>1</sup>, Table 5), which contribute 25% of total optimized emission changes (Inv3—inv2) between the early  
and late 2000s ( $21.9 \pm 5.7 \text{Tg yr}^{-1}$ , Table 5). As listed in Table 5, the largest emission increase due to OH  
interannual changes are calculated using MRI-ESM1r1 OH fields, for which a 1.1% global increase in  
OH can up to double the top-down estimation of CH<sub>4</sub> emission increase from the early to the late 2000s.  
This result indicates that a large bias likely exists in the former top-down estimation of the CH<sub>4</sub> emission  
520 trend calculated without considering OH changes (Saunois et al., 2017).

Keeping OH fields from 2000-2002, top-down estimated CH<sub>4</sub> emissions increase by  $16.9 \pm 1.9 \text{Tg yr}^{-1}$   
( $14.3\text{-}19.3 \text{Tg yr}^{-1}$ , Table 5) between the early 2000s (Inv2) to the late 2000s (Inv4) in response to  
increasing atmospheric CH<sub>4</sub> mixing ratios and temperature. This represents 75% of total optimized  
525 emission changes (Inv3—inv2) between the early and late 2000s ( $21.9 \pm 5.7 \text{Tg yr}^{-1}$ , Table 5). The  $1.9 \text{Tg}$   
 $\text{yr}^{-1}$  uncertainty (as standard deviation) is due to the different OH spatial and seasonal distributions,  
indicating that OH spatial and seasonal distributions, which are not considered in box-models, can also  
contribute to the uncertainties in optimized CH<sub>4</sub> emission changes.

### 530 3.2.2 Emission changes by source types and regions

**Total emission changes.** We further analyze the influence of OH (both spatial distributions and  
interannual variations) on the top-down estimated sectoral and regional CH<sub>4</sub> emission changes from the  
early 2000s (Inv2) to the late 2000s (Inv3). As shown in Fig. 6 (top panels), the smaller increase of the  
optimized global CH<sub>4</sub> emissions from the early 2000s to the late 2000s ( $21.9 \pm 5.7 \text{Tg yr}^{-1}$ ) compared to the  
535 prior change ( $39.4 \text{Tg yr}^{-1}$ ) is mainly due to decrease in wetland emissions over the southern tropics ( $-$   
 $4.4 \pm 1.5 \text{Tg yr}^{-1}$ ,  $15^{\circ}\text{S}\text{-}0^{\circ}$ ) and northern mid-latitude regions ( $-3.4 \pm 0.4 \text{Tg yr}^{-1}$ ,  $45^{\circ}\text{N}\text{-}60^{\circ}\text{N}$ ) in contrast to  
climatology prior wetland emissions, and a lower fossil fuel emission increase over  $30^{\circ}\text{N}\text{-}45^{\circ}\text{N}$  ( $3.7 \pm$   
 $0.4 \text{Tg yr}^{-1}$ ) compared to prior emission increase ( $8.9 \text{Tg yr}^{-1}$ ). Wetlands ( $-3.5 \pm 2.5 \text{Tg yr}^{-1}$ ) and agriculture  
and waste ( $14.2 \pm 2.1 \text{Tg yr}^{-1}$ ) contribute most of the total OH induced uncertainty in global total emission

540 changes ( $21.9 \pm 5.7 \text{Tg yr}^{-1}$ ) from the early 2000s (Inv2) to the late 2000s (Inv3) (Table 6), whereas fossil fuel emissions ( $8.7 \pm 0.8 \text{Tg yr}^{-1}$ ) show smaller uncertainty.

Considering emissions over latitudinal bands (Fig. 6, top panels), the largest spread of emission changes are found over the southern tropics ( $15^{\circ}\text{S}$  –tropics,  $-1.3$  to  $-6.5 \text{Tg yr}^{-1}$ ), northern subtropics ( $15^{\circ}\text{N}$ - $30^{\circ}\text{N}$ , 545  $15.5$  to  $20.0 \text{Tg yr}^{-1}$ ), and northern extratropical regions ( $30^{\circ}\text{N}$ - $45^{\circ}\text{N}$ ,  $7.6$  to  $10.7 \text{Tg yr}^{-1}$ ). The spread over the southern tropics is dominated by emission changes from wetlands ( $-2.3$  to  $-6.3 \text{Tg yr}^{-1}$ ), over northern subtropics by agriculture and waste ( $7.3$  to  $10.0 \text{Tg yr}^{-1}$ ), and over northern extratropical regions by agriculture and waste ( $3.7$  to  $5.1 \text{Tg yr}^{-1}$ ) and fossil fuels ( $3.3$  to  $4.3 \text{Tg yr}^{-1}$ ). At the regional scale (Fig. 7, top panels), northern South America ( $-1.2$  to  $-5.2 \text{Tg yr}^{-1}$ ), South Asia ( $9.1$  to  $12.4 \text{Tg yr}^{-1}$ ), and China ( $-$  550  $0.1$  to  $4.9 \text{Tg yr}^{-1}$ ) show the largest differences in emission changes from the early 2000s to the late 2000s. The multi-inversions calculated emission changes in China disagree in sign (Fig. 7; top panels), mainly due to differences in the agriculture and waste sector, which range from  $1.3 \text{Tg yr}^{-1}$  decrease to  $1.5 \text{Tg yr}^{-1}$  increase from the early 2000s to the late 2000s.

555 We now compare the uncertainty of top-down estimated  $\text{CH}_4$  emission changes from the early to the late 2000s due to different OH spatial-temporal variations with that ensemble of top-down studies given by Saunois et al. (2017). For the sectoral emissions, the emission changes from agriculture and waste and from wetland show the largest uncertainties (more than 50% of multi-inversions mean, Inv3 – Inv2 in Table 6) induced by OH spatial-temporal variations, comparable to that given by Saunois et al. (2017). 560 On the contrary, the uncertainty of fossil fuel emission changes (24% of multi-inversions mean) is much smaller than that given by Saunois et al. (2017). For regional  $\text{CH}_4$  emission changes, the uncertainty induced by OH spatial-temporal variations is usually larger than the multi-inversion mean emission changes (except South Asia) and similar to that given by Saunois et al. (2017). The large differences existing in different top-down estimated regional and sectoral emission changes are mainly attributed to

565 model transport errors in Saunio et al. (2017). Here, our results show that uncertainties due to OH spatio-temporal variations can lead to similar biases in top-down estimated CH<sub>4</sub> emission changes.

**Spatial versus temporal effects.** We now separate influences of OH interannual changes (Inv3—Inv4) on optimized regional CH<sub>4</sub> emission changes. As shown in the bottom panels of Fig. 6 and Fig. 7, at the regional scale, OH interannual changes mainly perturb top-down estimated CH<sub>4</sub> emission changes (Fig. 570 6; bottom panel) over the southern tropics (0°–15°S, -3.4–5.9Tg yr<sup>-1</sup>) and northern subtropics (15°N–30°N, 0–5.4Tg yr<sup>-1</sup>). This corresponds to the two largest spreads observed in Fig.7 (bottom panel) associated with wetland emissions over northern South America (-2.0–3.5Tg yr<sup>-1</sup>) and with agriculture and waste emissions over South Asia (-0.2–2.6Tg yr<sup>-1</sup>). Among the four emission sectors, wetland emissions (mainly southern tropical wetland) show the largest increase (3.3–4.8Tg yr<sup>-1</sup>) in response to OH temporal changes (Table 6), which account for 60% of total wetland emission changes between these two periods.

The OH spatial and seasonal distribution can lead to large uncertainties in regional CH<sub>4</sub> emission changes. For regional and latitudinal scales, the spreads (uncertainty ranges) of Inv4—inv2 (OH fixed to 2000–580 2002) (Fig. S5 and Fig. S6) are comparable to the spread of regional and latitudinal emission changes lead by both OH interannual changes and spatial and seasonal distributions (Inv3—Inv2) (top panels of Fig. 6 and Fig. 7) as mentioned above (e.g., 2.6–5.4Tg yr<sup>-1</sup> decrease over northern South America, a 6.1–11.1Tg yr<sup>-1</sup> increase over South Asia, and a 0.4–4.2Tg yr<sup>-1</sup> increase over China). These results show that even if the global total OH burden is well constrained (as in Inv4 and Inv2, where all OH fields are scaled to the same [OH]<sub>GM-CH<sub>4</sub></sub>, and the differences in optimized CH<sub>4</sub> emissions changes from the early 2000s to 585 the late 2000s are only due to different OH spatial distributions), top-down estimates of sectoral and regional temporal CH<sub>4</sub> emission changes remain highly uncertain.

### 3.3 Impacts of OH on year to year variations of CH<sub>4</sub> emissions from 2001 to 2015

590 To infer the influence of OH year-to-year variations on top-down optimized long-term CH<sub>4</sub> emission changes, we conducted two inversions, Inv5 and Inv6. Inv5 calculates optimized CH<sub>4</sub> emissions from 2001-2015 with the CESM1-WACCM OH field varying from one year to the next, while Inv6 uses the CESM1-WACCM OH field but fixed to the year 2000. The choice of the CESM1-WACCM OH field is explained in Sect. 2.3 above. As shown in Fig. 8, the [OH]<sub>GM-CH<sub>4</sub></sub> of the CESM1-WACCM OH field  
595 increases by  $0.47 \times 10^5$  molec cm<sup>-3</sup> (4.2%) from 2001 to 2011 and then decreases by  $0.13 \times 10^5$  molec cm<sup>-3</sup> (1.1%) from 2011 to 2015.

With OH fixed to the year 2000 (Inv6), global CH<sub>4</sub> emissions stall at  $550 \pm 2$  Tg yr<sup>-1</sup> during 2001-2003, decrease to 538 Tg yr<sup>-1</sup> in 2004, which is different from the continuous increase of CH<sub>4</sub> emissions given  
600 by the bottom-up inventory (Fig. 8, top panel). After 2004, global total CH<sub>4</sub> emissions show a positive trend of  $3.5 \pm 1.8$  Tg yr<sup>-2</sup> (P<0.05), but smaller than the prior bottom-up inventory ( $4.3 \pm 0.6$  Tg yr<sup>-2</sup> (P<0.05)). Both stalled/decreased emissions during 2001-2004 and increasing trend after 2004 are consistent with previous top-down estimations (Saunio et al., 2017).

605 The trend of global CH<sub>4</sub> emission during 2004-2016 calculated by Inv5 (using varying OH) is  $4.8 \pm 1.8$  Tg yr<sup>-2</sup> (P<0.05), which is 1.3 Tg yr<sup>-2</sup> (36%) higher than that calculated by Inv6 (OH fixed to 2000) due to the small increase in [OH], and also 0.5 Tg yr<sup>-2</sup> higher than the prior emission trend ( $4.3 \pm 0.6$  Tg yr<sup>-2</sup>). Accounting for the OH increasing trend leads to increasing the prior trend in Inv5 instead of decreasing it in Inv6. When calculating the differences between Inv5 and Inv6 for different latitude intervals, we find  
610 that before 2004, differences between Inv5 and Inv6 are mainly contributed by northern middle-latitude regions, whereas after 2004 they are dominated by tropical regions (Fig. 8, bottom).

We further compare CH<sub>4</sub> emission trends for the four previously defined emission sectors and the ten continental regions between Inv5 and Inv6. As shown in Fig. 9, the positive global CH<sub>4</sub> emission trend

615 during 2004-2016 is mainly contributed by anthropogenic sources from agriculture and waste, and fossil  
fuel-related activities, which are  $1.9 \pm 0.7 \text{Tg yr}^{-2}$ , and  $2.3 \pm 0.4 \text{Tg yr}^{-2}$ , respectively, as calculated by Inv6  
(fixed OH). Wetland emissions show a small negative trend ( $-0.5 \pm 0.7 \text{Tg yr}^{-2}$ ) and other natural emissions  
do not show a significant trend ( $0.04 \pm 0.6 \text{Tg yr}^{-2}$ ). Both sectors show large uncertainties in their trends  
reflecting large year-to-year variations. When considering [OH] variations, Inv5 estimates a higher  
620 agriculture and waste emission trend ( $2.4 \pm 0.8 \text{Tg yr}^{-2}$ ) compared to Inv6, mainly contributed by China  
( $1.5 \pm 0.5 \text{Tg yr}^{-2}$  for Inv6 versus  $1.7 \pm 0.5 \text{Tg yr}^{-2}$  for Inv5) and southern South America ( $-0.1 \pm 0.1 \text{Tg yr}^{-2}$  for  
Inv6 versus  $0.1 \pm 0.3 \text{Tg yr}^{-2}$  for Inv5). Accounting for interannual OH variations the negative wetland  
emission trend reduces to near zero ( $0.1 \pm 0.6 \text{Tg yr}^{-2}$ ), mainly due to increased emission trends over  
northern South America ( $-0.3 \pm 0.3 \text{Tg yr}^{-2}$  for Inv6 versus  $0.2 \pm 0.5 \text{Tg yr}^{-2}$  for Inv5). In contrast to  
625 agriculture and waste, and wetland emissions, fossil fuel emissions have a similar positive trend of  
 $2.4 \pm 0.4 \text{Tg yr}^{-2}$  in Inv5 and Inv6. This result comes from a higher  $\text{CH}_4$  emission trend over China  
calculated by Inv5 balanced by a lower  $\text{CH}_4$  emission trend over America and Russia ( $0.2 \pm 0.2 \text{Tg yr}^{-2}$   
for Inv6 versus  $0.1 \pm 0.3 \text{Tg yr}^{-2}$  for Inv5) since the CESM1-WACCM OH field shows a significant  
negative [OH] trend over America (Zhao et al., 2019).

630

#### 4 Conclusions and discussion

In this study, we have performed six groups of variational Bayesian inversions (top-down, 34 inversions  
in total) using up to 10 different prescribed OH fields to quantify the influence of OH burden, interannual  
variations, and spatial and seasonal distributions on the top-down estimation of i) global total, regional,  
635 and sectoral  $\text{CH}_4$  emissions, ii) emission changes between the early 2000s and late 2000s, and iii) year-  
to-year emission variations. Our top-down system estimates monthly  $\text{CH}_4$  emissions by assimilating  
surface observations with atmospheric transport of  $\text{CH}_4$  calculated by the offline version LMDz5B of the  
LMDz atmospheric model using different prescribed OH fields.

640 Based on the ensemble of 10 original OH fields ( $[\text{OH}]_{\text{GM-CH}_4}$ :  $10.3\text{-}16.3 \times 10^5 \text{ molec cm}^{-3}$ ), the global total  
CH<sub>4</sub> emissions inverted by our system vary from 518 to 757 Tg yr<sup>-1</sup> during the early 2000s, similar to the  
CH<sub>4</sub> emission range estimated by previous bottom-up syntheses and larger than the range reported by the  
top-down studies (Kirschke et al., 2013; Saunois et al, 2016;2019). The top-down estimated global total  
CH<sub>4</sub> emission varies linearly with  $[\text{OH}]_{\text{GM-CH}_4}$ , which indicates that at the global scale, a small uncertainty  
645 of  $1 \times 10^5 \text{ molec cm}^{-3}$  (10%)  $[\text{OH}]_{\text{GM-CH}_4}$  can result in 40.4 Tg yr<sup>-1</sup> uncertainties in optimized CH<sub>4</sub> emissions.

At regional scale (excluding the two highest OH fields), CH<sub>4</sub> emission uncertainties due to different OH  
global burdens and distributions are largest over South America (37% of multi-inversion mean), South  
Asia (24%), and China (39%), resulting in significant uncertainties in optimized emissions from the  
650 wetland and agriculture and waste sectors. These uncertainties are comparable in these regions with those  
due to model transport errors and inversion system set-up (Locatelli et al., 2013; Saunois et al., 2016).  
For these regions, the uncertainty due to OH is critical for understanding their methane budget. In other  
regions, OH leads to smaller uncertainties compared to that given by Locatelli et al. (2013) and Saunois  
et al. (2016). By performing inversions with globally-scaled OH fields, we calculated that emission  
655 uncertainties due to different OH spatial and seasonal distributions account for ~50% of total uncertainties  
(induced by both different OH burden and different OH spatial and seasonal distributions) over mid-high  
latitude regions and South America. CH<sub>4</sub> emission differences due to OH spatial distributions are the  
largest in northern South America and China but are negligible over South Asia and other northern tropical  
regions. Based on CH<sub>4</sub> emission optimization with surface observations, our study shows that tropical  
660 regions appear more sensitive to OH global burden (as less constrained regions used to achieve the global  
mass balance of the methane budget) and mid-to-high latitude regions are found sensitive to both OH  
global burden and spatial distributions.

The global CH<sub>4</sub> emission change between 2000-2002 and 2007-2009 as estimated by top-down inversions

665 using 6 different OH fields, is  $21.9 \pm 5.7 \text{ Tg yr}^{-1}$ , of which 25% ( $5.1 \pm 6.4 \text{ Tg yr}^{-1}$ ) is contributed by OH  
interannual variations (mainly by an increase in [OH]), while 75% can be attributed to emission changes  
resulting from the increase in observed CH<sub>4</sub> mixing ratios and atmospheric temperature (considering  
constant OH). Among the four emission sectors, wetland emissions (mainly southern tropical wetlands)  
show the largest increase of  $2.1 \pm 3.4 \text{ Tg yr}^{-1}$  in response to OH temporal changes, which account for 60%  
670 of total wetland emission changes between these two periods. For global total emission changes, OH  
spatial distributions lead to lower uncertainties than interannual variations ( $1.9 \text{ Tg yr}^{-1}$  versus  $6.4 \text{ Tg yr}^{-1}$ ),  
but at the regional scale, OH spatial distributions and interannual variations are of equal importance for  
quantifying CH<sub>4</sub> emission changes.

675 As the modeled OH used here mainly shows an increase in [OH] (meaning increasing CH<sub>4</sub> sink) during  
the 2000s, our inversion using year-to-year OH variations infers a 36% higher CH<sub>4</sub> emission trend  
compared with an inversion driven by climatological OH over the 2001-2015 period. The different OH  
fields from CCMI models consistently show increasing OH trends during 2000-2010 (Zhao et al., 2019).  
These variations disagree with MCF-constrained [OH], which show a decrease of  $8 \pm 11\%$  during 2004-  
680 2014 and 7% during 2003-2016 estimated by Rigby et al. (2017) and Turner et al. (2017), respectively. A  
drop of OH between 2006-2007 (Rigby et al., 2008, Bousquet et al., 2011) is captured by CESM1-  
WACCM OH fields but with (possibly) smaller changes (1%) compared to (the very uncertain)  $4 \pm 14\%$   
changes constraint by MCF (Rigby et al., 2008). This OH drop in 2006-2007 results in a  $6 \text{ Tg yr}^{-1}$  smaller  
increase of CH<sub>4</sub> emissions between 2006 and 2007 compared to that derived using constant OH. However,  
685 such [OH] drop is treated as a year-to-year variation instead of a trend, and cannot fully explain the  
resumption of CH<sub>4</sub> growth from 2006-2007. Thus, during 2004-2010, at the decadal timescale, if the  
CCMI models represent the OH trend properly, a higher increasing trend of CH<sub>4</sub> emissions is needed to  
match the CH<sub>4</sub> observations (compared to the CH<sub>4</sub> emission trend derived using constant OH). After 2010,  
CCMI models simulated OH trends of different signs (Zhao et al., 2019), thus the influence on the CH<sub>4</sub>

690 emission trend is more uncertain.

The trend and interannual variations of tropospheric OH burden are determined by both precursor emissions from anthropogenic and natural sources and climate change (Holmes et al., 2013; Murray et al., 2014). Based on satellite observations, Gauber et al. (2017) estimated that ~20% decrease in atmospheric CO concentrations during 2002-2013 led to an ~8% increase in atmospheric [OH]. The El Niño-Southern Oscillation (ENSO) has been proven to impact the tropospheric OH burden and CH<sub>4</sub> lifetime mainly through changes in biomass burning from CO (Nicely et al., 2020; Nguyen et al., 2020) and in NO emission from lightning (Murray et al., 2013; Turner et al., 2018). The ENSO signal is weak during the early 2000s, resulting in small interannual variations of tropospheric OH burden (Zhao et al., 2019). The mechanisms of OH variations related to ENSO and their impacts on the CH<sub>4</sub> budget need to be explored by inversions, but over a longer time period than this study (e.g. 1980-2010, Zhao et al., 2020).

Compared to previous box-model studies (e.g. Rigby et al., 2017; Turner et al. 2017), the inversions performed in this study take advantage of 4D OH fields from CCMI to quantify impacts on regional and sectoral emission estimations. Our results indicate that OH spatial distributions, which are difficult to obtain from proxy observations (e.g. MCF), are equally important as the global OH burden for constraining CH<sub>4</sub> emissions over mid- and high-latitude regions. Constraining global annual mean OH based on proxy observations (e.g. Zhang et al., 2018; Maasakkers et al., 2019) provides a constraint on global total methane emissions, through the necessity of balancing the global budget (sum of source – sum of sinks = atmospheric growth rate). It also largely reduces uncertainties in optimized CH<sub>4</sub> emissions due to OH over most of the tropical regions but not over South America and overall mid-high latitude regions. Also, the spatial and seasonal distributions of OH is found critical to properly infer temporal changes of regional and sectoral CH<sub>4</sub> emissions.

715 Top-down inversions, particularly variational Bayesian systems, are powerful tools to infer greenhouse  
gas budgets, in particular, methane the target of this study. However, they suffer from some limitations  
impacting the budget uncertainty. Some work has been done regarding atmospheric transport errors (e.g.,  
Locatelli et al., 2013, 2015) and sensitivity to observation constraints (Locatelli et al., 2015; Houweling  
et al., 2000), but less on the chemistry side of the budget. Overall, our study significantly contributes to  
720 assessing the impact of OH uncertainty on the CH<sub>4</sub> budget. We have shown that it is insufficient to  
consider a unique OH field, constant over time, to fully understand and assess the global CH<sub>4</sub> budget and  
its changes over time. Indeed, further work is needed to help determining OH fields to be used in future  
variational top-down inversion studies to properly account for changes in both source and sinks. There  
are different ways to optimize the current OH fields. One way can be to build semi-empirical OH fields  
725 by combining atmospheric chemistry models and observation-based meteorological data and chemical  
species concentrations (e.g. NO<sub>x</sub>, CO, VOCs. etc) as initiated in Spivakovsky et al. (2000); another way  
is conducting multi-species variational inversion of OH (e.g. Zheng et al., 2019) with such HFC species  
(Liang et al., 2017), formaldehyde (Glenn et al., 2019), CH<sub>4</sub> (Zhang et al., 2018; Maasakkers et al., 2019),  
or CO (Zheng et al., 2019). In addition, as suggested by Prather et al. (2017), the OH inversion would  
730 benefit from including in their prior data the responses of [OH] to variations of the precursor emissions  
(e.g. biomass burning and lighting) using the uncertainties estimated by 3D models. These resulting OH  
fields should include a mean 3D global [OH] distribution, associated with temporal variations and  
uncertainties. A lot remains to be done to better constrain the chemistry side of the global methane budget,  
a critical step toward its closure.

735

### **Data availability**

The CCMI OH fields are available at the Centre for Environmental Data Analysis  
(CEDA; <http://data.ceda.ac.uk/badc/wcrp-ccmi/data/CCMI-1/output>; Hegglin and Lamarque, 2015), the  
Natural Environment Research Council's Data Repository for Atmospheric Science and Earth  
740 Observation. The CESM1-WACCM outputs for CCMI are available

at <http://www.earthsystemgrid.org> (Climate Data Gateway at NCAR, 2019). The surface observations for CH<sub>4</sub> inversions are available at the World Data Centre for Greenhouse Gases (WDCGG, <https://gaw.kishou.go.jp/>, 2019). Other datasets, including INCA OH fields and optimized CH<sub>4</sub> emissions, can be accessed by contacting the corresponding author.

745

### **Author contributions**

YZ, MS, and PB designed the inversion experiments, analyzed results, and wrote the manuscript. BZ and XL helped with data preparation and inversion setup. JC and RJ discussed the results. AB developed the LMDz code for running CH<sub>4</sub> inversions. MH provided the CCMI OH fields. DW, ED, MR, and RL provided the atmospheric in situ data. All coauthors commented on the paper.

750

### **Acknowledgements**

This work benefited from the expertise of the Global Carbon Project methane initiative.

We acknowledge the modeling groups for making their simulations available for this analysis, the joint WCRP SPARC/IGAC Chemistry–Climate Model Initiative (CCMI) for organizing and coordinating the model simulations and data analysis activity, and the British Atmospheric Data Centre (BADC) for collecting and archiving the CCMI model output.

755

### **Financial support**

This research has been supported by the Gordon and Betty Moore Foundation (grant no. GBMF5439), “Advancing Understanding of the Global Methane Cycle”.

760

### **References**

Bloom, A. A., Bowman, K. W., Lee, M., Turner, A. J., Schroeder, R., Worden, J. R., Weidner, R., McDonald, K. C., and Jacob, D. J.: A global wetland methane emissions and uncertainty dataset for atmospheric chemical transport models (WetCHARTs version 1.0), *Geosci. Model Dev.*, 10, 2141-2156, 10.5194/gmd-10-2141-2017, 2017.

765

Bousquet, P., Hauglustaine, D. A., Peylin, P., Carouge, C., and Ciais, P.: Two decades of OH variability as inferred by an inversion of atmospheric transport and chemistry of methyl chloroform, *Atmos. Chem. Phys.*, 5, 2635-2656, 10.5194/acp-5-2635-2005, 2005.

Bousquet, P., Ringeval, B., Pison, I., Dlugokencky, E. J., Brunke, E. G., Carouge, C., Chevallier, F., Fortems-Cheiney, A., Frankenberg, C., Hauglustaine, D. A., Krummel, P. B., Langenfelds, R. L., Ramonet, M., Schmidt, M., Steele, L. P., Szopa, S., Yver, C., Viovy, N., and Ciais, P.: Source attribution of the changes in atmospheric methane for 2006–2008, *Atmospheric Chemistry and Physics*, 11, 3689-3700,

770

10.5194/acp-11-3689-2011, 2011.

775 Chevallier, F., Fisher, M., Peylin, P., Serrar, S., Bousquet, P., Brón, F.-M., Chédin, A., and Ciais, P.:  
Inferring CO<sub>2</sub> sources and sinks from satellite observations: Method and application to TOVS data,  
Journal of Geophysical Research: Atmospheres, 110, D24309, 10.1029/2005jd006390, 2005.

780 Ciais, P., Sabine, C., Bala, G., Bopp, L., Brovkin, V., al, e., and House, J. I.: Carbon and Other  
Biogeochemical Cycles, in: Climate Change 2013: The Physical Science Basis. Contribution of Working  
Group I to the Fifth Assessment Report of the Intergovernmental Panel on Climate Change Change,  
Cambridge University Press, Cambridge, United Kingdom and New York, NY, USA., 465–570, 2013.

Dalsøren, S. B., Myhre, C. L., Myhre, G., Gomez-Pelaez, A. J., Sørve, O. A., Isaksen, I. S. A., Weiss, R.  
F., and Harth, C. M.: Atmospheric methane evolution the last 40 years, Atmospheric Chemistry and  
Physics, 16, 3099-3126, 10.5194/acp-16-3099-2016, 2016.

785 Dee, D. P., Uppala, S. M., Simmons, A. J., Berrisford, P., Poli, P., Kobayashi, S., Andrae, U., Balmaseda,  
M. A., Balsamo, G., Bauer, P., Bechtold, P., Beljaars, A. C. M., van de Berg, L., Bidlot, J., Bormann, N.,  
Delsol, C., Dragani, R., Fuentes, M., Geer, A. J., Haimberger, L., Healy, S. B., Hersbach, H., Hóm, E. V.,  
Isaksen, L., Källberg, P., Köhler, M., Matricardi, M., McNally, A. P., Monge-Sanz, B. M., Morcrette, J.-  
J., Park, B.-K., Peubey, C., de Rosnay, P., Tavolato, C., Thépaut, J.-N., and Vitart, F.: The ERA-Interim  
790 reanalysis: configuration and performance of the data assimilation system, Quarterly Journal of the Royal  
Meteorological Society, 137, 553-597, doi:10.1002/qj.828, 2011.

Dlugokencky, E., Steele, L., Lang, P., and Masarie, K.: The growth rate and distribution of atmospheric  
methane, Journal of Geophysical Research: Atmospheres, 99, 17021-17043, 1994.

Dlugokencky, NOAA/ESRL ,[www.esrl.noaa.gov/gmd/ccgg/trends\\_ch4/](http://www.esrl.noaa.gov/gmd/ccgg/trends_ch4/), 2018

795 Emanuel, K. A.: A Scheme for Representing Cumulus Convection in Large-Scale Models, Journal of the  
Atmospheric Sciences, 48, 2313-2329, doi:10.1175/1520-0469(1991)048<2313:ASFRCC>2.0.CO;2,  
1991.

Etheridge, D. M., Steele, L. P., Francey, R. J., and Langenfelds, R. L.: Atmospheric methane between  
1000 A.D. and present: Evidence of anthropogenic emissions and climatic variability, Journal of  
Geophysical Research: Atmospheres, 103, 15979-15993, 10.1029/98jd00923, 1998.

800 Etminan, M., Myhre, G., Highwood, E. J., and Shine, K. P.: Radiative forcing of carbon dioxide, methane,  
and nitrous oxide: A significant revision of the methane radiative forcing, Geophysical Research Letters,  
43, 12,614-612,623, doi:10.1002/2016GL071930, 2016.

805 Fiore, A. M., West, J. J., Horowitz, L. W., Naik, V., and Schwarzkopf, M. D.: Characterizing the  
tropospheric ozone response to methane emission controls and the benefits to climate and air quality,  
Journal of Geophysical Research: Atmospheres, 113, 10.1029/2007jd009162, 2008.

Francey, R. J., Steele, L. P., Langenfelds, R. L., and Pak, B. C.: High Precision Long-Term Monitoring of  
Radiatively Active and Related Trace Gases at Surface Sites and from Aircraft in the Southern  
Hemisphere Atmosphere, Journal of the Atmospheric Sciences, 56, 279-285, 10.1175/1520-  
0469(1999)056<0279:hpltmo>2.0.co;2, 1999.

- 810 Gaubert, B., Worden, H. M., Arellano, A. F. J., Emmons, L. K., Tilmes, S., Barré J., Martínez Alonso, S., Vitt, F., Anderson, J. L., Alkemade, F., Houweling, S., and Edwards, D. P.: Chemical Feedback From Decreasing Carbon Monoxide Emissions, *Geophysical Research Letters*, 44, 9985-9995, 10.1002/2017gl074987, 2017.
- 815 Gilbert, J. C., and Lamaréchal, C.: Some numerical experiments with variable-storage quasi-Newton algorithms, *Mathematical programming*, 45, 407-435, 1989.
- He, J., Naik, V., Horowitz, L. W., Dlugokencky, E., and Thoning, K.: Investigation of the global methane budget over 1980–2017 using GFDL-AM4.1, *Atmos. Chem. Phys.*, 20, 805-827, 10.5194/acp-20-805-2020, 2020.
- 820 Hegglin, M. I. and Lamarque, J.-F.: The IGAC/SPARC Chemistry-Climate Model Initiative Phase-1 (CCMI-1) model data output, NCAS British Atmospheric Data Centre, [ADD ACCESS DATE], available at:<http://catalogue.ceda.ac.uk/uuid/9cc6b94df0f4469d8066d69b5df879d5>, 2015.
- Holmes, C. D., Prather, M. J., Søvde, O. A., and Myhre, G.: Future methane, hydroxyl, and their uncertainties: key climate and emission parameters for future predictions, *Atmospheric Chemistry and Physics*, 13, 285-302, 10.5194/acp-13-285-2013, 2013.
- 825 Houweling, S., Dentener, F., Lelieveld, J., Walter, B., and Dlugokencky, E.: The modeling of tropospheric methane: How well can point measurements be reproduced by a global model?, *Journal of Geophysical Research: Atmospheres*, 105, 8981-9002, 10.1029/1999jd901149, 2000.
- Kirschke, S., Bousquet, P., Ciais, P., Saunio, M., Canadell, J. G., Dlugokencky, E. J., Bergamaschi, P., Bergmann, D., Blake, D. R., Bruhwiler, L., Cameron-Smith, P., Castaldi, S., Chevallier, F., Feng, L., 830 Fraser, A., Heimann, M., Hodson, E. L., Houweling, S., Josse, B., Fraser, P. J., Krummel, P. B., Lamarque, J.-F., Langenfelds, R. L., Le Qué C., Naik, V., O'Doherty, S., Palmer, P. I., Pison, I., Plummer, D., Poulter, B., Prinn, R. G., Rigby, M., Ringeval, B., Santini, M., Schmidt, M., Shindell, D. T., Simpson, I. J., Spahni, R., Steele, L. P., Strode, S. A., Sudo, K., Szopa, S., van der Werf, G. R., Voulgarakis, A., van Weele, M., Weiss, R. F., Williams, J. E., and Zeng, G.: Three decades of global methane sources and sinks, 835 *Nature Geoscience*, 6, 813-823, <https://doi.org/10.1038/ngeo1955>, 2013.
- Lawrence, M. G., Jöckel, P., and von Kuhlmann, R.: What does the global mean OH concentration tell us?, *Atmos. Chem. Phys.*, 1, 37-49, 10.5194/acp-1-37-2001, 2001.
- Lelieveld, J., Dentener, F. J., Peters, W., and Krol, M. C.: On the role of hydroxyl radicals in the self-cleansing capacity of the troposphere, *Atmos. Chem. Phys.*, 4, 2337-2344, 10.5194/acp-4-2337-2004, 840 2004.
- Lelieveld, J., Gromov, S., Pozzer, A., and Taraborrelli, D.: Global tropospheric hydroxyl distribution, budget and reactivity, *Atmospheric Chemistry and Physics*, 16, 12477-12493, 10.5194/acp-16-12477-2016, 2016.
- 845 Levy, H.: Normal Atmosphere: Large Radical and Formaldehyde Concentrations Predicted, *Science*, 173, 141-143, 10.1126/science.173.3992.141, 1971.
- Lin, X., Ciais, P., Bousquet, P., Ramonet, M., Yin, Y., Balkanski, Y., Cozic, A., Delmotte, M., Evangelizou,

- 850 N., Indira, N. K., Locatelli, R., Peng, S., Piao, S., Saunois, M., Swathi, P. S., Wang, R., Yver-Kwok, C.,  
Tiwari, Y. K., and Zhou, L.: Simulating CH<sub>4</sub> and CO<sub>2</sub> over South and East Asia using the zoomed  
chemistry transport model LMDz-INCA, *Atmospheric Chemistry and Physics*, 18, 9475-9497,  
10.5194/acp-18-9475-2018, 2018.
- 855 Liang, Q., Chipperfield, M. P., Fleming, E. L., Abraham, N. L., Braesicke, P., Burkholder, J. B., Daniel,  
J. S., Dhomse, S., Fraser, P. J., Hardiman, S. C., Jackman, C. H., Kinnison, D. E., Krummel, P. B., Montzka,  
S. A., Morgenstern, O., McCulloch, A., Mühle, J., Newman, P. A., Orkin, V. L., Pitari, G., Prinn, R. G.,  
Rigby, M., Rozanov, E., Stenke, A., Tummon, F., Velders, G. J. M., Visionsi, D., and Weiss, R. F.: Deriving  
Global OH Abundance and Atmospheric Lifetimes for Long-Lived Gases: A Search for CH<sub>3</sub>CCl<sub>3</sub>  
Alternatives, *Journal of Geophysical Research: Atmospheres*, 122, 9114-9119, 2017,  
10.1002/2017jd026926, 2017.
- 860 Lin, X., Ciais, P., Bousquet, P., Ramonet, M., Yin, Y., Balkanski, Y., Cozic, A., Delmotte, M., Evangeliou,  
N., Indira, N. K., Locatelli, R., Peng, S., Piao, S., Saunois, M., Swathi, P. S., Wang, R., Yver-Kwok, C.,  
Tiwari, Y. K., and Zhou, L.: Simulating CH<sub>4</sub> and CO<sub>2</sub> over South and East Asia using the zoomed  
chemistry transport model LMDz-INCA, *Atmospheric Chemistry and Physics*, 18, 9475-9497,  
10.5194/acp-18-9475-2018, 2018.
- 865 Locatelli, R., Bousquet, P., Chevallier, F., Fortems-Cheney, A., Szopa, S., Saunois, M., Agusti-Panareda,  
A., Bergmann, D., Bian, H., Cameron-Smith, P., Chipperfield, M. P., Gloor, E., Houweling, S., Kawa, S.  
R., Krol, M., Patra, P. K., Prinn, R. G., Rigby, M., Saito, R., and Wilson, C.: Impact of transport model  
errors on the global and regional methane emissions estimated by inverse modelling, *Atmos. Chem. Phys.*,  
13, 9917-9937, 10.5194/acp-13-9917-2013, 2013.
- 870 Locatelli, R., Bousquet, P., Hourdin, F., Saunois, M., Cozic, A., Couvreux, F., Grandpeix, J. Y., Lefebvre,  
M. P., Rio, C., Bergamaschi, P., Chambers, S. D., Karstens, U., Kazan, V., van der Laan, S., Meijer, H. A.  
J., Moncrieff, J., Ramonet, M., Scheeren, H. A., Schlosser, C., Schmidt, M., Vermeulen, A., and Williams,  
A. G.: Atmospheric transport and chemistry of trace gases in LMDz5B: evaluation and implications for  
inverse modelling, *Geosci. Model Dev.*, 8, 129-150, 10.5194/gmd-8-129-2015, 2015.
- 875 Logan, J. A., Prather, M. J., Wofsy, S. C., and McElroy, M. B.: Tropospheric chemistry: A global  
perspective, *Journal of Geophysical Research*, 86, 7210, 10.1029/JC086iC08p07210, 1981.
- 880 Maasackers, J. D., Jacob, D. J., Sulprizio, M. P., Scarpelli, T. R., Nesser, H., Sheng, J. X., Zhang, Y.,  
Hersher, M., Bloom, A. A., Bowman, K. W., Worden, J. R., Janssens-Maenhout, G., and Parker, R. J.:  
Global distribution of methane emissions, emission trends, and OH concentrations and trends inferred  
from an inversion of GOSAT satellite data for 2010–2015, *Atmos. Chem. Phys.*, 19, 7859-7881,  
10.5194/acp-19-7859-2019, 2019.
- 880 McNorton, J., Chipperfield, M. P., Gloor, M., Wilson, C., Feng, W., Hayman, G. D., Rigby, M., Krummel,  
P. B., and Doherty, S., Prinn, R. G., Weiss, R. F., Young, D., Dlugokencky, E., and Montzka, S. A.:  
Role of OH variability in the stalling of the global atmospheric CH<sub>4</sub> growth rate  
from 1999 to 2006, *Atmospheric Chemistry and Physics*, 16, 7943-7956, 10.5194/acp-16-7943-2016,

2016.

885 McNorton, J., Wilson, C., Gloor, M., Parker, R. J., Boesch, H., Feng, W., Hossaini, R., and Chipperfield, M. P.: Attribution of recent increases in atmospheric methane through 3-D inverse modelling, *Atmos. Chem. Phys.*, 18, 18149-18168, 10.5194/acp-18-18149-2018, 2018.

890 Melton, J. R., Wania, R., Hodson, E. L., Poulter, B., Ringeval, B., Spahni, R., Bohn, T., Avis, C. A., Beerling, D. J., Chen, G., Eliseev, A. V., Denisov, S. N., Hopcroft, P. O., Lettenmaier, D. P., Riley, W. J., Singarayer, J. S., Subin, Z. M., Tian, H., Zürcher, S., Brovkin, V., van Bodegom, P. M., Kleinen, T., Yu, Z. C., and Kaplan, J. O.: Present state of global wetland extent and wetland methane modelling: conclusions from a model inter-comparison project (WETCHIMP), *Biogeosciences*, 10, 753-788, 10.5194/bg-10-753-2013, 2013.

895 Montzka, S. A., Krol, M., Dlugokencky, E., Hall, B., Jöckel, P., and Lelieveld, J.: Small Interannual Variability of Global Atmospheric Hydroxyl, *Science*, 331, 67-69, 10.1126/science.1197640, 2011.

900 Morgenstern, O., Hegglin, M. I., Rozanov, E., amp, apos, Connor, F. M., Abraham, N. L., Akiyoshi, H., Archibald, A. T., Bekki, S., Butchart, N., Chipperfield, M. P., Deushi, M., Dhomse, S. S., Garcia, R. R., Hardiman, S. C., Horowitz, L. W., Jöckel, P., Josse, B., Kinnison, D., Lin, M., Mancini, E., Manyin, M. E., Marchand, M., Mar écal, V., Michou, M., Oman, L. D., Pitari, G., Plummer, D. A., Revell, L. E., Saint-Martin, D., Schofield, R., Stenke, A., Stone, K., Sudo, K., Tanaka, T. Y., Tilmes, S., Yamashita, Y., Yoshida, K., and Zeng, G.: Review of the global models used within phase 1 of the Chemistry–Climate Model Initiative (CCMI), *Geoscientific Model Development*, 10, 639-671, 10.5194/gmd-10-639-2017, 2017.

905 Murray, L. T., Logan, J. A., and Jacob, D. J.: Interannual variability in tropical tropospheric ozone and OH: The role of lightning, *Journal of Geophysical Research: Atmospheres*, 118, 11,468-411,480, 10.1002/jgrd.50857, 2013.

Murray, L. T., Mickley, L. J., Kaplan, J. O., Sofen, E. D., Pfeiffer, M., and Alexander, B.: Factors controlling variability in the oxidative capacity of the troposphere since the Last Glacial Maximum, *Atmospheric Chemistry and Physics*, 14, 3589-3622, 10.5194/acp-14-3589-2014, 2014.

910 Naik, V., Voulgarakis, A., Fiore, A. M., Horowitz, L. W., Lamarque, J. F., Lin, M., Prather, M. J., Young, P. J., Bergmann, D., Cameron-Smith, P. J., Cionni, I., Collins, W. J., Dals øren, S. B., Doherty, R., Eyring, V., Faluvegi, G., Folberth, G. A., Josse, B., Lee, Y. H., MacKenzie, I. A., Nagashima, T., van Noije, T. P. C., Plummer, D. A., Righi, M., Rumbold, S. T., Skeie, R., Shindell, D. T., Stevenson, D. S., Strode, S., Sudo, K., Szopa, S., and Zeng, G.: Preindustrial to present-day changes in tropospheric hydroxyl radical and methane lifetime from the Atmospheric Chemistry and Climate Model Intercomparison Project (ACCMIP), *Atmospheric Chemistry and Physics*, 13, 5277-5298, 10.5194/acp-13-5277-2013, 2013.

915 Naus, S., Montzka, S. A., Pandey, S., Basu, S., Dlugokencky, E. J., and Krol, M.: Constraints and biases in a tropospheric two-box model of OH, *Atmos. Chem. Phys.*, 19, 407-424, 10.5194/acp-19-407-2019, 2019.

920 Nguyen, N. H., Turner, A. J., Yin, Y., Prather, M. J., and Frankenberg, C.: Effects of Chemical Feedbacks

- on Decadal Methane Emissions Estimates, *Geophysical Research Letters*, 47, e2019GL085706, 10.1029/2019gl085706, 2020.
- Nicely, J. M., Duncan, B. N., Hanisco, T. F., Wolfe, G. M., Salawitch, R. J., Deushi, M., Haslerud, A. S., Jöckel, P., Josse, B., Kinnison, D. E., Klekociuk, A., Manyin, M. E., Marćal, V., Morgenstern, O., Murray, L. T., Myhre, G., Oman, L. D., Pitari, G., Pozzer, A., Quaglia, I., Revell, L. E., Rozanov, E., Stenke, A., Stone, K., Strahan, S., Tilmes, S., Tost, H., Westervelt, D. M., and Zeng, G.: A machine learning examination of hydroxyl radical differences among model simulations for CCMI-1, *Atmos. Chem. Phys.*, 20, 1341-1361, 10.5194/acp-20-1341-2020, 2020.
- Patra, P. K., Houweling, S., Krol, M., Bousquet, P., Belikov, D., Bergmann, D., Bian, H., Cameron-Smith, P., Chipperfield, M. P., Corbin, K., Fortems-Cheiney, A., Fraser, A., Gloor, E., Hess, P., Ito, A., Kawa, S. R., Law, R. M., Loh, Z., Maksyutov, S., Meng, L., Palmer, P. I., Prinn, R. G., Rigby, M., Saito, R., and Wilson, C.: TransCom model simulations of CH<sub>4</sub> and related species: linking transport, surface flux and chemical loss with CH<sub>4</sub> variability in the troposphere and lower stratosphere, *Atmospheric Chemistry and Physics*, 11, 12813-12837, 10.5194/acp-11-12813-2011, 2011.
- Patra, P. K., Krol, M. C., Montzka, S. A., Arnold, T., Atlas, E. L., Lintner, B. R., Stephens, B. B., Xiang, B., Elkins, J. W., Fraser, P. J., Ghosh, A., Hints, E. J., Hurst, D. F., Ishijima, K., Krummel, P. B., Miller, B. R., Miyazaki, K., Moore, F. L., Muhle, J., O'Doherty, S., Prinn, R. G., Steele, L. P., Takigawa, M., Wang, H. J., Weiss, R. F., Wofsy, S. C., and Young, D.: Observational evidence for interhemispheric hydroxyl-radical parity, *Nature*, 513, 219-223, 10.1038/nature13721, 2014.
- Pison, I., Bousquet, P., Chevallier, F., Szopa, S., and Hauglustaine, D.: Multi-species inversion of CH<sub>4</sub>, CO and H<sub>2</sub> emissions from surface measurements, *Atmos. Chem. Phys.*, 9, 5281-5297, 10.5194/acp-9-5281-2009, 2009.
- Prather, M. J., Holmes, C. D., and Hsu, J.: Reactive greenhouse gas scenarios: Systematic exploration of uncertainties and the role of atmospheric chemistry, *Geophysical Research Letters*, 39, L09803, doi:10.1029/2012GL051440, 2012.
- Prather, M. J., and Holmes, C. D.: Overexplaining or underexplaining methane's role in climate change, *Proceedings of the National Academy of Sciences*, 114, 5324-5326, 10.1073/pnas.1704884114, 2017.
- Prinn, R. G., Huang, J., Weiss, R. F., Cunnold, D. M., Fraser, P. J., Simmonds, P. G., McCulloch, A., Harth, C., Salameh, P., O'Doherty, S., Wang, R. H. J., Porter, L., and Miller, B. R.: Evidence for Substantial Variations of Atmospheric Hydroxyl Radicals in the Past Two Decades, *Science*, 292, 1882-1888, 10.1126/science.1058673, 2001.
- Rigby, M., Prinn, R. G., Fraser, P. J., Simmonds, P. G., Langenfelds, R. L., Huang, J., Cunnold, D. M., Steele, L. P., Krummel, P. B., Weiss, R. F., O'Doherty, S., Salameh, P. K., Wang, H. J., Harth, C. M., Mühle, J., and Porter, L. W.: Renewed growth of atmospheric methane, *Geophysical Research Letters*, 35, L22805, 10.1029/2008gl036037, 2008.
- Rigby, M., Montzka, S. A., Prinn, R. G., White, J. W. C., Young, D., O'Doherty, S., Lunt, M. F., Ganesan, A. L., Manning, A. J., Simmonds, P. G., Salameh, P. K., Harth, C. M., Muhle, J., Weiss, R. F., Fraser, P.

- J., Steele, L. P., Krummel, P. B., McCulloch, A., and Park, S.: Role of atmospheric oxidation in recent methane growth, *Proc Natl Acad Sci U S A*, 114, 5373-5377, 10.1073/pnas.1616426114, 2017.
- 960 Saunois, M., Bousquet, P., Poulter, B., Peregon, A., Ciais, P., Canadell, J. G., Dlugokencky, E. J., Etiope, G., Bastviken, D., Houweling, S., Janssens-Maenhout, G., Tubiello, F. N., Castaldi, S., Jackson, R. B., Alexe, M., Arora, V. K., Beerling, D. J., Bergamaschi, P., Blake, D. R., Brailsford, G., Brovkin, V., Bruhwiler, L., Crevoisier, C., Crill, P., Covey, K., Curry, C., Frankenberg, C., Gedney, N., Höglund-Isaksson, L., Ishizawa, M., Ito, A., Joos, F., Kim, H. S., Kleinen, T., Krummel, P., Lamarque, J. F.,
- 965 Langenfelds, R., Locatelli, R., Machida, T., Maksyutov, S., McDonald, K. C., Marshall, J., Melton, J. R., Morino, I., Naik, V., O'Doherty, S., Parmentier, F. J. W., Patra, P. K., Peng, C., Peng, S., Peters, G. P., Pison, I., Prigent, C., Prinn, R., Ramonet, M., Riley, W. J., Saito, M., Santini, M., Schroeder, R., Simpson, I. J., Spahni, R., Steele, P., Takizawa, A., Thornton, B. F., Tian, H., Tohjima, Y., Viovy, N., Voulgarakis, A., van Weele, M., van der Werf, G. R., Weiss, R., Wiedinmyer, C., Wilton, D. J., Wiltshire, A., Worthy, D., Wunch, D., Xu, X., Yoshida, Y., Zhang, B., Zhang, Z., and Zhu, Q.: The global methane budget 2000–
- 970 2012, *Earth Syst. Sci. Data*, 8, 697-751, 10.5194/essd-8-697-2016, 2016.
- Saunois, M., Bousquet, P., Poulter, B., Peregon, A., Ciais, P., Canadell, J. G., Dlugokencky, E. J., Etiope, G., Bastviken, D., Houweling, S., Janssens-Maenhout, G., Tubiello, F. N., Castaldi, S., Jackson, R. B., Alexe, M., Arora, V. K., Beerling, D. J., Bergamaschi, P., Blake, D. R., Brailsford, G., Bruhwiler, L.,
- 975 Crevoisier, C., Crill, P., Covey, K., Frankenberg, C., Gedney, N., Höglund-Isaksson, L., Ishizawa, M., Ito, A., Joos, F., Kim, H. S., Kleinen, T., Krummel, P., Lamarque, J. F., Langenfelds, R., Locatelli, R., Machida, T., Maksyutov, S., Melton, J. R., Morino, I., Naik, V., O'Doherty, S., Parmentier, F. J. W., Patra, P. K., Peng, C., Peng, S., Peters, G. P., Pison, I., Prinn, R., Ramonet, M., Riley, W. J., Saito, M., Santini, M., Schroeder, R., Simpson, I. J., Spahni, R., Takizawa, A., Thornton, B. F., Tian, H., Tohjima, Y., Viovy, N.,
- 980 Voulgarakis, A., Weiss, R., Wilton, D. J., Wiltshire, A., Worthy, D., Wunch, D., Xu, X., Yoshida, Y., Zhang, B., Zhang, Z., and Zhu, Q.: Variability and quasi-decadal changes in the methane budget over the period 2000–2012, *Atmos. Chem. Phys.*, 17, 11135-11161, 10.5194/acp-17-11135-2017, 2017.
- Saunois, M., Stavert, A. R., Poulter, B., Bousquet, P., Canadell, J. G., Jackson, R. B., Raymond, P. A., Dlugokencky, E. J., Houweling, S., Patra, P. K., Ciais, P., Arora, V. K., Bastviken, D., Bergamaschi, P.,
- 985 Blake, D. R., Brailsford, G., Bruhwiler, L., Carlson, K. M., Carrol, M., Castaldi, S., Chandra, N., Crevoisier, C., Crill, P. M., Covey, K., Curry, C. L., Etiope, G., Frankenberg, C., Gedney, N., Hegglin, M. I., Höglund-Isakson, L., Hugelius, G., Ishizawa, M., Ito, A., Janssens-Maenhout, G., Jensen, K. M., Joos, F., Kleinen, T., Krummel, P. B., Langenfelds, R. L., Laruelle, G. G., Liu, L., Machida, T., Maksyutov, S., McDonald, K. C., McNorton, J., Miller, P. A., Melton, J. R., Morino, I., Müller, J., Murgia-Flores, F.,
- 990 Naik, V., Niwa, Y., Noce, S., O'Doherty, S., Parker, R. J., Peng, C., Peng, S., Peters, G. P., Prigent, C., Prinn, R., Ramonet, M., Regnier, P., Riley, W. J., Rosentretter, J. A., Segers, A., Simpson, I. J., Shi, H., Smith, S. J., Steele, L. P., Thornton, B. F., Tian, H., Tohjima, Y., Tubiello, F. N., Tsuruta, A., Viovy, N., Voulgarakis, A., Weber, T. S., van Weele, M., van der Werf, G. R., Weiss, R. F., Worthy, D., Wunch, D., Yin, Y., Yoshida, Y., Zhang, W., Zhang, Z., Zhao, Y., Zheng, B., Zhu, Q., Zhu, Q., and Zhuang, Q.: The

- 995 Global Methane Budget 2000-2017, *Earth Syst. Sci. Data Discuss.*, 2019, 1-136, 10.5194/essd-2019-128, 2019.
- Spivakovsky, C. M., Logan, J. A., Montzka, S. A., Balkanski, Y. J., Foreman-Fowler, M., Jones, D. B. A., Horowitz, L. W., Fusco, A. C., Brenninkmeijer, C. A. M., Prather, M. J., Wofsy, S. C., and McElroy, M. B.: Three-dimensional climatological distribution of tropospheric OH: Update and evaluation, *Journal of Geophysical Research: Atmospheres*, 105, 8931-8980, 10.1029/1999jd901006, 2000.
- 1000 Szopa, S., Balkanski, Y., Schulz, M., Bekki, S., Cugnet, D., Fortems-Cheiney, A., Turquety, S., Cozic, A., D'andréis, C., Hauglustaine, D., Idelkadi, A., Lathi ère, J., Lefevre, F., Marchand, M., Vuolo, R., Yan, N., and Dufresne, J.-L.: Aerosol and ozone changes as forcing for climate evolution between 1850 and 2100, *Climate Dynamics*, 40, 2223-2250, 10.1007/s00382-012-1408-y, 2013.
- 1005 Terrenoire, E., D. A. Hauglustaine, R. Valorso, and A. Cozic, Impact of present and future aircraft NO<sub>x</sub> and aerosol emissions on atmospheric composition and radiative forcing of climate, *Atmos. Chem. Phys.* in preparation, 2019.
- Tiedtke, M.: A Comprehensive Mass Flux Scheme for Cumulus Parameterization in Large-Scale Models, *Monthly Weather Review*, 117, 1779-1800, 10.1175/1520-0493(1989)117<1779:acmfsf>2.0.co;2, 1989.**
- 1010 Tohjima, Y., Kubo, M., Minejima, C., Mukai, H., Tanimoto, H., Ganshin, A., Maksyutov, S., Katsumata, K., Machida, T., and Kita, K.: Temporal changes in the emissions of CH<sub>4</sub> and CO from China estimated from CH<sub>4</sub>/CO<sub>2</sub> and CO / CO<sub>2</sub> correlations observed at Hateruma Island, *Atmos. Chem. Phys.*, 14, 1663-1677, 10.5194/acp-14-1663-2014, 2014.
- Turner, A. J., Frankenberg, C., Wennberg, P. O., and Jacob, D. J.: Ambiguity in the causes for decadal trends in atmospheric methane and hydroxyl, *Proc Natl Acad Sci U S A*, 114, 5367-5372, 10.1073/pnas.1616020114, 2017.
- 1015 Turner, A. J., Frankenberg, C., and Kort, E. A.: Interpreting contemporary trends in atmospheric methane, *Proceedings of the National Academy of Sciences*, 116, 2805-2813, 10.1073/pnas.1814297116, 2019.
- Voulgarakis, A., Naik, V., Lamarque, J. F., Shindell, D. T., Young, P. J., Prather, M. J., Wild, O., Field, R. D., Bergmann, D., Cameron-Smith, P., Cionni, I., Collins, W. J., Dals øren, S. B., Doherty, R. M., Eyring, V., Faluvegi, G., Folberth, G. A., Horowitz, L. W., Josse, B., MacKenzie, I. A., Nagashima, T., Plummer, D. A., Righi, M., Rumbold, S. T., Stevenson, D. S., Strode, S. A., Sudo, K., Szopa, S., and Zeng, G.: Analysis of present day and future OH and methane lifetime in the ACCMIP simulations, *Atmospheric Chemistry and Physics*, 13, 2563-2587, 10.5194/acp-13-2563-2013, 2013.
- 1025 Wolfe, G. M., Nicely, J. M., St. Clair, J. M., Hanisco, T. F., Liao, J., Oman, L. D., Brune, W. B., Miller, D., Thames, A., Gonz ález Abad, G., Ryerson, T. B., Thompson, C. R., Peischl, J., McKain, K., Sweeney, C., Wennberg, P. O., Kim, M., Crouse, J. D., Hall, S. R., Ullmann, K., Diskin, G., Bui, P., Chang, C., and Dean-Day, J.: Mapping hydroxyl variability throughout the global remote troposphere via synthesis of airborne and satellite formaldehyde observations, *Proceedings of the National Academy of Sciences*, 116, 11171-11180, 10.1073/pnas.1821661116, 2019.
- 1030 Zhang, Y., Jacob, D. J., Maasackers, J. D., Sulprizio, M. P., Sheng, J. X., Gautam, R., and Worden, J.:

Monitoring global tropospheric OH concentrations using satellite observations of atmospheric methane, *Atmos. Chem. Phys.*, 18, 15959-15973, 10.5194/acp-18-15959-2018, 2018.

1035 Zhao, Y., Saunio, M., Bousquet, P., Lin, X., Berchet, A., Hegglin, M. I., Canadell, J. G., Jackson, R. B., Hauglustaine, D. A., Szopa, S., Stavert, A. R., Abraham, N. L., Archibald, A. T., Bekki, S., Deushi, M., Jöckel, P., Josse, B., Kinnison, D., Kirner, O., Maréchal, V., O'Connor, F. M., Plummer, D. A., Revell, L. E., Rozanov, E., Stenke, A., Strode, S., Tilmes, S., Dlugokencky, E. J., and Zheng, B.: Inter-model comparison of global hydroxyl radical (OH) distributions and their impact on atmospheric methane over the 2000–2016 period, *Atmos. Chem. Phys.*, 19, 13701-13723, 10.5194/acp-19-13701-2019, 2019.

1040 Zhao, Y., Saunio, M., Bousquet, P., Lin, X., Berchet, A., Hegglin, M. I., Canadell, J. G., Jackson, R. B., Deushi, M., Jöckel, P., Kinnison, D., Kirner, O., Strode, S., Tilmes, S., Dlugokencky, E. J., and Zheng, B.: On the role of trend and variability of hydroxyl radical (OH) in the global methane budget, *Atmos. Chem. Phys. Discuss.*, 2020, 1-28, 10.5194/acp-2020-308, 2020.

1045 Zheng, B., Chevallier, F., Yin, Y., Ciais, P., Fortems-Cheiney, A., Deeter, M. N., Parker, R. J., Wang, Y., Worden, H. M., and Zhao, Y.: Global atmospheric carbon monoxide budget 2000–2017 inferred from multi-species atmospheric inversions, *Earth Syst. Sci. Data*, 11, 1411-1436, 10.5194/essd-11-1411-2019, 2019.

**Table 1.** Global tropospheric mean [OH] ( $\times 10^5$  molec  $\text{cm}^{-3}$ ) and inter-hemispheric OH ratios (N/S) averaged over 2000-2002 for 10 OH fields used in this study. The global tropospheric [OH] weighted by reaction with  $\text{CH}_4$  ( $[\text{OH}]_{\text{GM-CH}_4}$ ) and weighted by dry air-mass ( $[\text{OH}]_{\text{GM-M}}$ ) are both given.

	$[\text{OH}]_{\text{GM-CH}_4}$	$[\text{OH}]_{\text{GM-M}}$	N/S
TransCom	10.6	10.0	1.0
INCA NMHC-AER-S	10.3	9.4	1.3
INCA NMHC	11.1	10.4	1.2
CESM1-WACCM	11.9	11.4	1.3
CMAM	12.2	11.3	1.2
EMAC-L90MA	11.8	11.5	1.2
GEOSCCM	12.6	12.3	1.2
MOCAGE	15.0	12.5	1.5
MRI-ESM1r1	10.9	10.6	1.2
SOCOL3	16.3	14.4	1.5
Mean $\pm$ SD	12.3 $\pm$ 3.8	11.4 $\pm$ 2.8	1.3 $\pm$ 0.3
Mean $\pm$ SD (8 OH) <sup>1</sup>	11.3 $\pm$ 0.8	10.9 $\pm$ 0.9	1.2 $\pm$ 0.1

<sup>1</sup> The OH fields simulated by SOCOL3 and MOCAGE are excluded.

**Table 2.** The global total, hemispheric  $\text{CH}_4$  emissions, and inter-hemispheric difference of  $\text{CH}_4$  emissions calculated by Inv1 and Inv2 during the early 2000s (2000/07/01-2002/06/01) in  $\text{Tg yr}^{-1}$ .

Unit: $\text{Tg yr}^{-1}$	Inv1 original OH				Inv2 scaled OH			
	Global	0-90°N	90°S-0	N-S <sub>Inv1</sub>	Global	0-90°N	90°S-0	N-S <sub>Inv2</sub>
<b>Prior</b>	522	384	138	246	522	384	138	246
<b>TransCom</b>	530	368	162	206	549	377	172	205
INCA NMHC-AER-S	518	380	138	242	553	399	154	245
INCA NMHC	552	392	160	232	552	392	160	232
CESM1-WACCM	587	420	166	254	551	400	151	249
CMAM	599	419	180	239	553	399	154	245
EMAC-L90MA	589	414	175	239	555	396	159	237
GEOSCCM	611	424	187	237	550	392	159	233

<b>MOCAGE</b>	716	/ <sup>a</sup>	/	/	/	/	/	/	/
<b>MRI-ESM1r1</b>	553	396	156	240	548	396	152	244	
<b>SOCOL3</b>	757	/	/	/	/	/	/	/	
<b>Mean±SD</b>	601±78	401±21	166±15	236±14	551±2	393±7	158±7	236±14	

<sup>a</sup> We do not analyze the hemispheric CH<sub>4</sub> emission estimated with MOCAGE and SOCOL3 OH field since inversions using the two OH fields calculate much higher CH<sub>4</sub> emissions than using other OH fields.

**Table 3.** Global, latitudinal, and regional CH<sub>4</sub> emission in Tg yr<sup>-1</sup> (mean±SD and the [min-max] range of the inversions) calculated by Inv1 and Inv2 during the early 2000s (2000/07/01-2002/06/01) in Tg yr<sup>-1</sup> (excluding MOCAGE and SOCOL-3). The uncertainties (Unc.= (max – min)/multi-inversions mean) lead by using different OH fields are compared with the uncertainties in CH<sub>4</sub> emissions given by Sauniois et al. (2016) and Locatelli et al. (2013).

Study	This study (Impact of OH)				Sauniois et al. (2016)	Locatelli et al. (2013)
Period	2000/07/01-2002/06/01				2000-2009	2005
Experiment	Inv1 (Original OH)		Inv2 (Scaled OH)		TD ensemble	Transport model errors
Region	Mean±SD[range <sup>1</sup> ]	Unc.	Mean±SD [range]	Unc.	Unc.	Unc.
global	567±34[518-611]	17%	551±2[548-555]	1%	6%	5%
60 °-90 °N	29±1[27-30]	12%	29±1[27-30]	12%	50%	10%(NH)
30 °N-60 °N	174±8[158-183]	14%	172±6[159-178]	11%	20%	
0 °-30 °N	199±14[178-217]	20%	192±1[191-194]	1%	13% (<30 °N)	
0 °-30 °S	147±14[121-167]	30%	140±6[133-153]	14%		24%(SH)
30 °S-90 °S	19±1[17-20]	18%	18±1[18-19]	9%	25%	37% (North America)
America	45±2[42-48]	11%	45±1 [42-46]	8%	70%	
Canada	27±1[24-28]	17%	27±1 [24-28]	13%	43%	23%
Europe	27±1 [25-28]	12%	27±1 [25-28]	12%	31%	38%
Russia	33±1 [30-35]	13%	33±1 [30-34]	20%	11%	25% (Asia)
China	42±5 [33-50]	39%	40±3 [35-43]	3%	42%	
Southeast Asia	38±3 [34-41]	20%	37±0.3 [36-37]	4%	44%	
South Asia	59±6 [51-66]	24%	57±0.8 [56-58]			

Northern South America	73 ± 9 [58-85]	37%	69 ± 4 [65-77]	17%	44%	48% (South America)
Southern South America	33 ± 4 [27-39]	37%	31 ± 2 [29-36]	20%	94%	
Africa	76 ± 4 [68-82]	18%	74 ± 1 [73-77]	6%	42%-45%	30%

1070

**Table 4.** Global and latitudinal percentage changes of CH<sub>4</sub> reaction weighted [OH] from 2000-2002 to 2007-2009.

	90-30 S	30 S-0 °	0 °-30 N	30 °-90 N	Global
<b>TransCom</b>	0.0%	0.0%	0.0%	0.0%	0.0%
<b>INCA NMHC</b>	-0.5%	-0.9%	-0.3%	-0.2%	-0.5%
<b>CESM1-WACCM</b>	1.1%	1.6%	2.5%	1.2%	1.8%
<b>EMAC-L90MA</b>	-0.1%	0.1%	1.3%	1.1%	0.7%
<b>GEOSCCM</b>	-0.3%	1.1%	1.4%	1.0%	1.0%
<b>MRI-ESM1r1</b>	-2.0%	0.2%	2.4%	1.7%	1.1%

1075

**Table 5.** Global total emission changes (in Tg yr<sup>-1</sup>) from the early 2000s (2000/07/01-2002/06/01) to the late 2000s (2007/07/01-2009/06/01) calculated to identify the effect of OH fields (Inv3 – Inv2), of OH fixed to early 2000s (Inv4 – Inv2), and the contribution of OH changes from the early to late 2000s to top-down estimated CH<sub>4</sub> emissions changes (Inv3 – Inv4).

	Inv3 – Inv2	Inv4 – Inv2	Inv3 – Inv4
TransCom	17.2	17.2	0.0
INCA NMHC	16.6	19.3	-2.7
CESM1-WACCM	30.0	18.5	11.5
EMAC-L90MA	20.4	15.3	5.1
GEOSCCM	19.1	16.1	3.0
MRI-ESM1r1	27.8	14.3	13.5
Mean ± SD	21.9 ± 5.7	16.9 ± 1.9	5.1 ± 6.4

1080

**Table 6.** Global sectoral emission changes (in Tg yr<sup>-1</sup>) from the early 2000s (2000/07/01-2002/06/01) to the late 2000s (2007/07/01-2009/06/01) (mean ±SD and the [min-max] range).

	Inv3—Inv2	Inv4—Inv2	Inv3—Inv4	Prior
Wetland	-3.5 ±2.5[-6.4- -0.3]	-5.6 ±1.3[-6.8- -3.0]	2.1 ±3.4[3.3-4.8]	0.0
Agri-waste	14.2 ±2.1[12.2-17.2]	12.3 ±0.7[11.1-13.2]	1.9 ±2.3[-0.4-5.3]	19.0
Fossil fuel	8.7 ±0.8[8.0-10.1]	8.1 ±0.8[7.1-9.6]	0.6 ±0.9[-0.1-2.2]	18.0
Other	2.4 ±0.5[2.1-3.1]	2.0 ±0.2[1.7-2.2]	0.5 ±0.5[-0.1-1.2]	2.5
Total	21.9 ±5.7[16.7-30.0]	16.8 ±1.9[14.3-19.3]	5.1 ±6.4[-2.5-13.1]	39.4

## Figures

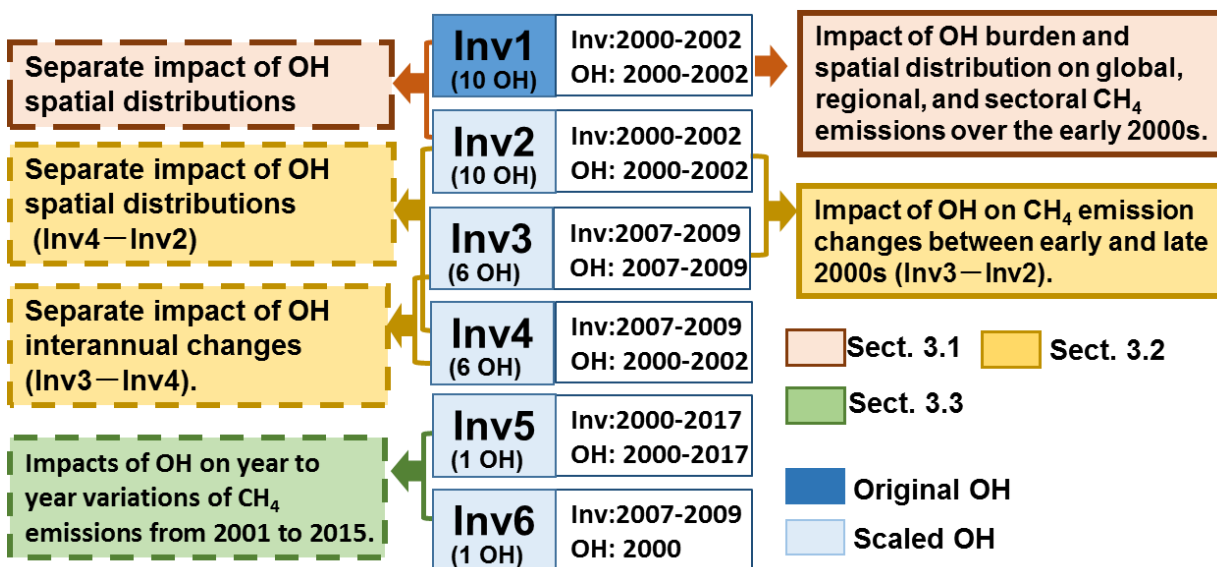
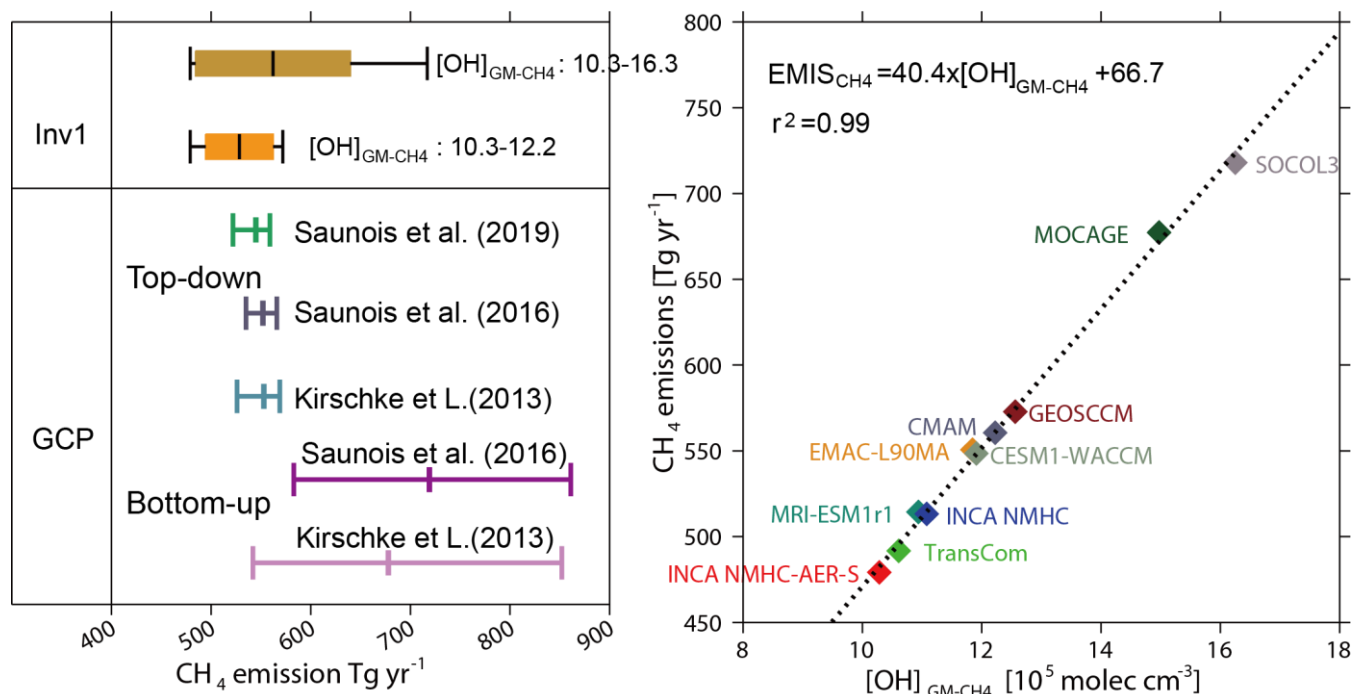


**Figure 1.** A diagram showing inversion experiments (Inv1–Inv6) performed in this study. For each experiment, “Inv” gives the time period of inversion, and “OH” gives the time period of the OH fields used in the inversion. Inv1 is performed using the original OH field, whereas Inv2–Inv5 are performed using scaled OH fields. The colored boxes on the left and right show analyses of inversions we did to examine the OH impacts on inverted CH<sub>4</sub> emissions. The brown, yellow, and green textboxes correspond to analyses presented in Section 3.1, Section 3.2, and Section 3.3, respectively.



1100 **Figure 2.** Left: The global CH<sub>4</sub> emissions from Inv1 (averaged over 2000/07/01-2002/06/01). The  
 1105 bottom-up and top-down estimations over 2000-2009 from previous GCP (Kirschke et al., 2013; Saunois  
 et al., 2016; 2019) are also presented for comparison. The brown box plot shows the inversion results  
 using 10 OH fields, while the orange one shows the results that exclude the largest estimates from the  
 SOCOL3 and MOCAGE OH fields. The left, middle and right whisker chart (vertical lines) represent the  
 minimum, mean, and maximum values of different inversion, and the left and right edges of boxes  
 represent the mean  $\pm$ one standard deviation. The definition of the box plot is applicable to all those  
 hereafter. Right: The relationship between the optimized CH<sub>4</sub> emissions (Tg yr<sup>-1</sup>) in Inv1 and the  
 corresponding [OH]<sub>GM-CH<sub>4</sub></sub> ( $\times 10^5$  mole cm<sup>-3</sup>). The correlation coefficient (r) and the linear regression  
 equation fitted to the data are shown inset.

1110

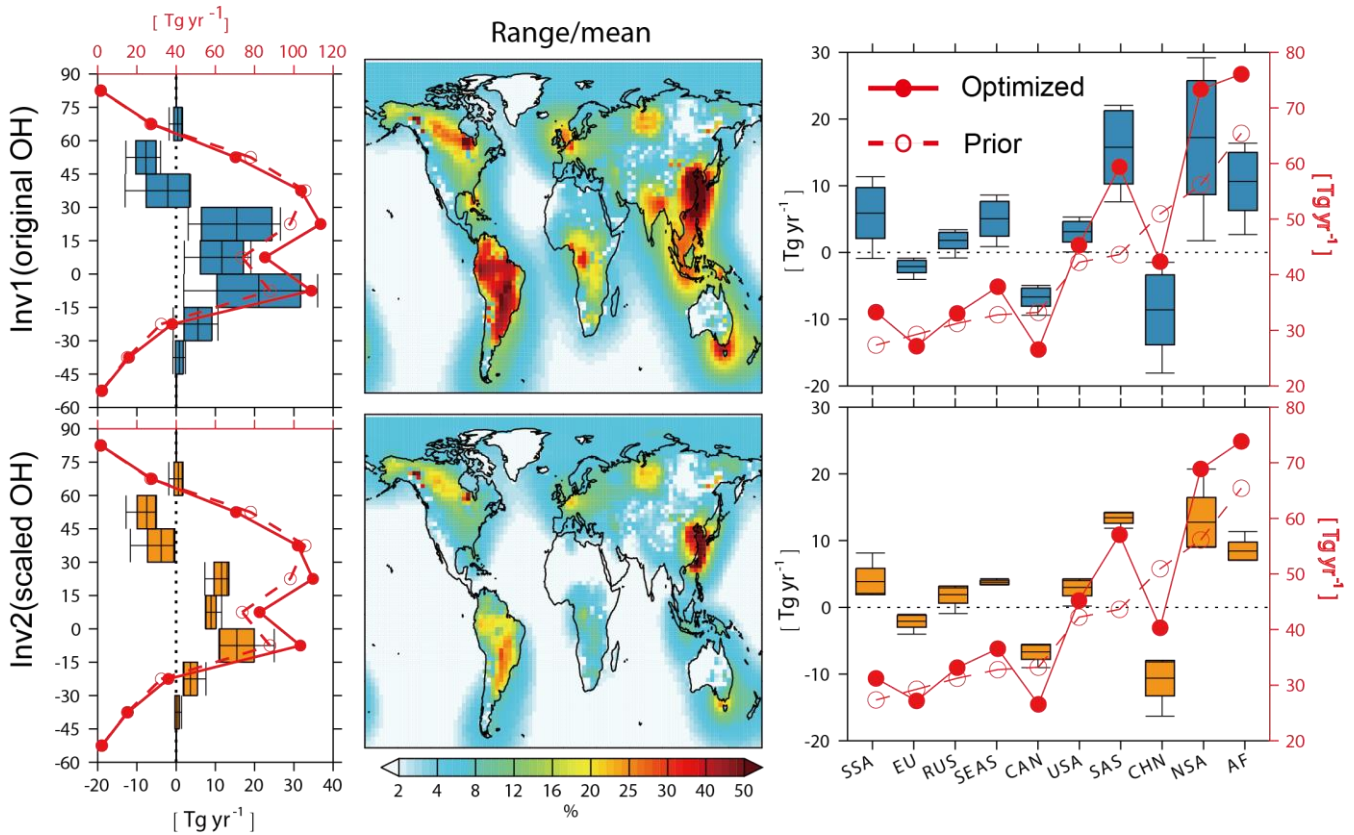


**Figure 3.** Zonal (left), and regional averages (right) of CH<sub>4</sub> emissions calculated by Inv1 (top row) and Inv2 (bottom row) with 8 OH fields from 2000/07/01 to 2002/06/01. Left and right panels: prior (dash red line) and mean optimized (solid red line) CH<sub>4</sub> emissions for every 15-degree latitudinal band and 10 regions, respectively. Where USA=America, CAN=Canada, EU=Europe, RUS=Russia, CHN=China, SEAS=Southeast Asia, SAS=South Asia, NSA=northern South America, SSA=southern South America, AF=Africa. The differences between prior and optimized emissions (optimized minus prior) are shown by the box plots (defined in Fig. 1). Prior and optimized emissions values correspond to the right axes and their differences correspond to the left axes. Middle panel: the ratio of the **uncertainty range** of emissions estimated with different OH fields (**max-min**) in each grid-cell calculated by Inv1 (top) and Inv2 (bottom) to multi-inversion mean CH<sub>4</sub> emissions.

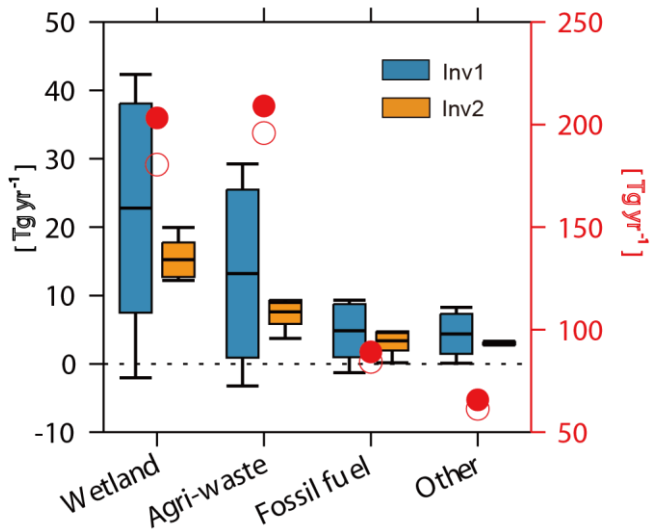
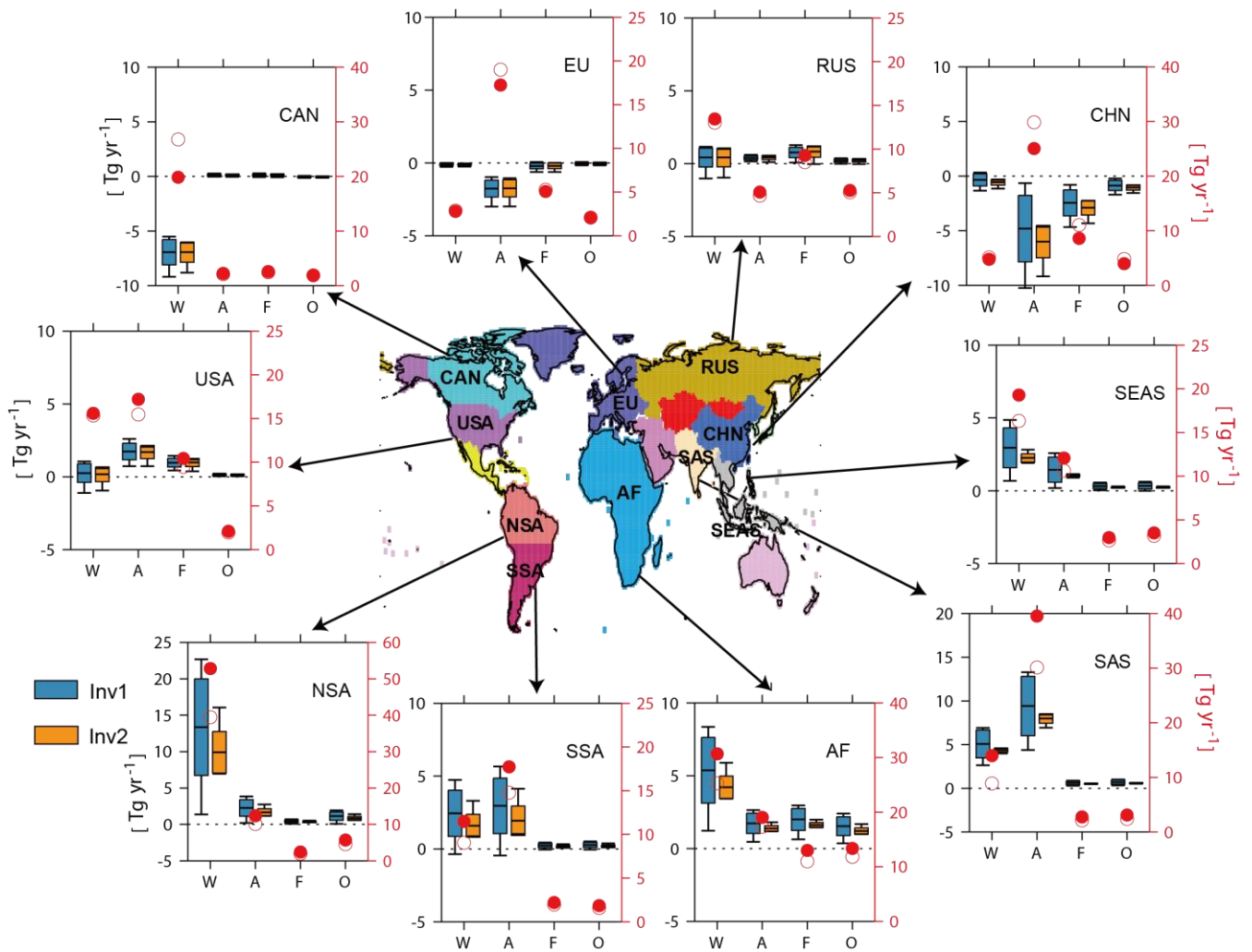
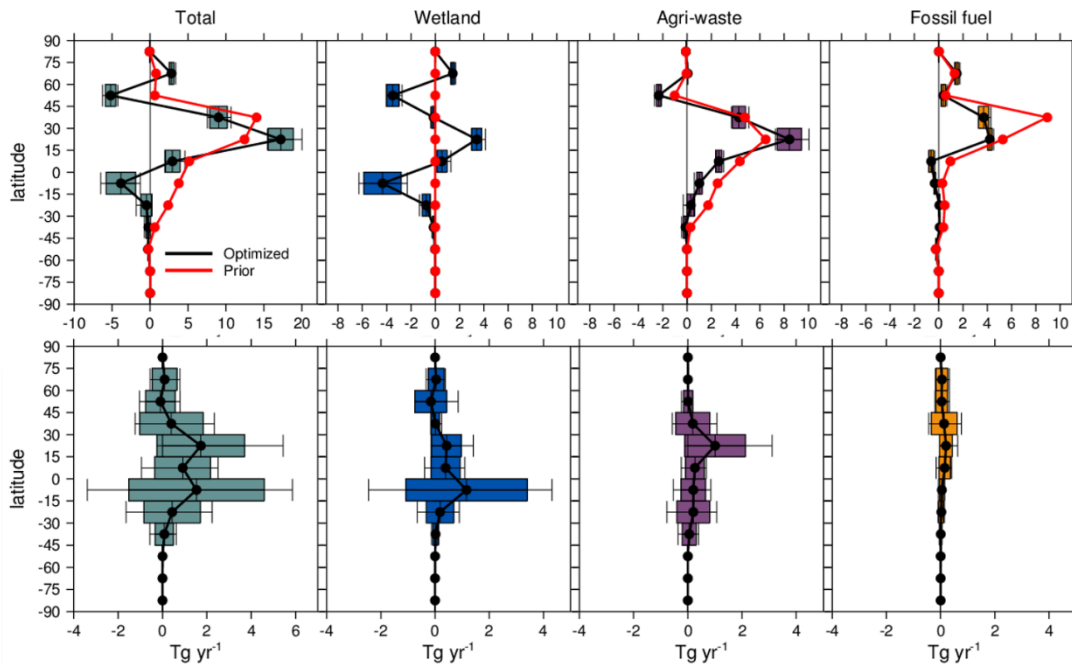


**Figure 4.** Global total CH<sub>4</sub> emissions from four broad categories from 2000/07/01-2002/06/01 in Tg yr<sup>-1</sup>. The red circles and dots show the prior emissions and mean optimized emissions, respectively, as calculated by Inv1 (right axes), and the box plots (defined in Fig. 1) show the difference between optimized emissions calculated by Inv1 (blue) and Inv2 (yellow) and prior emissions (optimized minus prior, left axes).



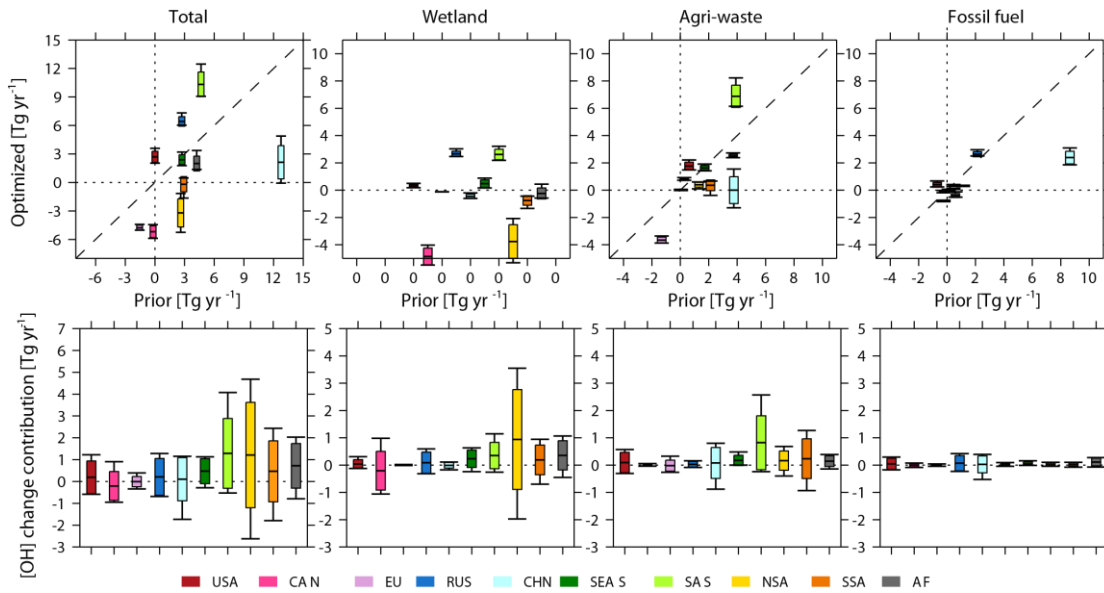
1135 **Figure 5.** Same as Fig. 4 but for prior and optimized emissions over 10 emitting regions covering most of the emitting lands. W=Wetlands, A=Agri-waste, F=Fossil fuels, and O=Others. In  $\text{Tg yr}^{-1}$ .



1140

**Figure 6.** Top panel: latitudinal emission (every 15-degree latitudinal band) changes in  $\text{Tg yr}^{-1}$  from the early 2000s (2000/07/01-2002/06/01) to the late 2000s (2007/07/01-2009/06/01) of total, wetlands, agriculture and waste, and fossil fuel emissions ( $\text{Inv3} - \text{Inv2}$ ). Bottom panel: contribution of OH changes on top-down estimated  $\text{CH}_4$  emission changes between the two periods ( $\text{Inv3} - \text{Inv4}$ ). The red lines are changes of prior emissions and the black lines are the mean changes of optimized emissions. The box plots (defined by Fig. 1) show the standard deviations and ranges calculated with different OH fields.

1145



1150 **Figure 7.** Top panel: optimized global total and sectoral regional emission changes in Tg yr<sup>-1</sup> from the  
 1155 early 2000s to the late 2000s (y-axis) plotted against prior emission changes between the two time periods  
 (x-axis) as derived from Inv2 and Inv3. The prior wetland emissions are constant over time, thus show  
 zero changes (all '0' on the x-axis). Bottom panel: contribution of OH changes between the two periods  
 on top-down estimated emission changes (Inv3 – Inv4). The box plots (defined by Fig. 1) show the  
 standard deviations and ranges calculated with different OH fields.

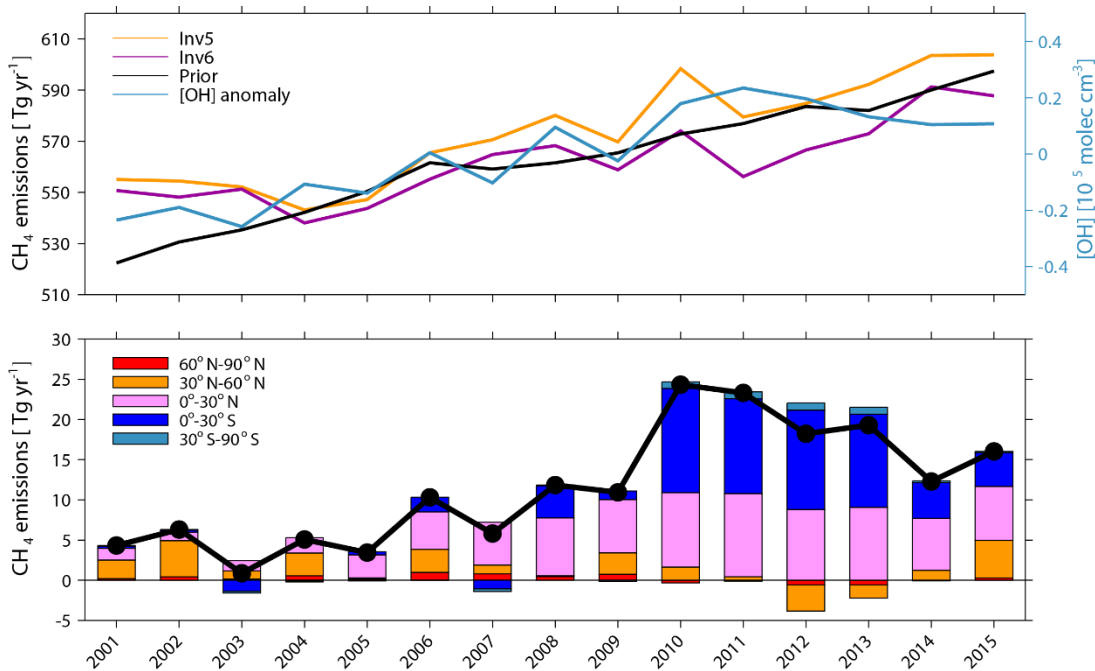


**Figure 8.** Top panel: Time series of global total  $\text{CH}_4$  emissions calculated by Inv5 (yellow) and Inv6 (purple) plotted together with prior emissions (black), and  $[\text{OH}]_{\text{GM-CH}_4}$  anomaly of CESM OH fields (blue). Bottom panel: the difference of global total (black line) and latitudinal (stack bar plots)  $\text{CH}_4$  emissions between Inv5 and Inv6 (Inv5-Inv6).

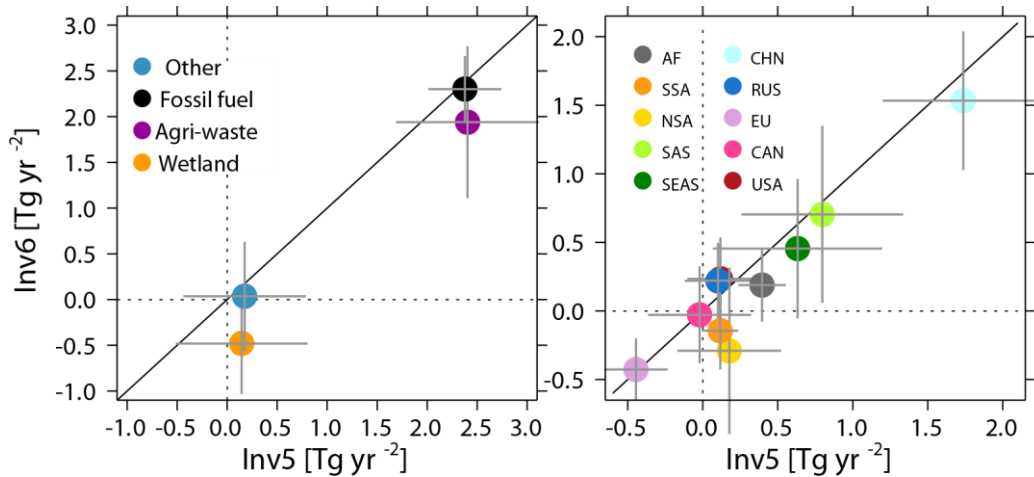


**Figure 9.** Comparison between Inv5 (x-axis) and Inv6 (y-axis) estimated global total  $\text{CH}_4$  emissions trends in  $\text{Tg yr}^{-2}$  between 2004 and 2015 for the four categories (left) and over the ten continental regions (right). The error bars show the trend with 95% confidence intervals.